ABSTRACT

Title of Thesis:	EFFECTS OF SEAWATER SR/CA VARIABILITY ON CORAL PALEOTHERMOMETRY IN THE FLORIDA KEYS AND VIRGIN ISLANDS REVEALED BY MULTI-YEAR CONTINUOUS MONITORING
	Hunter Passman Hughes, Master of Science, 2020
Thesis Directed By:	Associate Research Professor, K. Halimeda Kilbourne and Associate Professor, Johan Schijf, Chesapeake Biological Laboratory

Coral skeletal Sr/Ca is a widely applied proxy indicator for tropical sea surface temperature (SST) because the elemental ratio in coral aragonite is influenced by both SST and seawater Sr/Ca. Application of the methodology assumes that seawater Sr/Ca is a constant in coral reef environments, and the ratio can be used to solve for paleotemperatures based upon an established coral Sr/Ca – SST relationship. This study tests that assumption by documenting seawater Sr/Ca variability in the Florida Keys and in the U.S. and British Virgin Islands using continuous osmotic pumps. Samples are analyzed for Sr/Ca using a novel method via Inductively Coupled Plasma – Atomic Emission Spectrometry. While mean seawater Sr/Ca did not vary significantly between sites, all sites exhibited significant annual variability (~0.5 – 0.1 mmol/mol), with the greatest variability observed in locations most impacted by freshwater discharge. These findings correspond to large temperature offsets (>2°C) in standard coral Sr/Ca-based SST reconstructions.

EFFECTS OF SEAWATER SR/CA VARIABILITY ON CORAL PALEOTHERMOMETRY IN THE FLORIDA KEYS AND VIRGIN ISLANDS REVEALED BY MULTI-YEAR CONTINUOUS MONITORING

by

Hunter Passman Hughes

Thesis submitted to the Faculty of the Graduate School of the
University of Maryland, College Park, in partial fulfillment
of the requirements for the degree of
Master of Science
2020

Advisory Committee:
Associate Research Professor K. Halimeda Kilbourne, Chair
Associate Professor Johan Schijf
Professor Lee Cooper

Acknowledgements

More individuals than I can list helped in making this body of work. To highlight a few that deserve the utmost thanks, I would like to start with my advisors, Dr. Hali Kilbourne and Dr. Johan Schijf. They nurtured my curiosity, guided my exuberance, and kept their expectations high to mold me into the best student of science I can be. I am forever indebted to both of them for their passion and hard-work to bring this project to fruition. I would also like to thank Dr. Lee Cooper, whose combination of positivity and expertise brought a much-welcomed perspective to this thesis.

I would like to thank the National Science Foundation for research supported through grants to my advisors. I would also like to thank the Geological Society of America, and the Cove Point Natural Heritage Trust for additional analytical funding. I would like to thank the Chesapeake Biological Laboratory Graduate Education Committee and the University of Maryland Jacob K. Goldhaber award for supporting presentations of my work at two international conferences. I have made lifelong friends and associates at these meetings, and the benefits of these travels have yet to be fully realized.

A sincere thanks is owed to the staff at the Keys Marine Laboratory, who made all of our work in the Florida Keys possible. Captains Shaun Kadison in St. Thomas and Kelly Faulkner in Anegada also deserve thanks for guiding us through the beautiful waters of the Virgin Islands. A special thanks goes to the Nutrient Analytical Services Laboratory, particularly Jerry Frank and Kim Blodnikar, who worked seamlessly with me to ensure that all of the samples could be analyzed for this thesis. I would also like to thank all of the faculty, staff, and students at the Chesapeake Biological Laboratory who work tirelessly to create a wonderful atmosphere that fosters intellectual curiosity and supports higher learning.

Finally, a special thanks goes to my close friends and family. To Rori and Bob Lowe, who encouraged me to take bold strokes and chase my passions. To my sisters, who cultivated and challenged my ambitions. To the Oxford Gentlemen, I'm with you 'til the end of the line. And finally, to Marissa, who gave so much to me so that I could give to this.

This research was conducted in the Florida Keys National Marine Sanctuary under the authority of permits FKNMS-2016-099 and FKNMS-2016-099-A2

Table of Contents

Acknowledgements ii
Table of Contents iv
List of Tables v
List of Figures vi
Chapter 1: Introduction 1
1.1 Earth's Climate History and the Coral Paleothermometer 1
1.2 The Coral Sr/Ca Paleothermometer 3
1.3 Previous Investigations into Seawater Sr/Ca Variability 5
1.4 Potential Mechanisms of Seawater Sr/Ca Variability on Coral Reefs 7
1.5 Potential Impacts of Seawater Sr/Ca Variability on Coral Paleothermometry ... 9
1.6 Measuring Seawater Sr/Ca in the Florida Keys and the Virgin Islands 12
Chapter 2: Materials and Methods 14
2.1 Site Descriptions 14
2.2 Continuous Water Sampling via OsmoSampler 18
2.3 ICP-AES Analysis 20
2.4 Supporting Data 25
Chapter 3: Results 27
3.1 Age Models 27
3.2 Temporal Variability of Seawater Sr/Ca in the Tropical Western Atlantic 29
3.3 Temporal Variability of Seawater Sr/Ca in the Florida Keys 31
3.4 Temporal Variability of Seawater Sr/Ca in the Virgin Islands 35
3.5 Seawater Sr/Ca and $\delta^{18}O$ 36
3.6 Seawater Sr/Ca and [Sr] 39
Chapter 4: Discussion 41
4.1 Seawater Sr/Ca Variability in the Tropical Western Atlantic 41
4.2 Seawater Sr/Ca Variability in Florida Bay 44
4.3 Seawater Sr/Ca Variability in the Virgin Islands 48
4.4 Implications for Coral Sr/Ca-based Paleothermometry 52
4.4.1 Implications for Coral Sr/Ca-based SST Reconstructions 52
4.4.2 Implications for Seawater Sr/Ca Variability Across the FKRT 56
Chapter 5: Conclusion 60
Appendix 62
Bibliography 80

List of Tables

Table 1. Comparison of analytical precision for two ICP-AES procedures used in this study. Improvements in the modified method can largely be attributed to using a baffled spray chamber. 22

Table 2. Mean and standard deviation of seawater reference materials (CASS-5 and CASS-6) and in-house standards (GoM and GoM SPLIT). Percent relative standard deviation is abbreviated % RSD. Data from standards provide a measure of the ICP-AES method analytical performance. 24

Table 3. Summary statistics of seawater Sr/Ca collected via OsmoSampler. Mean, standard deviation, and range are in units of mmol/mol. Mean seawater Sr/Ca is similar across sites, but standard deviation and range vary significantly. *Samples from STJN estimated to be pumped between Oct. 24th and Nov. 25th 2018 were removed from this dataset. 31

Table 4. Summary statistics of seawater $\delta^{18}O$ at our OS1, OS4, and ANEE sites. Note the similarities at OS4 and ANEE compared to OS1, particularly with respect to standard deviation and range. Mean, standard deviation and range in ‰ relative to Vienna Standard Mean Ocean Water (V-SMOW). 36

Table 5. Mean seawater Sr/Ca and standard error at both VI sites prior to and after June 2018. All units are in mmol/mol. *Samples from STJN that were estimated to be collected between Oct. 24th and Nov. 25th 2018 were clearly an unusual local event and were therefore not included in this analysis (see text). 49

Table 6. A summary of the error for the pseudo SST reconstructions at OS1, OS4, ANEE, and STJN. Values are reported as the difference between measured in situ SST and SST theoretically obtained from a coral growing under the measured in situ seawater Sr/Ca conditions (pseudo SST). Negative values indicate that pseudo SST is lower than in situ SST. Absolute mean temperature offset is low at all sites except for OS1, where the temperature offset is seasonal rather than episodic. 56

List of Figures

Figure 1. Locations of the four water monitoring stations in the Florida Keys, Florida, USA. Stations were located in various benthic environments at different depths forming an offshore transect. The OS1 site is ~8 km from NOAA buoy PKYF1. Inset box outlines the approximate area of the detailed map.. 15

Figure 2. Locations of two water monitoring stations in Coral Bay on St. John, USVI (STJN) and on the fringing reef off the east end of Anegada, BVI (ANEE). Inset box outlines the approximate area of the detailed map.. 16

Figure 3. Seawater Sr/Ca from six water monitoring stations in the Florida Keys and Virgin Islands. Black error bars at the beginning of the time series represent analytical uncertainty (0.01 mmol/mol, 1σ). Crossed boxes indicate when deployment periods begin. ANEE and STJN constitute a single deployment. Light portions of the time series indicate where there is less confidence in the age model. Gray portions indicate where data were not considered in the discussion. Note the high degree of seasonality at OS1 and, to a lesser extent, OS2. 30

Figure 4. A bean-box hybrid plot of seawater Sr/Ca at all sites. The gray area behind each boxplot represents the probability density curve of the distribution of seawater Sr/Ca ratios at each site. The bold horizontal lines indicate the median at each site. An Anderson-Darling test for normality (e.g., Thode, 2002) indicates a relatively normal distribution of the data at OS1 and OS2 ($p > 0.05$), where an annual cycle is evident. 34

Figure 5. Time series of seawater Sr/Ca and $\delta^{18}O$ data from the ANEE OsmoSampler. The Sr/Ca – $\delta^{18}O$ relationship is significant, but substantially weaker than in the Florida Keys ($p = 0.01$). 38

Figure 6. Time series of seawater Sr/Ca and [Sr] at OS1. Analytical error for [Sr] is 0.003 mM. Correlation coefficients were calculated using a Pearson correlation test. Seawater Sr/Ca and [Sr] are modestly correlated at OS1, and typically exhibit co-occurring summer maxima and winter minima. 39

Figure 7. Monthly mean seawater Sr/Ca at OS1 (orange) and OS2 (green) over the study period. The shaded regions around each line indicate the range of ratios observed in that month throughout the three-year study. Note that despite substantial interannual variability, local maxima consistently occur in July. Minima typically occur in November, December, or January. 43

Figure 8. A conservative water mass mixing model between measured seawater Sr/Ca and [Sr] from samples at OS1. Endmembers are indicated by red boxes. The freshwater endmember was determined using Everglades measurements from Surge and Lohmann (2002). Mean seawater Sr/Ca and [Sr] at OS4 were taken as the upper end member.

The area between the dashed lines represents the possible range of values obtained from two-endmember mixing, given the variance observed for each endmember. Vertical red bars represent 10% increments of mixing. Analytical errors in [Sr] and Sr/Ca are represented by the crosshairs at the top-left of the graph. Note how some lower values fall directly in the center of the mixing model, while higher values show substantial scatter. 46

Figure 9. Seawater Sr/Ca at the ANEE site (black line) plotted with satellite-derived SSS measurements acquired during the study period (Kerr et al., 2010) (dashed lines). The color of each dashed line corresponds to SSS integrated over an area indicated by the inset map during the study period. Errors for Sr/Ca (solid) and SSS (dashed) are 0.01 mmol/mol and 0.28, respectively. Salinity in each region is positively correlated with seawater Sr/Ca from ANEE ($r^2 > 0.54$), most strongly in the Northeast quadrant ($r^2 = 0.61$). 49

Figure 10. Seawater Sr/Ca at the STJN OsmoSampler plotted with (A) precipitation data from the east end of St. Thomas (~15 km from STJN) collected by the Community Collaborative Rain, Hail, and Snow Network (Reges et al., 2016), and (B) barometric pressure measurements from National Data Buoy Center Station 41052 (Hamilton, 1986), approximately 10 km south of Cruz Bay on the southwest corner of St. John. The negative excursion in seawater Sr/Ca from STJN is coincident with a sustained drop in barometric pressure, but available precipitation data does not appear anomalous at this time. 52

Figure 11. Coral Sr/Ca-based reconstructed pseudo SST (red) versus in situ SST (blue) measured using Onset HOBO© loggers at OS1 (A), OS4 (B), ANEE (C), and STJN (D). Pseudo SST was calculated using the coral Sr/Ca – SST regression from Swart et al. (2002). Pseudo SST is more variable at all sites compared to in situ SST. In November 2018, pseudo SST at STJN peak at almost 40ºC, which is clearly an unrealistic temperature. 55

Figure 12. (A) Monthly averages of measured seawater Sr/Ca at OS1 (orange) and OS2 (green). (B) Monthly averages of measured seawater $\delta^{18}O$ at OS1. (C) Monthly averages of calculated seawater Sr/Ca at Looe Key (Smith et al., 2006) using calibration equations from Smith et al. (1979) (red) and Swart et al. (2002) (green). (D) Monthly averages of calculated seawater $\delta^{18}O$ at Looe Key (Smith et al., 2006) using a calibration equation from Leder et al. (1996). The shaded regions in (A) and (B) represent the range of values observed at OS1 during the study period, while the shaded regions in (C) and (D) represent the standard deviation of the reported values associated with sampling. Notes the similarities in the summer maxima and winter minima between the current study and Smith et al. (2006). 58

Chapter 1: Introduction

1.1 Earth's Climate History and the Coral Paleothermometer

The climate system is driven by the unequal distribution of the Sun's energy across the Earth's surface that is skewed towards the tropical oceans (Peixoto & Oort, 1992). The tropical oceans therefore play an important role as a primary recipient of solar heat, which is then dissipated through atmospheric and oceanic circulation. Tropical sea surface temperature (SST) is linked to many critical climate variables such as atmospheric moisture content and temperature, cloud cover, and patterns of atmospheric circulation (Hastenrath, 1991). While there is still much to explore, the available literature demonstrates that understanding tropical climate is essential to understanding how Earth's climate functions as a whole (McPhaden et al., 1998).

Tropical SST is a key part of the meridional heat transport that reduces the heat gradient between the tropics and the poles, dictating global hydroclimate patterns on seasonal timescales (Barry & Chorley, 2009). Tropical Pacific SST anomalies are diagnostic of the El Niño-Southern Oscillation, the leading mode of Earth's interannual climate variability, and are linked to extreme weather events across the globe (Emile-Geay et al., 2016; Felis et al., 2000; Philander, 1990). While there is an ongoing debate regarding the persistence and predictability of climate variability on multidecadal timescales (Mann et al., 2020; Smith et al., 2020) multidecadal variations in tropical SST during the industrial era have been linked to Atlantic hurricane activity (Gray et al., 1997), as well as summer rainfall in India and the Sahel (Wang & Zhang, 2013).

Changes in tropical SST have even been used to explain centennial-scale changes in global hydroclimate during the Medieval Climate Anomaly and the Little Ice Age (Burgman et al., 2010; Mann et al., 2009). Reconstructions of past climate, or paleoclimate, specifically of tropical SST, are thus an important tool for understanding the fundamental mechanisms of the climate system over a range of time scales (IPCC, 2014).

Forecasting climate variability through the 21st century requires validating climate models with observations (Hackert et al., 2020). However, globally interpolated instrumental data sets only date back to the late 1800s, which does not encompass enough time to accurately identify modes of climate variability on multidecadal and longer timescales, or how they impact seasonal and interannual climate variability (Smerdon & Pollack, 2016). This problem is exacerbated in the tropics, where historical SST measurements are relatively scarce compared to the extra-tropical Northern Hemisphere (Kennedy et al., 2011; Morice et al., 2012).

To reconstruct tropical climate variability, paleoclimatologists extend the observed instrumental record both spatially and temporally using climate indicators recorded by massive reef-building corals, which are well suited as low-latitude, shallow-water, high-resolution climate proxies (Jones et al., 2009). Restricted both geographically and bathymetrically to shallow water in tropical and subtropical oceans, the skeletons of reef-building scleractinian corals incorporate numerous chemical constituents of ambient seawater that can serve as geochemical proxies for a variety of environmental parameters (Jones et al., 2009). Annual changes in skeletal density provide excellent chronologies, and a single coral colony can grow to be several meters high over decadal to centennial time-scales, making them ideal tools for studying seasonal to centennial scale climate variability (Grottoli, 2001). Furthermore, coral skeletons can persist for millennia in the geologic record, offering glimpses of climate well before the modern era (Guilderson et al., 1994; Hughen et al., 1999; Kilbourne et al., 2004; Shackleton & Matthews, 1977).

1.2 The Coral Sr/Ca Paleothermometer

Two of the most widespread coral skeletal geochemical proxies are the oxygen isotopic composition ($\delta^{18}O$) of aragonite and the strontium-to-calcium ratios (Sr/Ca) in the same carbonate structure, often utilized together to reconstruct both sea surface salinity (SSS) and SST (Gagan et al., 1998; Kilbourne et al., 2004). Coral skeletal Sr/Ca and $\delta^{18}O$ are influenced primarily by the temperature and, respectively, Sr/Ca and $\delta^{18}O$ of ambient seawater (Corrège, 2006). Seawater $\delta^{18}O$ varies generally as a function of salinity (Epstein & Mayeda, 1953), but seawater Sr/Ca is considered stable and invariable over the small salinity variations that occur in coral reef environments (Beck et al., 1992).

The relationship between temperature and the distribution coefficient ratio (K) of Sr and Ca between aragonite and seawater was determined by Kinsman and Holland (1969) and Smith et al. (1979). The former observed the temperature dependence of Sr/Ca in authigenic aragonite precipitated from solution, while the latter empirically defined this dependence for coral aragonite in seawater.

$$K(T) = \frac{(Sr/Ca)_{aragonite}}{(Sr/Ca)_{seawater}} \tag{1}$$

$$K(T) = 1.30 - 0.0094T \quad (2)$$

If $(Sr/Ca)_{seawater}$ is known, then equations (1) and (2), in combination with precise measurements of $(Sr/Ca)_{aragonite}$, will yield a unique value for temperature (T, in ºC). Using laboratory experiments, Smith et al. (1979) manipulated seawater Sr/Ca at constant temperatures and confirmed its predicted impact on coral Sr/Ca. However, when the authors collected corals for field reconstructions, they assumed a constant value of seawater Sr/Ca at ~8.6 mmol/mol (Kinsman & Holland, 1969), which was consistent with their empirical coral Sr/Ca – SST calibration.

$$(Sr/Ca)_{coral} = 8.6 \times (1.30 - 0.0094T) \sim 11.32 - 0.082T \quad (3)$$

At the time, the methodology used for determining $Sr/Ca_{aragonite}$ (atomic absorption spectrometry) was insufficiently precise and resulted in errors as large as ~2ºC in predicted temperatures during aragonite synthesis. A methodological improvement was achieved when Beck et al. (1992) used thermal ionization mass spectrometry, which reduced the analytical error for coral Sr/Ca-based temperature reconstructions to ~0.5ºC. As with Smith et al. (1979), Beck et al. (1992) assumed constant seawater Sr/Ca in view of the long residence times of Sr and Ca in the global oceans (6 million years and 0.7 million years, respectively; Pilson, 2012), and likewise used a linear coral Sr/Ca – SST calibration. After this initial success, coral Sr/Ca paleothermometry was adapted to Inductively Coupled Plasma – Atomic Emission Spectrometry (ICP-AES) for more rapid and cost-effective analysis while retaining the necessary level of precision (de Villiers et al., 2002; Schrag, 1999). Over the following decades, the coral Sr/Ca method became widely utilized in the paleoclimate community for regional-to-global-scale reconstructions, establishing itself as a reliable tropical paleothermometer (Felis et al., 2018; Tierney et al., 2015).

Shortly after Beck et al. (1992) showed the robustness of the coral Sr/Ca paleothermometer, de Villiers et al. (1994) demonstrated that mean seawater Sr/Ca, which Smith et al. (1979) showed to have a direct impact on the coral Sr/Ca – SST relationship, can vary by ~2% between sites across the tropical Pacific and Atlantic. If seawater Sr/Ca were to vary locally within the range observed in that study, it could skew the local calibration and create errors in reconstructed SST of more than 2°C, equivalent to the seasonal temperature range in many tropical regions (Hastenrath, 1991). However, within the coral paleoclimate community, this knowledge of Sr/Ca variations is not regarded as a major limitation, because the primary findings of de Villiers and co-workers apply to Sr/Ca changes in upwelling zones and at depth in the open ocean, neither of which are prime habitat for reef-forming scleractinian corals.

1.3 Previous Investigations into Seawater Sr/Ca Variability

The justification for assuming constant seawater Sr/Ca is based on an early finding by Forchhammer (1865) that was later confirmed by Dittmar (1884). These studies form the basis of the Principle of Constant Proportions, which states that the concentrations of the major ions in seawater are invariable with respect to one another regardless of salinity. Over a century later, Horibe et al. (1974) convincingly showed non-conservative behavior of Ca in salinity-normalized vertical profiles, namely relative depletion in shallow waters and enrichment at depth. Later studies by Bernstein et al. (1987, 1992) showed similar behavior for Sr. Further studies in the last ~30 years have established a more nuanced understanding of seawater Sr/Ca variability over geologic time (Stoll & Schrag, 1998), depth (de Villiers et al., 1994), and in estuaries (Macdonald & Crook, 2010).

In the broader context of Earth's geologic history, seawater Sr/Ca can vary substantially due to changes in carbonate mineralization and sea level that differentially alter the Sr and Ca budgets of the global ocean (Steuber & Veizer, 2002; Stoll & Schrag, 1998). However, such variations in seawater Sr/Ca occur on temporal scales (millennial and longer) far exceeding those recorded by a single coral colony, and would only impact mean reconstructed SST over much longer periods of time. The amplitude and frequency of reconstructed short-term (centennial and shorter) SST variability should thus be preserved, unless more rapid or localized changes in seawater Sr/Ca were occurring.

Most studies measuring seawater Sr/Ca variability on more local spatiotemporal scales report a nutrient-like profile, where Sr/Ca increases with depth (Alibert et al., 2003; de Villiers et al., 1994). This is likely caused by biogeochemical release of these elements from plankton (Bernstein et al., 1987, 1992; Horibe et al. 1974). The saturation state of Sr is lower than that of Ca in the global ocean, so celestite ($SrSO_4$) tests dissolve at a much shallower depth than those made of calcite or aragonite, resulting in deep seawater Sr/Ca that is higher by 1-2% than the surface water, with a particularly steep gradient in the upper 200 meters and maximum Sr/Ca ratios found at less than 1000 meters (de Villiers, 1999).

In estuaries, Sr/Ca is a non-linear function of salinity (Surge & Lohmann, 2002). This is used to advantage in fisheries science, where Sr/Ca in fish otoliths can be used to the track the history of fish movements in and out of estuaries (Gillanders, 2005). Although Sr/Ca in river systems can vary greatly depending on drainage basin geology, Sr/Ca ratios are generally lower than in seawater (Brennan et al., 2014; English et al., 2000). However, because seawater has much higher Sr and Ca concentrations than river water, Sr/Ca in estuaries is typically only distinguishable from seawater at salinities considered below the viable range for corals (Dodd & Crisp, 1982).

1.4 Potential Mechanisms of Seawater Sr/Ca Variability on Coral Reefs

The current body of knowledge regarding the marine geochemical behavior of Sr and Ca over geologic time, depth, and in estuaries (see Section 1.3) can provide a framework for understanding seawater Sr/Ca variability over relatively short timescales in coral reef environments. Potential mechanisms of variability in coral reef environments may include: (1) inputs from local landmasses, (2) upwelling, or (3) local changes in carbonate mineralization due to seasonal changes in reef productivity.

Discharge from land could give rise to variations in seawater Sr/Ca in coral reef environments in the form of runoff or submarine groundwater discharge (SGD). Given what is known about Sr/Ca in river systems and estuaries (Brennan et al., 2014; Macdonald & Crook, 2010), seawater Sr/Ca variability on reefs that are sufficiently close to sources of runoff may be correlated with regional precipitation patterns. The effects of this runoff could even have more regional effects as seasonal variations in runoff leave traceable signatures in water masses across the tropical western Atlantic (Hu et al., 2004).

Alternatively, SGD in coral reef environments is an area of active research with major implications for nutrient cycling and hydrologic interactions in reef waters (Lubarsky et al., 2018; Paytan et al., 2006). Groundwater Sr/Ca values can vary depending on its source (modified seawater *vs.* rainwater) and local watershed geology (silicate *vs.* carbonate) (Andersson et al., 1992; Basu et al., 2001; Khaska et al., 2013). In carbonate systems, remineralization of aragonite to calcite or dolomite can lead to higher Sr/Ca in groundwater due to progressive exclusion of Sr from the crystal lattice (Katz et al., 1972; Lerouge et al., 2010; Malone & Baker, 1999; Schijf & Byrne, 2007). However, fresh (as opposed to saline) groundwater in the same carbonate system may instead have low Sr/Ca, more akin to runoff (Stalker et al., 2009). Therefore, SGD may cause shifts of Sr/Ca in different coral reef environments depending on the flux and Sr/Ca ratio of the groundwater.

Despite the Sr/Ca depth gradient in the upper ocean, upwelling is likely to play at most a minor role in seawater Sr/Ca variability in coral reef environments. Most tropical coral reefs are found in nutrient-poor waters, where the nutrient-like profile in seawater Sr/Ca ratios is much less pronounced (de Villiers et al., 1994). Furthermore, sampling constraints mean that most coral Sr/Ca skeletal samples are integrated over a minimum of biweekly time periods (DeLong et al., 2013). Transient upwelling events common on reefs would likely not be sufficient to significantly impact coral Sr/Ca, unless (1) these events were common enough to shift mean seawater Sr/Ca, and (2) the upwelling event triggered secondary responses such as stress and bleaching (Hetzinger et al., 2016).

Diel-to-seasonal variations in reef productivity could, in theory, vary local seawater Sr/Ca through changes in calcification and dissolution of Sr and Ca containing minerals (Muehllehner et al., 2016). Diel changes in calcification rates, resulting from changes in photosynthesis and respiration, mirror similar changes between summer maxima and winter minima in photosynthesis and calcification rates on seasonal timescales (Muehllehner et al., 2016; Schneider et al., 2009). Over an annual cycle in most tropical regions, temperature can fluctuate near the value (~31.9°C) where K (Eq. 2) for aragonite is equal to unity (Smith et al., 1979). For most of the year, however, temperature remains well below this value (Lough, 2012), corresponding to a K that is slightly higher than unity. Given the complicated dynamics of biogenic calcification in coral reef environments, variations in aragonite and calcite precipitation and dissolution rates could alter ambient seawater Sr/Ca values on seasonal timescales.

1.5 Potential Impacts of Seawater Sr/Ca Variability on Coral Paleothermometry

A number of studies (e.g., Quinn et al., 2006; Smith et al., 2006; Swart et al., 2002; Wei et al., 2000) have speculated that the accuracy of coral Sr/Ca – SST calibrations can be affected by seawater Sr/Ca variability, but seawater Sr/Ca measurements are not often made, and the significance of impacts on calibrations vary. For example, there is evidence that coral Sr/Ca – SST calibrations have been affected by seawater Sr/Ca variability from substantial terrestrial runoff (Shen et al., 1996; Wei et al., 2000). Even in regions with little runoff, differences in calibrations between corals from back-reef and forereef environments have been observed (Fowell et al., 2016; Saenger et al., 2008); complexities include potential non-temperature related factors. To the best of my knowledge, only two field studies have measured Sr/Ca in seawater from which a coral core was collected for paleothermometry (Saenger et al., 2008; de Villiers et al., 1994). In only one of these, coral Sr/Ca – SST calibrations were normalized at each site using the observed mean seawater Sr/Ca ratio (de Villiers et al., 1994). Although seawater Sr/Ca measurements from these studies were limited both spatially and temporally, significant variations were found with depth and between study sites (de Villiers et al., 1994), or between different reef environments (Saenger et al., 2008).

Smith et al. (2006) provide a robust argument for the potential complication of coral Sr/Ca – SST reconstructions by seawater Sr/Ca variations, under some circumstances. Rearranging equation (2) above, these authors used coral Sr/Ca and local values of SST from the HadISST dataset (Rayner et al., 2003) to estimate seawater Sr/Ca at Looe Key, Florida, over the previous 41 years. Their calculations projected that local seawater Sr/Ca exhibits an annual cycle slightly out of phase with temperature, with minima and maxima spanning ~0.3 mmol/mol on average (equivalent to ~5ºC in reconstructed SST) between February and August. Similar calculations for the $\delta^{18}O$ data indicated a positive relationship between seawater Sr/Ca and $\delta^{18}O$ at Looe Key (Smith et al., 2006; their Eq. 8).

Recently, Khare (2018) corroborated the seawater Sr/Ca variations predicted by Smith et al. (2006) by measuring surface seawater Sr/Ca in a ~400 km^2 grid adjacent to the Florida Keys over two consecutive summer and winters. Offshore ratios were relatively invariant (±0.02 mmol/mol), while the nearshore environment alternated between high summer and low winter ratios with a range of ~0.1 mmol/mol. Spatial variability in seawater Sr/Ca was well represented in that study, but the limited semi-annual sampling resolution may have aliased the full extent of the annual cycle.

Despite its great potential impact on coral Sr/Ca, seawater Sr/Ca variability has received relatively little attention compared to other non-temperature related variables that can affect coral Sr/Ca-based SST reconstructions (Cohen et al., 2001; Grove et al., 2013; Maupin et al., 2008) such as biological controls on coral skeletal Sr/Ca (de Villiers et al., 1995; Hirabayashi et al., 2013; Sinclair et al., 2006). While several studies have shown that coral Sr/Ca is highly reproducible between corals growing on the same reef (DeLong et al., 2011), others have found significant offsets in corals from the same location (Meibom et al., 2006). The cause of these "vital effects" is still a subject of active research (D'Olivo et al., 2018; Flannery et al., 2017), but has garnered much attention and is thought of as a dominant confounding variable for coral Sr/Ca paleothermometry (de Villiers et al., 1994; Ross et al., 2019; Saenger et al., 2008).

Analytical limitations have also contributed to a lack of knowledge of seawater Sr/Ca variability. The instrumentation typically used for seawater Sr/Ca analysis, thermal ionization mass spectrometry, has a high capital acquisition cost, and high analytical costs with low sample throughput. However, in the same way that coral Sr/Ca measurements were adapted for ICP-AES analysis (Schrag, 1999; de Villiers et al., 2002; Watanabe et al., 2020), the scientific community is working to develop more accessible and user-friendly methods for measuring Sr/Ca (Khare, 2018), and particularly Ca (He et al., 2020), in seawater

1.6 Measuring Seawater Sr/Ca in the Florida Keys and the Virgin Islands

This thesis investigates whether seawater Sr/Ca variability can significantly affect coral Sr/Ca-based temperature reconstructions. Comprehensive and targeted seawater Sr/Ca studies over various reef environments are needed in order to characterize the temporal variability of seawater Sr/Ca, with the ultimate goal of assessing the importance of a potentially confounding variable in coral Sr/Ca paleothermometry. This study makes innovative use of continuous water sampling methodologies (Jannasch et al., 2004) and a modification of a novel analytical method (Khare, 2018) to quantify the temporal variability of seawater Sr/Ca across various coral reefs in the Florida Keys and the British and U.S. Virgin Islands.

The three locations included in this study (Florida Keys, USA; St. John, U.S. Virgin Islands; Anegada, British Virgin Islands) are areas of previous and active coral Sr/Ca-based paleoclimate studies (Kuffner et al., 2013; Reich et al., 2013; Xu et al., 2015), and are therefore relevant to paleoclimatic applications. Furthermore, previous studies at two of these three locations suggest that seawater Sr/Ca variability affects coral Sr/Ca ratios (Reich et al., 2013; Smith et al., 2006; Swart et al., 2002). The sites were selected to represent a hydrologic and geologic gradient along which many coral reefs can be found, from a continental-scale carbonate platform (Florida Keys) to a high-relief siliciclastic island (St. John, U.S. Virgin Islands).

At each site, the use of continuous *in situ* water samplers over multiple years allowed a comprehensive observation of the annual cycle in seawater Sr/Ca. The experimental design was meant to facilitate understanding of which reef environments are more susceptible, if at all, to significant seawater Sr/Ca variations. Seawater Sr/Ca measurements were supplemented by measurements of seawater $\delta^{18}O$. Given its proposed correlation with seawater Sr/Ca in the Florida Keys (Smith et al., 2006), this separate indicator may help to elucidate potential mechanisms of seawater Sr/Ca variability.

Chapter 2: Materials and Methods

2.1 Site Descriptions

The first site observed in this study consisted of four water monitoring stations located in the Florida Keys, a crescent-shaped chain of islands stretching from just southeast of Miami to the Dry Tortugas, ~290 km to the southwest (Halley et al., 1997). These islands are located in a tropical climate regime (Kottek et al., 2006), with the wet season typically lasting from May to October. Precipitation and freshwater runoff only exceed evaporation between mid-May and mid-September (Duever et al., 1994; Stabenau & Kotun, 2012). Tropical cyclones, which usually arrive in late summer and fall, can contribute as much as 15-20% of annual precipitation (Prat & Nelson, 2013). Based on environmental criteria, the Florida Keys are geographically divided into three sub-regions (Shinn et al., 1989): The Upper Keys (Soldier Key to Upper Matecumbe Key), the Middle Keys (Upper Matecumbe Key to Big Pine Key), and the Lower Keys (Big Pine Key to the Dry Tortugas).

The Florida Keys water monitoring stations (OS1 – OS4) were located in the Middle Keys, ranging from 2.5 km north to 8 km seaward of Long Key (Figure 1). These stations constitute a transect that covers a variety of habitats along the Florida Keys Reef Tract (FKRT), which extends up to 10 km offshore and delineates an area of dynamic interactions between water masses from the open ocean (Lee & Williams, 1999; Leichter et al., 2003), groundwater (Paul et al., 1997; Reich et al., 2002; Top et al., 2001), and Florida Bay (Lloyd, 1964; Swart & Price, 2002; Swart et al., 1989b). The dominant hydrographic interactions over the reefs are from competing influences of the open ocean Florida Current and anti-estuarine (hypersaline) Florida Bay (Davis et al., 2008; Lee et al., 1992; Pitts, 1994). This can be observed in a seaward 'green-to-blue-water' front that migrates daily in response to wind and tidal forcing (Lee, 1986).

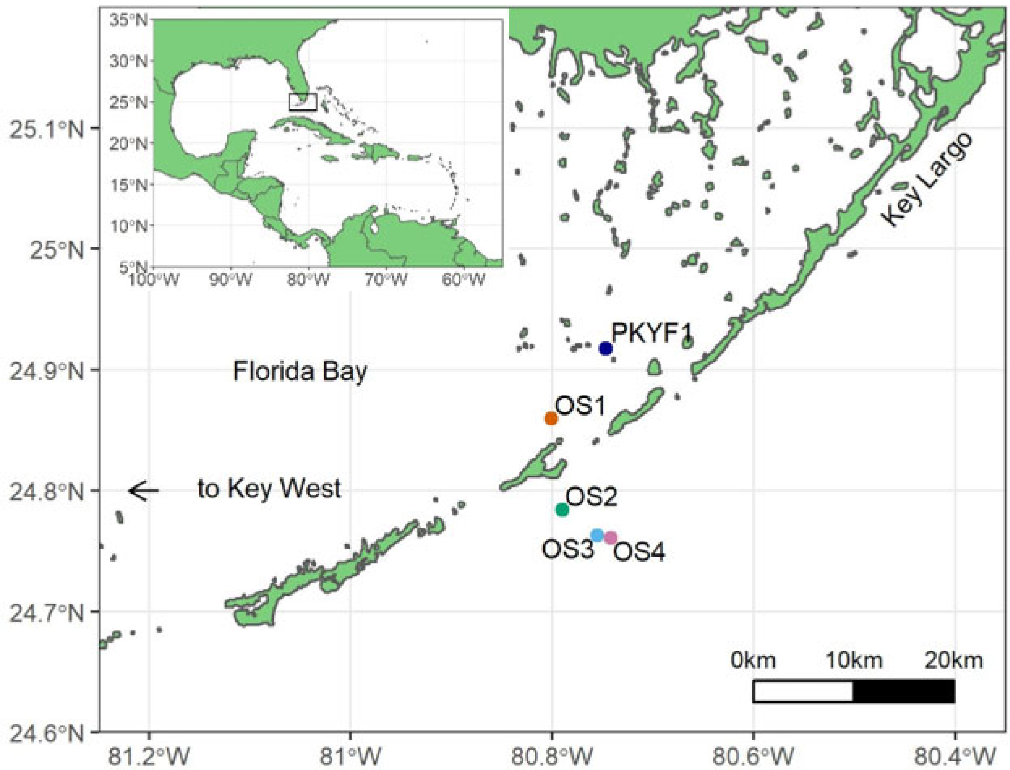

Figure 1. Locations of the four water monitoring stations in the Florida Keys, Florida, USA. Stations were located in various benthic environments at different depths forming an offshore transect. The OS1 site is ~8 km from NOAA buoy PKYF1. Inset box outlines the approximate area of the detailed map.

Stations OS1 – OS4 were located along a transect between Florida Bay and the forereef to determine if temporal variability in seawater Sr/Ca changed with distance from shore. The shallowest station (OS1) was located ~2.5 km north of Long Key in Florida Bay, where few corals grow (Swart et al., 1996), at a bottom depth of 3 m. The second (OS2) was deployed in a sandy patch among seagrass beds in Hawk Channel at

6 m bottom depth, ~3 km south of Long Key. The third (OS3) was placed in a sand patch along a spur-and-groove formation (i.e., ridges of coral limestone and valleys of sand) in Tennessee Reef, ~9 km south of Lower Matecumbe Key at 9 m bottom depth. The final station (OS4) was placed on the forereef among large-scale sand ripples, ~10.5 km south of Lower Matecumbe Key at 18 m bottom depth. Over the course of this study, shifting sediments revealed ubiquitous hard ground at OS4, intermittently buried by sand.

Two additional water monitoring stations (Figure 2) were located in St. John,

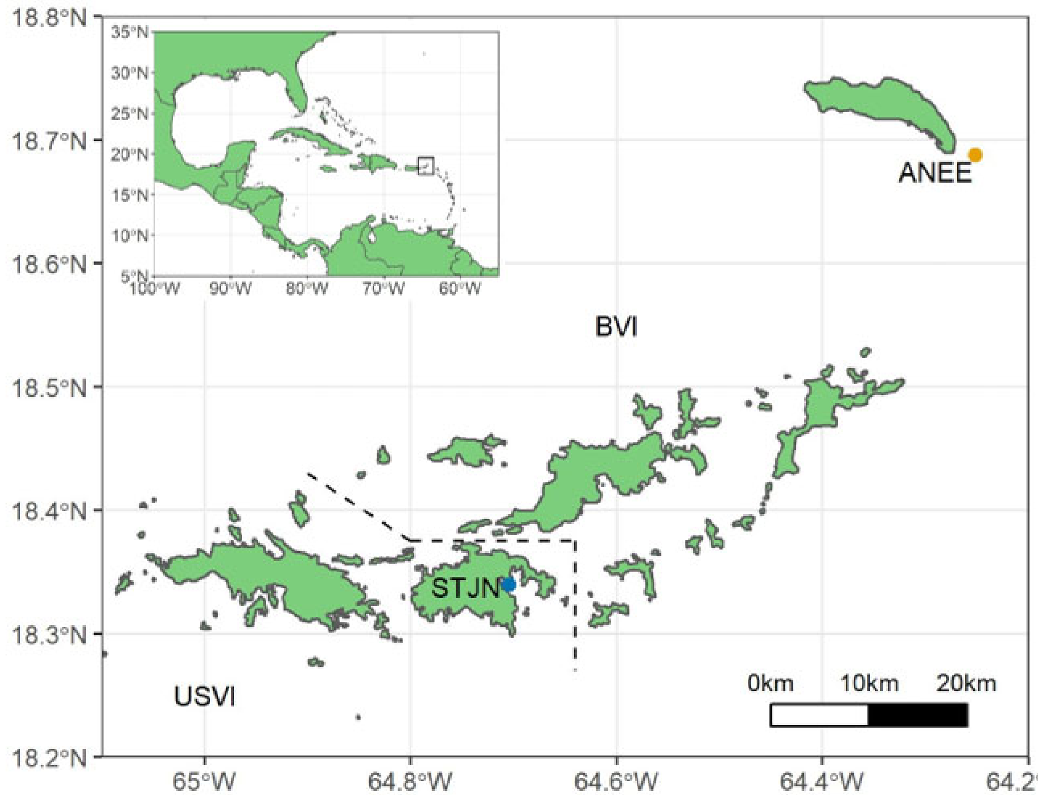

Figure 2. Locations of two water monitoring stations in Coral Bay on St. John, USVI (STJN) and on the fringing reef off the east end of Anegada, BVI (ANEE). Inset box outlines the approximate area of the detailed map.

U.S. Virgin Islands (USVI), and Anegada, British Virgin Islands (BVI). These two islands lie within 75 km of each other and experience a similar dry tropical climate regime (Bowden et al., 1970), so that any differences in seawater Sr/Ca between these two sites could be attributed to more local processes. Most rainfall generated between May and November derives from tropical cyclones, while cold fronts are an important source of precipitation for the rest of the year (Calvesbert, 1970).

St. John is mainly composed of siliciclastic rocks of volcanic origin, with a maximum elevation of 474 m (Donnelly, 1966; Rankin, 2002). It is distinct from our sites in the Florida Keys both geologically (silicate *vs.* carbonate) and hydrographically. The water monitoring station on the east end of St. John (STJN) is situated in Coral Bay, surrounded on three sides by steep terrain. Given its relative size, depth, surrounding topography, and siliciclastic bedrock, it is likely that the major water masses interacting in this coastal zone stem from surface runoff and groundwater discharge on the shore side, and from northwestern tropical Atlantic seawater and Caribbean seawater on the ocean side (Cosner, 1972; Johns et al., 2002).

Anegada is an emergent reef island located on the northeastern edge of the Puerto Rico-Virgin Island carbonate platform. Its area (~54 km^2) is nearly equal to that of St. John (51 km^2), but with a maximum elevation of only 8 m (Martin-Kaye, 1959). Anegada is a carbonate island of Pleistocene origin, like the Florida Keys, but shares hydrographic similarities with St. John as a small island influenced by northwestern tropical Atlantic Ocean water and Caribbean Sea water (Brown & Dunne, 1980; Johns et al., 2002). Lacking steep slopes and consisting of karst terrain, Anegada is not likely subject to strong influences of terrestrial runoff. Given the relative age of the sediments

(Pleistocene) and the maximum predicted thickness of the freshwater lens on Anegada prior to any drawdown via human consumption (~30 m; Budd & Vacher, 1991), it is likely that groundwater interactions on the reef are predominantly through tidal pumping of seawater (Mather, 1988; Robins, 2012). The water monitoring station near Anegada (ANEE) is located on the eastern edge of the fringing reef, ~2 km from shore and well-flushed by open-ocean currents.

2.2 Continuous Water Sampling via OsmoSampler

Historically, most temporal studies of seawater chemistry have been limited by the length and number of expeditions. The development of osmotically driven water pumps, or OsmoSamplers (Jannasch et al., 2004) has provided a reliable means of continuous autonomous sample collection. These battery-free pumps collect water samples for months or even years at a time with minimal maintenance, utilizing a strong salinity gradient between deionized (Milli-Q, 18MΩ) water and a saturated sodium chloride solution separated by one or more semi-permeable membranes in parallel. Osmosis drives Milli-Q water through the semi-permeable membrane into the brine reservoir, from which excess fluid is then expelled to the outside. Saturation is maintained in the brine reservoir by an excess of solid NaCl.

A long coil of Teflon® tubing filled with Milli-Q water is connected to the Milli-Q reservoir of the pump. The open end of the Teflon® tubing acts as an inlet for seawater as Milli-Q water is pulled through the tubing across the semi-permeable membrane. A Rhizon, a hydrophilic microporous filter typically used in sampling porewater (Seeberg-Elverfeldt et al., 2005), was not placed on the end of the tubing (Gelesh et al., 2016) in order to prevent possible contamination from the filter itself.

The rate of pumping, which is slightly modified by ambient temperature, is used to calculate an age model by relating the volume of sample collected in the tubing to the total deployment time (see Ch. 3). The small diameter of the Teflon® tubing (~0.2 mm) minimizes diffusion, ensuring that the collected sample can be subdivided with weekly or even daily resolution, depending on the required aliquot size (Jannasch et al., 2004).

The OsmoSamplers used in the Florida Keys (OS1 – OS4) were deployed for 3 years and serviced every 6 months. The OsmoSamplers used in the Virgin Islands were deployed for two years (STJN) and for one year (ANEE), continuously without servicing. Each OsmoSampler was accompanied by an Onset HOBO© temperature logger, which recorded *in situ* temperature every two hours. During servicing in the Florida Keys, OsmoSamplers were retrieved from the seafloor, separated from the Teflon® coil cartridge, cleaned, refilled with brine and Milli-Q water, and redeployed with a new Teflon® coil cartridge within 24 hours. These new cartridges were prepared using a peristaltic pump to fill them with 2% nitric acid, after which they soaked for 2-3 weeks before they were thoroughly rinsed and filled with Milli-Q water. Teflon® coil cartridges containing seawater sample were immediately capped at both ends, and returned to Chesapeake Biological Laboratory (CBL) for analysis.

Upon return to CBL, the Teflon® coil cartridges were stored at room temperature until subsampling within a week of recovery. Prior to subsampling, the Teflon® coil cartridges were scrubbed to remove organic matter and/or sediment from the outer surface. Subsampling was conducted using a clean work area, nitrile gloves, and a lab bench covered with Kimwipes® to minimize contamination. The Teflon® coil was unspooled while cutting it into ~5-m sections, transferring the contents of each section into 7-mL polypropylene snap-cap tubes (Argos Technologies, part number T2076S-CA). A 750-µL aliquot was pipetted from each sample tube into an airtight glass vial (Specialty Bottle, 1/6-dram perfume sampler) with minimal headspace for $\delta^{18}O$ analysis. An additional 100-µL aliquot was pipetted from the first sample and every fifth sample after that for salinity measurement by handheld refractometer. The start of the first sample was indicated by zero salinity (Milli-Q water). For the preceding sample, usually comprising a mixture of seawater and Milli-Q water, the primary sample was retained, but the $\delta^{18}O$ aliquot was not. All samples were stored in a dark refrigerator (4°C) until analysis for Sr/Ca and $\delta^{18}O$ using ICP-AES and Isotope Ratio Mass Spectrometry (IRMS), respectively.

The length of each section was chosen to contain a nominal sample volume of about 5 mL, corresponding to an average collection time of ~8 days, to minimize the potential impact of tidal fluctuations on the results. The ~5-mL samples provided sufficient volume for replicate analysis and minimized potential sample storage artifacts due to evaporation or contamination. Part of the OS1 Teflon® coil from the winter 2018 collection from the Florida Keys was cut into smaller sections (~680 µL aliquots) to capture daily changes in seawater chemistry during Hurricane Irma's passage over the Florida Keys. These high-resolution samples (~26 hours/aliquot) were not stored, but analyzed immediately.

2.3 ICP-AES Analysis

Seawater samples were analyzed for Sr/Ca with a Perkin Elmer Optima 8300DV ICP-AES using the method developed by Khare (2018). This method was based on the coral Sr/Ca method originally developed by Schrag (1999) and modified by de Villiers et al. (2002). Samples were measured for Sr/Ca intensity ratios (Sr 421.552 nm, Ca 422.673 nm) and converted to Sr/Ca concentration ratios. After the five calibration standards, which were analyzed first, each run comprised five repetitions of a block consisting of 33 seawater samples, two in-house standards, two external reference materials, five quality control standards (an in-house standard treated as a sample), and a non-matrix-matched blank (70% trace-metal-grade nitric acid diluted to 2% using Milli-Q water). The latter was used to correct the raw intensity of each sample measured within the same block.

In accordance with Schrag (1999), a single in-house standard (Gulf of Mexico – GoM) was measured before and after each sample. A correction factor for each sample was then calculated by averaging the two bracketing GoM solutions and normalizing the mean to its known value measured independently via Inductively Coupled Plasma Mass Spectrometry (ICP-MS). A single value for each sample was reported by calculating the average of the five replicate GoM-corrected measurements in each block. This GoM correction (hereafter termed a Schrag correction) adjusts for instrumental drift over the course of each 6-11 hour run. Suppression of instrumental variability and drift by means of the Schrag correction facilitates identification of subtle natural variability in the seawater Sr/Ca ratio.

Some changes were made to the instrument configuration during the analysis of our samples. The first twelve ICP-AES sample runs were as described by Khare (2018). For the last ten runs, a non-baffled spray chamber was replaced with a baffled spray-chamber to prevent sample build-up at the base of the injector. This sample build-up is intermittently injected into the plasma, creating an anomalous ‘glitch’ in plasma conditions. These glitches would occasionally extinguish the plasma and appeared to be the primary source of analytical outliers throughout this study. Using a baffled spray chamber not only remedied the plasma instability, but also improved analytical precision by a number of metrics (Table 1). Other method parameter adjustments included (a) increasing carrier gas flow rate from 0.6 to 0.7 L/min, and (b) adjusting the torch mount position from –3.0 mm to –4.5 mm. Both modifications yielded better sensitivity and precision for the analytes of interest.

Table 1. Comparison of analytical precision for two ICP-AES procedures used in this study. Improvements in the modified method can largely be attributed to using a baffled spray chamber.

Analytical Metric	**Initial Method (First 12 Runs) (Khare 2018)**	**Modified Method (Last 10 Runs)**
GoM RSD	0.12%	0.09%
GoM Short-term RSD	0.08%	0.05%
CASS-5 RSD	0.23%	0.09%
CASS-6 RSD	0.17%	0.09%
GoM SPLIT RSD	0.10%	0.07%

In addition to the optimized configuration, certain sample introduction parameters were also modified from Khare (2018) to reduce run time from ~10.5 hours to ~6.5 hours. A rapid sample introduction protocol, or "flush", was implemented to speed up introduction of sample into the plasma. Pump speed was increased to 4.5 mL/min until sample was aspirating in the plasma for 1-2 seconds, at which point pump speed was reduced to 1.5 mL/min. Spectrometer readings were then delayed by 15 seconds to allow the plasma to stabilize after the flush. Between samples, the sample introduction system is rinsed with 2% nitric acid to prevent cross-contamination. This "wash" protocol was modified by reducing the wash time from 30 seconds to 10 seconds, and increasing the wash pump speed from 1.5 mL/min to 3.0 mL/min.

Seawater samples were diluted 1:100 using 2% trace metal grade nitric acid to minimize seawater matrix effects and maintain an adequate balance of instrument sensitivity and precision. Calibration solutions contained concentrations of Ca, Na, and Mg equal to seawater concentrations diluted 1:100, to match the matrix of our samples and reduce matrix effects (Olesik, 1991). Strontium concentrations in the calibration solutions were varied to obtain a range of Sr/Ca ratios, from 0 mmol/mol (matrix-matched blank) to ~17 mmol/mol, approximately twice the value of seawater. The matrix-matched blank was used to correct the other four calibration standards, and a calibration line was produced by performing a linear regression between the Sr 421 / Ca 422 intensity ratio and the calculated Sr/Ca concentration ratio of each standard. Calibration standards were measured gravimetrically using certified reference materials of Sr (PerkinElmer® 1,000 mg/L), Ca (Inorganic Ventures® 10,000 mg/L), Mg (PerkinElmer® 1,000 mg/L), and Na (SPEX CertiPrep® 10,000 mg/L).

Four reference materials were used in this study. No certified seawater reference standard exists for either Sr or Ca. Therefore, a large batch of aged and filtered seawater collected at 400 m depth in the Gulf of Mexico was used as an in-house reference standard (GoM) and measured externally by ICP-MS using standard addition. The three other reference standards used in this study were: a 125-mL aliquot of GoM stored separately from the in-house standard (GoM SPLIT), and two additional coastal seawater reference materials, not certified for Sr and Ca, supplied by the National Research Council of Canada (CASS-5 and CASS-6).

The average relative standard deviation (RSD) was 0.20% (< 0.02 mmol/mol), indicating that the Schrag correction accounted well for instrumental drift. Average RSD was calculated from the five replicate Sr/Ca ratio measurements made for each sample in a single run. Direct measurements of the Sr/Ca ratio in each sample (rather than individual measurements of Sr and Ca concentrations) precludes the issue of error propagation (de Villiers et al., 2002). Mean Sr/Ca, standard deviations (1σ), and RSDs for the various standards are listed in Table 2, demonstrating the long-term precision of this study across all runs. Average short-term precision for our samples (RSD of the five quality control standards within a single run) was 0.07%. Out of 521 seawater samples reported in this study, 93 were run 2-4 times on separate days. The average long-term precision for these samples was 0.12%.

Table 2. Mean and standard deviation of seawater reference materials (CASS-5 and CASS-6) and in-house standards (GoM and GoM SPLIT). Percent relative standard deviation is abbreviated % RSD. Data from standards provide a measure of the ICP-AES method analytical performance.

	Long-term (22 Runs)	
Standard	**Mean Sr/Ca (mmol/mol)**	**% RSD**
GoM Reference Material	8.69 ± 0.01 (n = 110)	0.11%
CASS-5	8.74 ± 0.02 (n = 22)	0.18%
CASS-6	8.73 ± 0.01 (n = 22)	0.13%
GoM SPLIT	8.70 ± 0.01 (n = 16)	0.08%

2.4 Supporting Data

A subset of the seawater samples was analyzed for $\delta^{18}O$ values using a ThermoFisher DeltaPlus XL stable isotope mass spectrometer at CBL. The methodology is based upon the carbon dioxide equilibration method first described by Epstein and Mayeda (1953). Briefly, tank gas with a known CO_2 isotopic composition is injected into the vial head-space with high-purity helium, with sufficient flushing to remove all other gas. Following equilibration of the water sample with the tank gas at 25°C, an aliquot of the gas is removed, and any water in it is removed by a ThermoFisher GasBench preparation device and transferred to a Thermo Delta Plus mass spectrometer for mass spectrometric measurement of the ^{18}O / ^{16}O ratio of the water samples. Results are reported in delta notation (δ, ‰) relative to the international reference standard Vienna Standard Mean Ocean Water (V-SMOW; Coplen, 1996).

$$\delta^{18}O = \left(\frac{\left(\frac{^{18}O}{^{16}O}\right)_{sample}}{\left(\frac{^{18}O}{^{16}O}\right)_{standard}} - 1 \right) * 1000\ ‰ \quad (4)$$

Long-term precision for $\delta^{18}O$ analysis in the CBL isotope laboratory is < 0.1‰ (Cooper et al., 2016).

Strontium concentrations ([Sr]) were calculated for nearly all samples for comparative analysis (see Ch. 4). This was made possible by the fact that the five ratio calibration standards also constitute a concentration calibration line for Sr, but not for Ca. Since the Schrag correction that is applied to our intensity ratios cannot be used for concentration data, only measurements made from the first block of each run were considered for analysis in order to minimize the effect instrumental drift. The standard deviation associated with the [Sr] measurements is 0.003 mM (3.29% RSD), based on the five quality control standards measured over all 22 runs.

Salinity and meteorological data (rainfall and barometric pressure) from environmental monitoring programs were also used in this study for comparison with our results. Satellite-derived sea surface salinity measurements from the Caribbean were acquired through NOAA Coastwatch from the MIRAS SMOS satellite mission (Kerr et al., 2010; Mecklenburg et al., 2012). Discrete rainfall data for St. John were acquired through the Community Collaborative Rain, Hail, and Snow Network (Reges et al., 2016). Discrete barometric pressure data from St. John were obtained from the National Data Buoy Center (NDBC; Hamilton, 1986)

Chapter 3: Results

3.1 Age Models

Temperature-corrected age models are often implemented with OsmoSampler data (Gelesh et al., 2016; Wheat et al., 2011), but they are known to be less reliable in environments with substantial temperature variations such as estuaries or the surface ocean (Jannasch et al., 2004). Therefore, a 'non-temperature-corrected' age model was constructed for each OsmoSampler deployment by relating the total volume of sample to the number of days deployed. The first and last samples of each deployment were constrained by the deployment and recovery dates of each OsmoSampler. Daily OsmoSampler pumping rates were calculated for each deployment by dividing the total volume of seawater in the Teflon® coil by the total number of deployment days. Time was determined for each sample by multiplying the volume of that sample by the calculated pumping rate specific to each OsmoSampler deployment. This accounts for changes in volume between samples caused by the occasional presence of gas pockets inside the Teflon® coil. If gas comprised a substantial fraction of the sample volume, age model uncertainty was considered higher for that deployment. Most tubing recovered did not contain gas pockets.

For comparative purposes, both a non-temperature-corrected and a temperature-corrected age model were applied to the OS1 deployment that pumped during Hurricane Irma's passage over Florida Bay. The temperature-corrected model placed the geochemical signal of the event 13 days before the actual September 10th event, whereas the non-temperature-corrected model placed the signal closer, September 2nd. Hurricane Irma's date offset indicates an age-model uncertainty that is on the order of days for most samples.

A potential source of uncertainty in the age models could be the treatment of gas pockets found in the lines. Gas pockets in the submerged pre-filled pump tubing typically occurred in tubing that contained small plugs of sediment or were visibly pinched during deployment. Such blockages in the Teflon® coil likely cause cavitation and gas pockets. Treating these simply as 'displaced water' only accounts for changes in volume between samples, and may not accurately capture evident fluctuations in pumping rates associated with their formation.

The age model for the STJN OsmoSampler was the only one constructed differently from all others. This was because the STJN OsmoSampler was deployed in March 2017, but could not be recovered until January 2019 due to adverse weather conditions. By then, seawater had been drawn through the coil into the Milli-Q reservoir (MR) of the pump, indicated by a refractometer-based salinity measurement in the MR of 77 ± 5. As a result, the first samples were lost and could not be tied to the deployment date in an age model. Instead, the amount of seawater drawn into the pump and the average pumping rate provided enough information to calculate an estimated start date. A key assumption is that the change in pumping rate due to the change in salinity of the MR is negligible.

The total volume of seawater drawn into the pump was calculated by the following equation:

$$V_X = \left(\frac{S_{mr}}{S_{sw}}\right) * V_{mr} \tag{5}$$

In equation 5, S_{mr} is the salinity of the MR (77), S_{sw} is the salinity of seawater (35), and V_{mr} is the volume of the MR (138 mL). This equation yields a volume of seawater taken into the MR (V_x) of 303.6 mL. The sample coil from the STJN OsmoSampler contained 340.5 mL of seawater. Adding the volume of seawater in the coil to the volume of seawater in the MR yields a total sample volume of 644.1 mL collected over 691 days, yielding an average pumping rate of 6.5 mL/week. Dividing the total volume of sample in the coil (340.5 mL) by this pumping rate yields the collection time represented by the sample coil (366 days). Given the assumptions and uncertainty of the salinity measurement, age model uncertainty for the STJN OsmoSampler is estimated to be on the order of weeks to months.

3.2 Temporal Variability of Seawater Sr/Ca in the Tropical Western Atlantic

A total of 521 seawater samples were collected from the six water monitoring stations across the Florida Keys and Virgin Islands. Four OsmoSamplers in the Florida Keys (OS1 – OS4) were deployed from 9/21/2016 to late summer of 2020. Only collections up to 8/13/2019 are presented here. OsmoSamplers OS1 – OS4 were recovered and redeployed semi-annually, comprising six deployments in total throughout the study period. The Sr/Ca data at each station exhibit good continuity across deployments, with smooth transitions from the last sample of one deployment to the first sample of the next deployment (Figure 3). Seawater samples from the Virgin Islands were collected in a single deployment for each OsmoSampler. The OsmoSampler in Anegada, BVI (ANEE) was deployed between 1/20/2018 and 2/10/2019. The OsmoSampler in St. John, USVI (STJN) was deployed from 3/16/2017 to 2/5/2019. Adverse weather conditions prevented service in January 2018. Samples prior to 2/4/2018 were lost, as explained in Section 3.1.

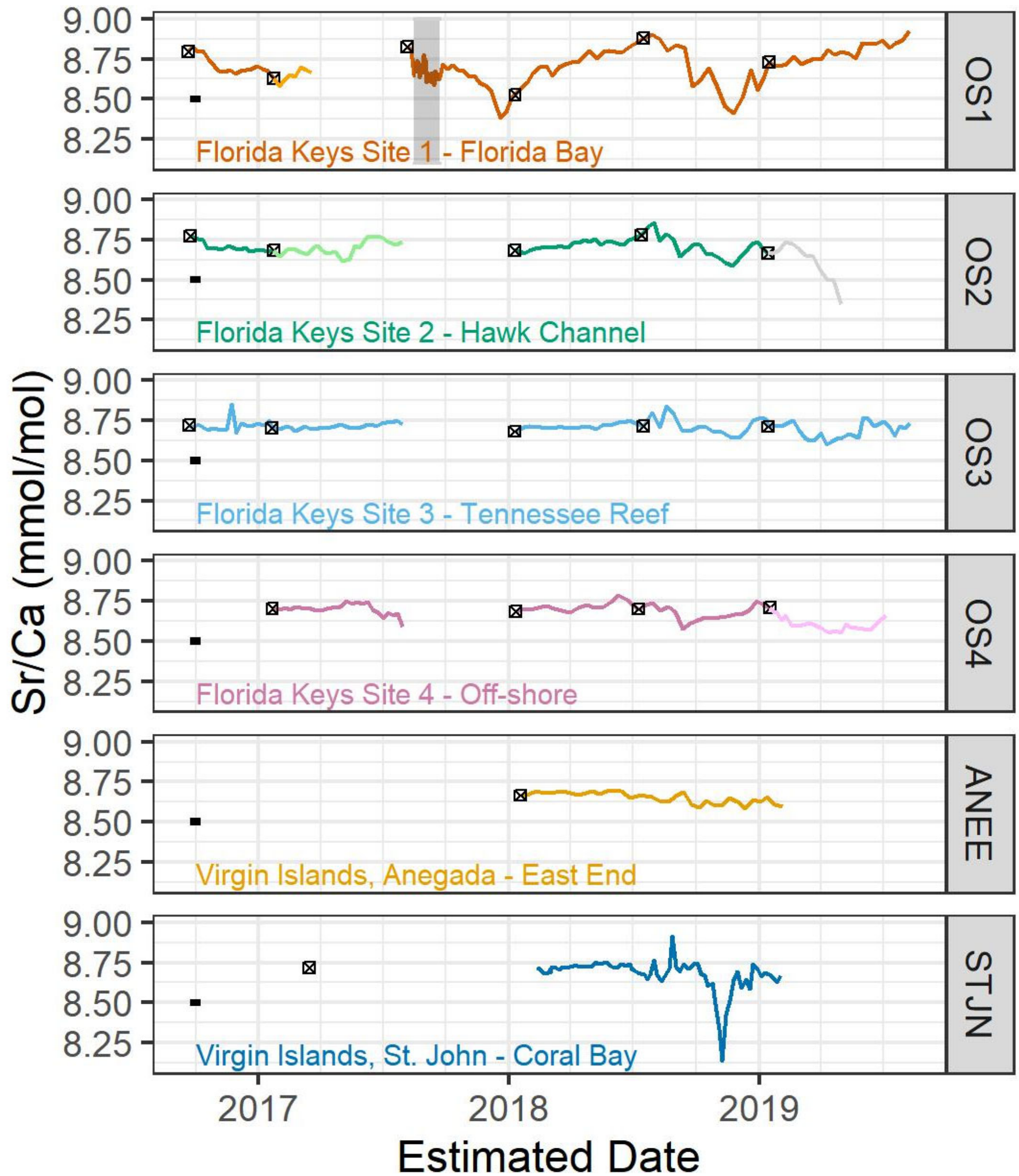

Figure 3. Seawater Sr/Ca from six water monitoring stations in the Florida Keys and Virgin Islands. Black error bars at the beginning of the time series represent analytical uncertainty (0.01 mmol/mol, 1σ). Crossed boxes indicate when deployment periods begin. ANEE and STJN constitute a single deployment. Light portions of the time series indicate where there is less confidence in the age model. Gray portions indicate where data were not considered in the discussion. Note the high degree of seasonality at OS1 and, to a lesser extent, OS2.

The mean, standard deviation, and range of seawater Sr/Ca at each site are reported in Table 3. All errors are reported as 1σ of the mean. Across all sites, mean seawater Sr/Ca was 8.69 ± 0.07 mmol/mol. This is statistically equivalent to our GoM standard. Deployments where substantial gas pockets were present and/or calculated pumping rates were anomalously low are represented by lighter colors in Figure 3, indicating increased age model uncertainty. Data missing from OS2 – OS4 in the final months of 2017 are due to Hurricane Irma storm damage.

Table 3. Summary statistics of seawater Sr/Ca collected via OsmoSampler. Mean, standard deviation, and range are in units of mmol/mol. Mean seawater Sr/Ca is similar across sites, but standard deviation and range vary significantly. *Samples from STJN estimated to be pumped between Oct. 24th and Nov. 25th 2018 were removed from this dataset.

OsmoSampler	Site Names	n	Mean	Std. Dev.	Range
OS1	Florida Bay	137	8.69	0.10	0.54
OS2	Hawk Channel	83	8.71	0.05	0.26
OS3	Tennessee Reef	111	8.71	0.04	0.25
OS4	FKRT Forereef	81	8.68	0.05	0.23
ANEE	Anegada, BVI	36	8.65	0.03	0.10
STJN (no excursion) *	St. John, USVI	68	8.70	0.05	0.33
STJN (with excursion)	St. John, USVI	73	8.68	0.10	0.78
GoM (in-house standard)	Gulf of Mexico	110	8.69	0.01	0.12

3.3 Temporal Variability of Seawater Sr/Ca in the Florida Keys

The average sampling resolution at OS1 was ~9 days except from mid-August to late-September, 2017, when the sample coil was cut into shorter sections and sampling resolution was increased to ~26 hours (see Ch. 2). When the OsmoSampler was serviced on 8/2/2017, the exposed Teflon® tubing connecting the pump to the sample coil was found severed and pinched, indicating that sample collection had ceased sometime after the most recent deployment date (1/20/2017), possibly caused by fish biting the exposed Teflon® tubing. Compared to the average pumping rate of the OS1 OsmoSampler across all deployments (4.4 ± 0.8 mL/week), this deployment's calculated average pumping rate was anomalously low (1.6 mL/week). Therefore, an estimated correction was made for samples during this deployment period by adjusting the pumping rate to match the previous deployment. Using this *ad hoc* correction, sample collection was estimated to have ceased after 3/23/2017, until it was resumed following servicing on 8/2/2017. The data support this rough estimation by showing good continuity in the first and poor continuity in the last sample of this deployment. Tube damage by fish was avoided in future deployments with the addition of protective casing coiled around the exposed tubing. Mean seawater Sr/Ca at OS1 was 8.69 ± 0.10 mmol/mol, with minimum and maximum values observed in December 2017 (8.38 mmol/mol) and August 2019 (8.92 mmol/mol), respectively. Despite the uncertainty in absolute dates of the collections, a clear annual cycle is evident in the overall record between winter minima (Jan. 2017, Dec. 2017, Dec. 2018) and summer maxima (Sep. 2016, Jul. 2017, Jul. 2018, Aug. 2019); the winter minimum is conspicuously smaller in Jan. 2017.

The average sampling resolution at OS2 was ~8 days. Age model uncertainty was higher for samples collected between 1/20/2017 and 8/2/2017 due to the presence of significant gas pockets throughout the sample coil, potentially caused by a small sediment plug observed at the sample intake during retrieval. Samples collected between 1/14/2019 and 8/13/2019 (indicated as gray in Figure 3) were preceded by a large, ~20 cm plug of sediment in the Teflon® coil. Sample volume was anomalously low during this deployment; hence these samples were excluded from the analysis.

Mean seawater Sr/Ca at OS2 (excluding the final deployment) was 8.71 ± 0.05 mmol/mol, with minimum and maximum values observed in November 2018 (8.59 mmol/mol) and July 2018 (8.85 mmol/mol). Winter minima (May 2017, Nov. 2018) and summer maxima (Sep. 2016, Jun. 2017, Jul. 2018) were present at OS2, albeit less pronounced than at OS1.

The average sampling resolution at OS3 was ~8 days. No apparent issues with blockages, gas pockets, or pumping rates were observed throughout the study period. Mean seawater Sr/Ca at OS3 was 8.71 ± 0.04 mmol/mol, with minimum and maximum values observed in April 2019 (8.60 mmol/mol) and November 2016 (8.85 mmol/mol). Unlike OS1 and OS2, there is no apparent annual cycle at OS3, potentially due to its position further offshore. Positive excursions from the mean appear random both in magnitude and timing, while negative excursions (appearing later in the time series) lasted as long as 12 weeks.

The average sampling resolution at OS4 was ~9 days. The OsmoSampler malfunctioned in the first deployment and no sample was collected between 9/21/2016 and 1/19/2017. Age model uncertainty was higher for samples collected between 1/14/2019 and 8/13/2019, where sediment was found at the sample intake and significant gas pockets were present throughout the sample coil. Mean seawater Sr/Ca at OS4 was 8.68 ± 0.05 mmol/mol, with minimum and maximum values observed in April 2019 (8.55 mmol/mol) and June 2018 (8.78 mmol/mol). Seawater Sr/Ca variability at OS4 exhibited small but significant positive and negative excursions about the mean that typically last multiple weeks. However, like OS3, there was little evidence for an annual cycle, again potentially due to its greater distance from the shore.

Significant inter-site differences in seawater Sr/Ca distributions were observed throughout the study period (Figure 4). Variance comparisons using Levene's Test for

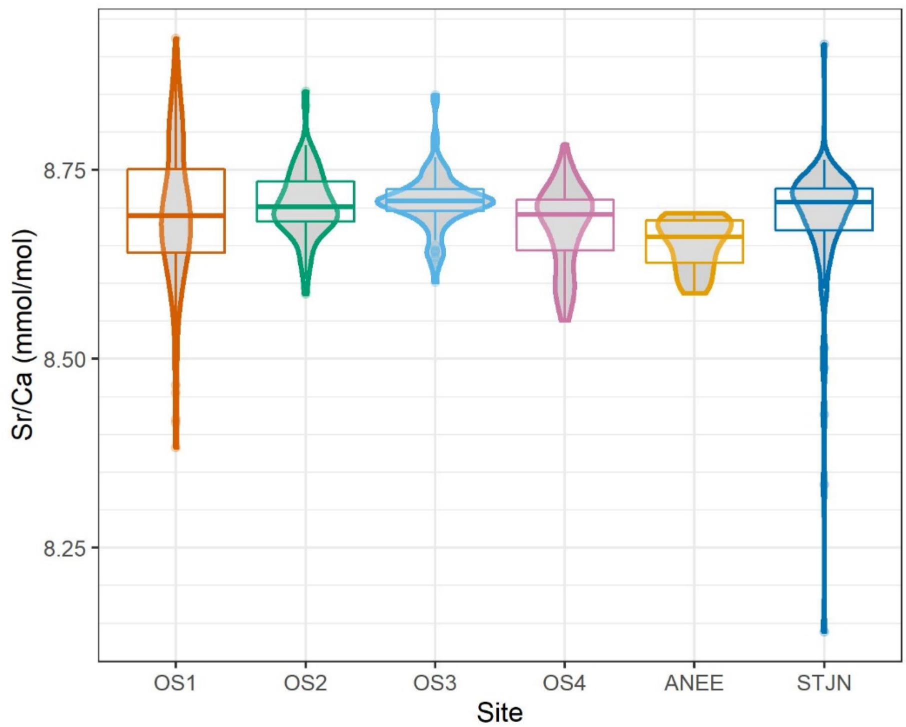

Figure 4. A bean-box hybrid plot of seawater Sr/Ca at all sites. The gray area behind each boxplot represents the probability density curve of the distribution of seawater Sr/Ca ratios at each site. The bold horizontal lines indicate the median at each site. An Anderson-Darling test for normality (e.g., Thode, 2002) indicates a relatively normal distribution of the data at OS1 and OS2 ($p > 0.05$), where an annual cycle is evident.

Homogeneity of Variance (Levene, 1960) demonstrates that OS1 is the only site in the Florida Keys with a statistically different variance, exhibiting the highest range and standard deviation ($p < 0.001$). Site OS2 exhibits the second highest range among the Florida Keys sites, and its maximum and minimum seawater Sr/Ca values coincide with the summer 2018 maximum and winter 2018 minimum observed at OS1. Site OS3 has the smallest standard deviation out of all Florida Keys sites in this study, exhibiting a near-constant seawater Sr/Ca value from September 2017 until July 2018. The mean at OS4 is significantly different from both OS2 and OS3 (Wilcoxon Rank Sum Test, $p < 0.05$), and OS4 has the smallest range out of all sites in the Florida Keys.

3.4 Temporal Variability of Seawater Sr/Ca in the Virgin Islands

The average sampling resolution at ANEE was ~11 days. Three soft plugs, possibly composed of organic matter, were observed in the sample coil, and nearly every sample contained small gas pockets. Mean seawater Sr/Ca at ANEE is 8.65 ± 0.03 mmol/mol, with minimum and maximum values observed in December 2018 (8.57 mmol/mol) and February 2018 (8.71 mmol/mol). Seawater Sr/Ca appears relatively constant at this site from February 2018 until June 2018, after which the mean decreases and the standard deviation (i.e., variance) increases from 8.68 ± 0.01 mmol/mol to 8.63 ± 0.03 mmol/mol.

The average sampling resolution at STJN was ~5 days, the highest sampling resolution (i.e., fastest pumping rate) for all OsmoSamplers during the study period. Similar to ANEE, small gas pockets were present in nearly every sample, and one small sediment plug was removed from the sample coil. Mean seawater Sr/Ca at STJN is 8.68 ± 0.10 mmol/mol, with minimum and maximum values observed in November 2018 (8.14 mmol/mol) and August 2018 (8.92 mmol/mol). The large range and variance in seawater Sr/Ca at this site was due to a pronounced negative excursion in October and November 2018. Excluding this single excursion, mean seawater Sr/Ca at STJN is 8.70 ± 0.05 mmol/mol, with a maximum range of 0.33 mmol/mol. Also similar to ANEE, seawater Sr/Ca is relatively stable at STJN from February 2018 to June 2018, after which mean and variance shift from 8.72 ± 0.02 mmol/mol to 8.65 ± 0.12 mmol/mol including the excursion, and 8.69 ± 0.06 mmol/mol excluding the excursion.

Seawater Sr/Ca at both ANEE and STJN exhibited a decreased mean and increased variance after June 2018. It is beyond the scope of this study to determine if the decreased mean ratio and variance is persistent or an annual variation due to the relatively short time series recovered from this location (~1 year) relative to the FLKS OsmoSamplers (~3 years). However, no excursions of this magnitude were observed at any of the other sites. Even excluding the large negative excursion, variations at STJN are larger than at ANEE.

3.5 Seawater Sr/Ca and $\delta^{18}O$

Out of 521 seawater samples collected for Sr/Ca measurements, 155 were also analyzed for $\delta^{18}O$. A summary of these data is provided in Table 4. Samples from OS1, OS4, and ANEE were selected for $\delta^{18}O$ analysis to enable comparisons with other hydrographic data. Additional samples from OS1 were analyzed to document impacts of Hurricane Irma in Florida Bay in 2017.

Table 4. Summary statistics of seawater $\delta^{18}O$ at our OS1, OS4, and ANEE sites. Note the similarities at OS4 and ANEE compared to OS1, particularly with respect to standard deviation and range. Mean, standard deviation and range in ‰ relative to Vienna Standard Mean Ocean Water (V-SMOW).

Site	n	Mean	Std. Dev.	Range	Start Date	End Date
OS1 (Florida Bay)	89	0.8	0.7	2.4	2017-08-11	2019-01-08
OS4 (FKRT Forereef)	31	0.8	0.1	0.3	2018-01-20	2019-01-07
ANEE (Anegada, BVI)	35	0.7	0.2	0.8	2018-01-26	2019-02-04

Seawater $\delta^{18}O$ at OS1 and OS4 shows a weak but significant correlation with seawater Sr/Ca that seems to be primarily driven by seasonal changes (OS1: $r^2 = 0.27$, $N = 89$, $p < 0.001$; OS4: $r^2 = 0.32$, $N = 31$, $p = 0.001$) (Figure 5). However, the time series is short and provides for only limited quantitative analysis for separating annual from higher frequency variability. At OS1, the minimum seawater $\delta^{18}O$ value is observed in September 2017 (–0.5‰), concurrent with the arrival of Hurricane Irma, while the maximum value is observed in April 2018 (+2.0‰), which is earlier in the year than one would expect evaporation to exceed precipitation in this region (Stabenau & Kotun, 2012; Swart & Price, 2002). At OS4, the minimum $\delta^{18}O$ value is observed in September 2018 (+0.6‰), while the maximum value is observed in May 2018 (+0.9‰). Like seawater Sr/Ca, the range and variance of seawater $\delta^{18}O$ at OS1 is significantly larger than at OS4, likely due to the greater impacts of evaporation and runoff in Florida Bay at OS1 relative to OS4. Maximum and minimum values of Sr/Ca and $\delta^{18}O$ at each site are not coincident, except at OS4 in September 2018.

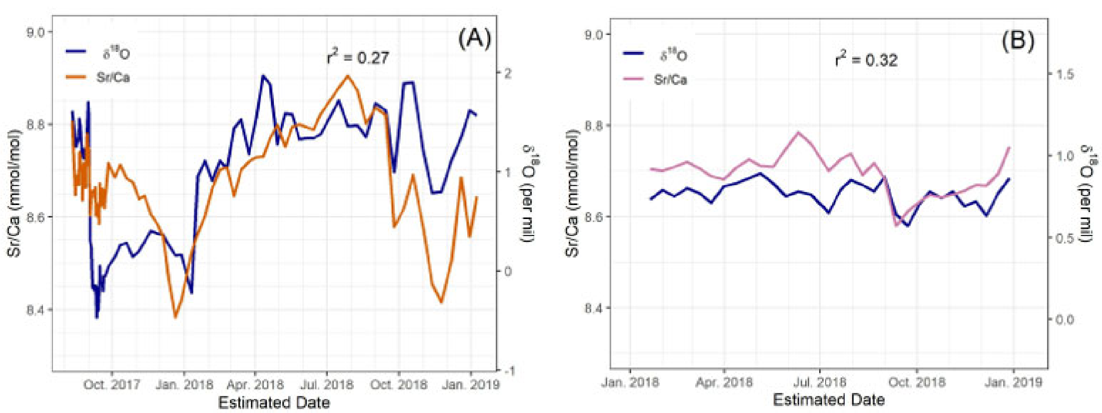

Figure 5. Time Series of Sr/Ca and $\delta^{18}O$ at OS1 (A) and OS4 (B). Absolute analytical error for $\delta^{18}O$ is 0.1‰. Correlation coefficients were calculated using a Pearson correlation test ($p \leq 0.001$). Seawater Sr/Ca and $\delta^{18}O$ are moderately correlated at both sites despite differences in local hydrography.

Seawater δ^{18}O at ANEE shows the weakest correlation with seawater Sr/Ca out of all sites ($r^2 = 0.18$, n = 35, p = 0.01) (Figure 6). This is likely because absolute analytical error (0.1‰) is large relative to sample variability. However, unlike OS1 and OS4, minimum and maximum values of seawater Sr/Ca and δ^{18}O are nearly coincident, indicating that both could be phase-locked to the seasonal cycle of salinity. The maximum δ^{18}O value is observed in April 2018, while the minimum value is observed in November 2018. Student's t-test shows that mean seawater δ^{18}O before and after June 2018 are statistically different (0.8 *vs.* 0.7‰, p = 0.01), while Levene's test indicates no significant change in variance (0.2 *vs.* 0.2‰, p = 0.93).

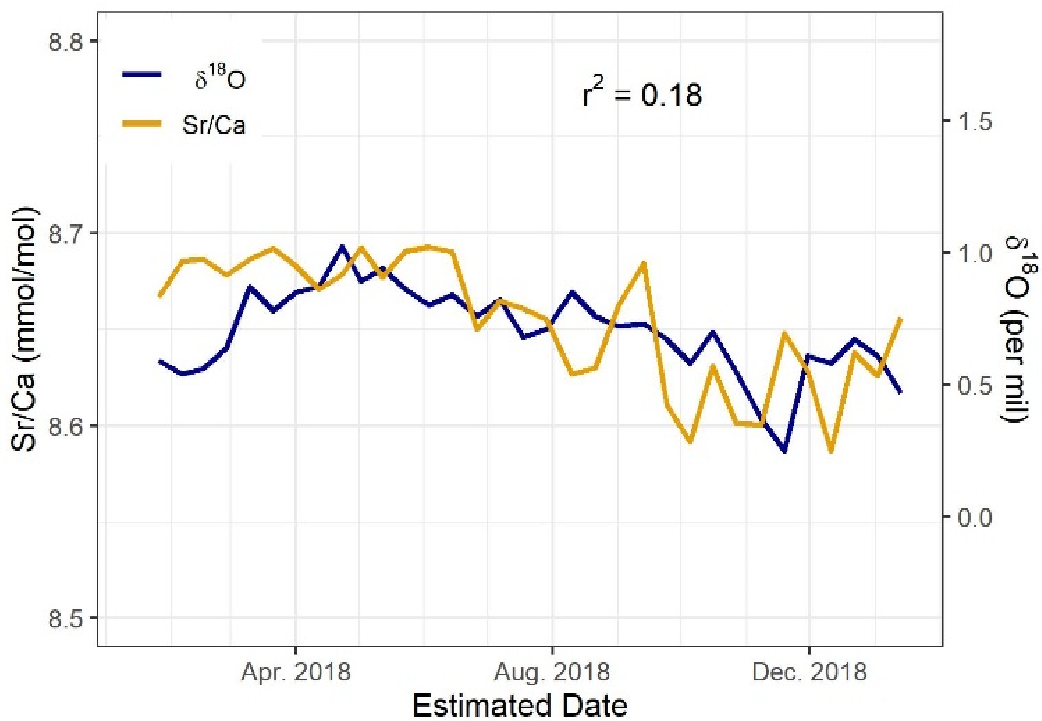

Figure 5. Time series of seawater Sr/Ca and δ^{18}O data from the ANEE OsmoSampler. The Sr/Ca – δ^{18}O relationship is significant, but substantially weaker than in the Florida Keys (p = 0.01).

3.6 Seawater Sr/Ca and [Sr]

Strontium concentrations ([Sr], in mM) were calculated for 96 of the 137 seawater samples collected from OS1 to compare seawater Sr/Ca at this site with a conservative tracer (Figure 7). The samples collected at daily resolution in August and

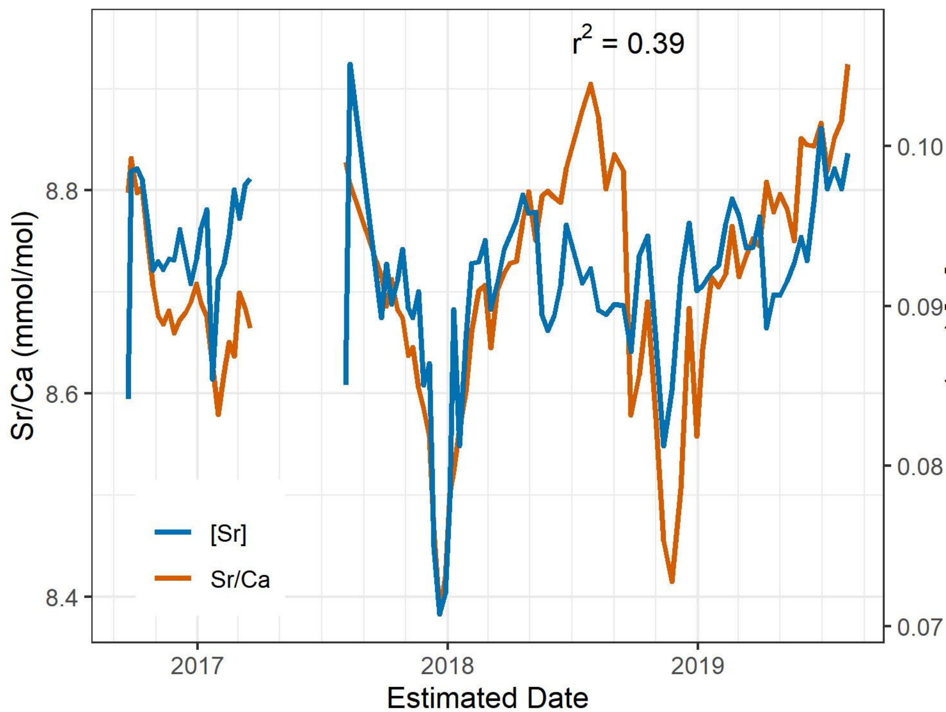

Figure 6. Time series of seawater Sr/Ca and [Sr] at OS1. Analytical error for [Sr] is 0.003 mM. Correlation coefficients were calculated using a Pearson correlation test. Seawater Sr/Ca and [Sr] are modestly correlated at OS1, and typically exhibit co-occurring summer maxima and winter minima.

September 2017 were excluded from this calculation. Mean seawater [Sr] at OS1 is 0.092 ± 0.006 mM, with the minimum value observed in December 2017 (0.071 mM), coincident with the seawater Sr/Ca minimum. The maximum seawater [Sr] value is observed in August 2017 (0.105 mM), a few weeks prior to the Hurricane Irma event.

Throughout the study period, seawater Sr/Ca and [Sr] exhibit a modest correlation at OS1 ($r^2 = 0.39$, $n = 96$, $p < 0.001$). Summer maxima and winter minima are generally observed in the seawater [Sr] time series except for the summer 2018, when seawater [Sr] does not deviate significantly from the mean. These maxima and minima are consistent with expected periods of maximum and minimum salinity in Florida Bay (Stabenau & Kotun, 2012).

Chapter 4: Discussion

4.1 Seawater Sr/Ca Variability in the Tropical Western Atlantic

This study was designed to determine if seawater Sr/Ca varies in three different Atlantic basin coral reef systems. Continuous *in situ* measurements across these geologically and hydrographically distinct coral reef environments reveal substantial seawater Sr/Ca variability at each of the six water monitoring stations, with significant implications for coral Sr/Ca-based paleothermometry (see Section 4.4). Moreover, while there are similarities among some sites (i.e., an annual cycle), each site exhibits different behavior in seawater Sr/Ca, despite the fact that four of the six sites were within a 12.5 km transect. This is perhaps most clearly demonstrated by OS3 and OS4, which appear to have little in common despite their relative proximity to each other (~ 1.4 km). These observations emphasize the importance of local factors in dictating seawater Sr/Ca variability.

Notwithstanding the importance of these local factors, adjoining landscape geology appears to play a minor role in seawater Sr/Ca variability compared to hydrography. When omitting the one major negative excursion, the mean and variance of seawater Sr/Ca at the STJN site, which is surrounded on three sides by a mountainous island with siliciclastic geology, are statistically similar to all the sites situated on carbonate platforms. Although the deviations at STJN are greater in magnitude and shorter in duration than at other sites, this is likely due to its steeper topography, increasing the likelihood of transient environmental signals resulting from meteorological events.

Unlike geology, local and regional hydrography have a notable influence over seawater Sr/Ca variability. Khare (2018) found that seawater Sr/Ca variability along the middle portion of the FKRT was linked to variability in Florida Bay and hypothesized that it might be seasonal. The Sr/Ca ratio data from the two most inshore sites, OS1 and OS2, confirm that the two summer maxima (September 2016 and July/August 2017) and two winter minima (January 2016 and 2017) observed by Khare (2018) are indicative of an annual cycle. While Khare (2018) reported a Sr/Ca range of ~0.1 mmol/mol near Florida Bay based on semi-annual samples, weekly integrated seawater sampling in the present study yields a more comprehensive record of its true variability.

Seawater Sr/Ca at OS1 and OS2 were binned into monthly values and then averaged over each month for the duration of the study period to obtain a monthly climatological average (Figure 8). At OS1, winter ratio minima typically occur between November and January, while summer maxima consistently occur in July, corresponding to an annual cycle of variation spanning ~0.5 mmol/mol at OS1 and ~0.25 mmol/mol at OS2 over a period of 4-7 months. Given an average coral Sr/Ca – SST calibration slope of 0.04 – 0.08 mmol/mol per ºC, these changes constitute an equivalent apparent SST variability of 3-13˚C over 4-7 months. The shaded regions in Figure 8 also indicate that substantial year-to-year variability in the annual cycle is observed at both OS1 and OS2. Whereas pronounced seasonal extremes are observed at OS1 in the latter two years of the study period, the first year exhibits a conspicuously weaker annual cycle, particularly with respect to the winter ratio minimum. Sample-to-sample variability was also substantial at OS1, with an average absolute difference between consecutive samples of 0.041 ± 0.039 mmol/mol. These weekly variations are on the same order of magnitude as common coral Sr/Ca – SST slopes (0.04 – 0.08 mmol/mol per ºC).

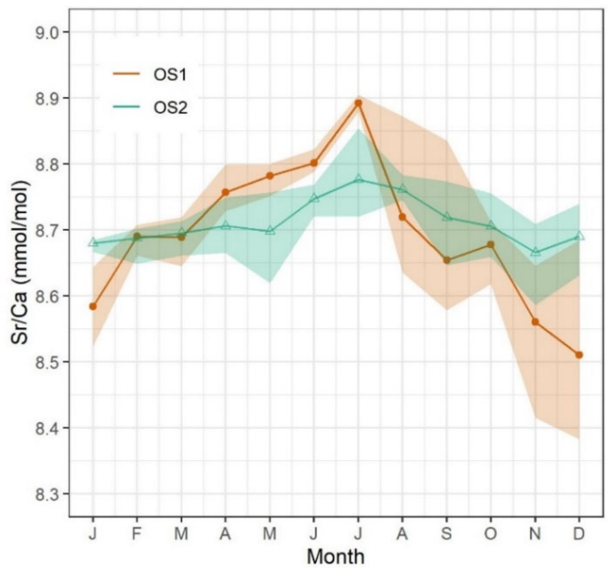

Figure 7. Monthly mean seawater Sr/Ca at OS1 (orange) and OS2 (green) over the study period. The shaded regions around each line indicate the range of ratios observed in that month throughout the three-year study. Note that despite substantial interannual variability, local maxima consistently occur in July. Minima typically occur in November, December, or January.

Unlike at OS1 and OS2, seawater Sr/Ca variability at OS3 and OS4 lacks any clear pattern. Interestingly, OS4 exhibits greater variability than OS3, despite its greater distance from Florida Bay. It is therefore reasonable to expect that seawater Sr/Ca variations at OS3 (0.04 mmol/mol, 1σ) and OS4 (0.05 mmol/mol, 1σ) are influenced both by variability in Florida Bay and by annual and interannual meanders in the Florida Current, which can cause upwelling along the FKRT (Lee et al., 1992, 1994; Leichter et al., 2003). These upwelling events are a potential mechanism of seawater Sr/Ca variability if seawater originates at sufficient depth (de Villiers, 1999). However, analysis of *in situ* temperature and seawater Sr/Ca at OS2, OS3, and OS4 (following the method of Leichter et al., 2003) shows little evidence of upwelling at our sites or any concomitant change in seawater Sr/Ca. Aside from interannual variability, potential reasons are (1) the Tennessee Reef area only rarely experiences high-frequency upwelling (Leichter et al., 2003), or (2) even our most offshore site is too shallow to experience upwelling from a sufficiently deep (i.e, hundreds of meters) source (Kourafalou & Kang, 2012; Lee et al., 1992).

Just as OS1 and OS2 have higher variance than the more offshore OS3 and OS4 in the Florida Keys, the relatively coastal USVI site (STJN) has a higher Sr/Ca variance compared to the open-ocean exposed ANEE site in the BVI. The STJN site may be more influenced by runoff and groundwater discharge (Cosner, 1972) than ANEE, given the steep topography surrounding STJN on three sides and its location very close to shore. Meanwhile, the Anegada OsmoSampler lies close to the seaward edge of a high-energy reef with substantial currents from offshore, ~2 km from a low carbonate island with little, if any, runoff. However, it is interesting to note that, excluding the large negative excursion at STJN in late 2018, the shift in mean and variance observed at both VI sites after June 2018 is similar in both timing and magnitude. The implication is that a single process, or combination of processes, could be partly responsible for seawater Sr/Ca variability at both sites.

4.2 Seawater Sr/Ca Variability in Florida Bay

Given the evidence for strong impacts of Florida Bay on seawater Sr/Ca ratios along the FKRT, potential sources of Sr/Ca variability in Florida Bay warrant discussion. Specifically, the features of interest are the pronounced winter minima and summer maxima that persist year-to-year at OS1. The three most likely causes of seawater Sr/Ca variability in Florida Bay are (1) freshwater runoff (Surge & Lohmann, 2002), (2) groundwater (saline or fresh) (Schijf & Byrne, 2007; Stalker et al., 2009), and (3) changes in carbonate precipitation and dissolution (Millero et al., 2001; Muehllehner et al., 2016; Yates & Halley, 2006).

While exploring all sources of seawater Sr/Ca variability are outside the scope of this thesis, one way to explore the impact of freshwater runoff on seawater Sr/Ca in Florida Bay is to examine the relationship between Sr/Ca and [Sr] at OS1, because [Sr] is generally found to be conservative (i.e., correlated with salinity) in South Florida (Dwyer & Cronin, 2001). Therefore, a two-endmember mixing model can be superposed on a cross plot of Sr/Ca and [Sr] at OS1, to assess the potential impact of fresh Everglades water on Sr/Ca variability in Florida Bay (Figure 9). The values of the freshwater endmember (i.e., Everglades water) for Sr/Ca and [Sr] are 1.15 ± 2.91 mmol/mol and 0.002 ± 0.003 mM, respectively (Surge & Lohmann, 2002). The values of the upper endmember (i.e., seawater) for Sr/Ca and [Sr] are 8.68 ± 0.05 mmol/mol and 0.087 ± 0.004 mM, respectively. The seawater endmember values were obtained by averaging all of the samples from OS4 throughout the entire study period. The area between the dashed curves represents the range of possible values that could be obtained by two-endmember-mixing, given the variance (1σ) observed in both endmembers. The model assumes that evaporation and precipitation impact [Sr] through concentration and dilution, respectively, but do not impact Sr/Ca, hence the horizontal line at [Sr] greater than mean seawater.

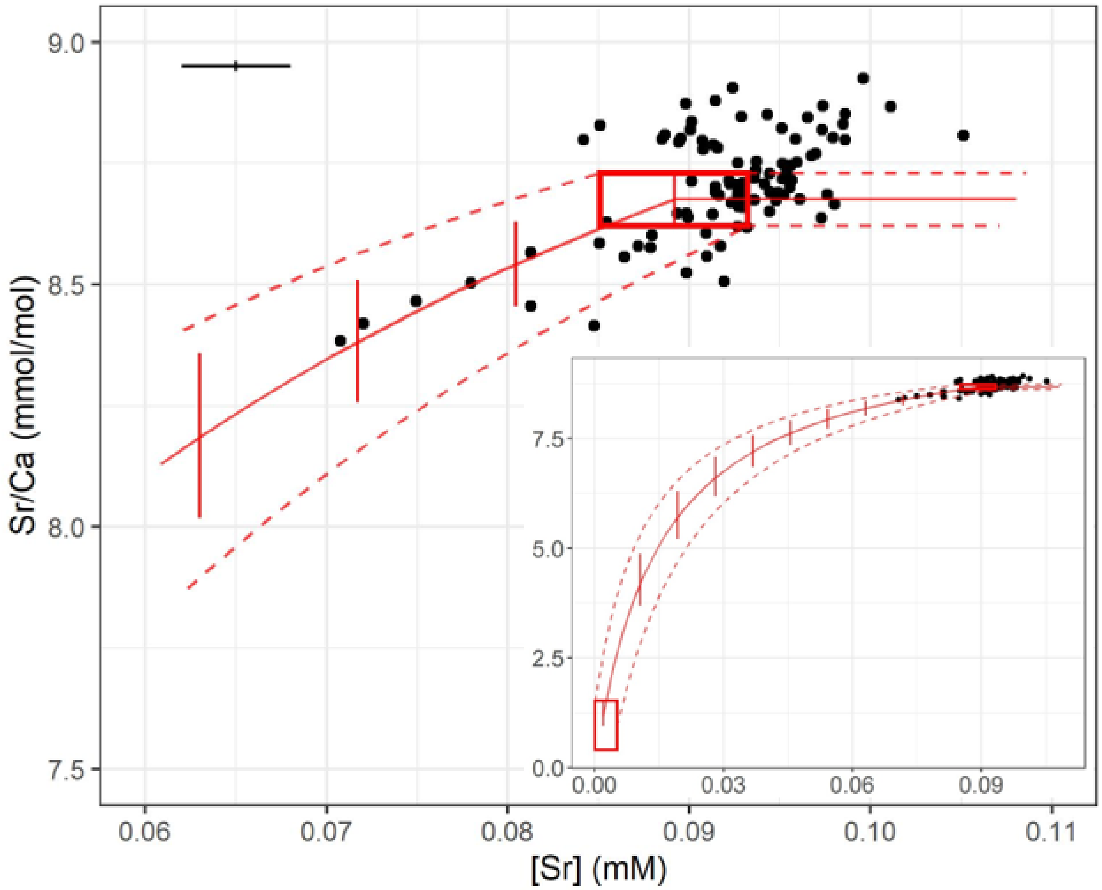

Figure 8. A conservative water mass mixing model between measured seawater Sr/Ca and [Sr] from samples at OS1. Endmembers are indicated by red boxes. The freshwater endmember was determined using Everglades measurements from Surge and Lohmann (2002). Mean seawater Sr/Ca and [Sr] at OS4 were taken as the upper end member. The area between the dashed lines represents the possible range of values obtained from two-endmember mixing, given the variance observed for each endmember. Vertical red bars represent 10% increments of mixing. Analytical errors in [Sr] and Sr/Ca are represented by the crosshairs at the top-left of the graph. Note how some lower values fall directly in the center of the mixing model, while higher values show substantial scatter.

A subset of the data falls within the bounds of the conservative mixing model, with lower values of both Sr/Ca and [Sr] following directly along the projected mixing curve. It can thus be inferred that periods of time such as the 2017-2018 winter minimum are well explained by conservative mixing of seawater and runoff from the

Everglades. However, most of the remaining data show significant scatter and fall well above the bounds of the mixing model, indicating that (1) the upper endmember is poorly defined, (2) seawater is not the upper endmember, and/or (3) seawater Sr/Ca variability in Florida Bay is non-conservative by nature.

These results confirm prior studies concerning the complexity of Sr/Ca variability in Florida Bay (e.g., Stabenau & Kotun, 2012; Swart & Price, 2002; Swart et al., 1989a). Florida Bay geochemistry is known to be a complex mixture of different water masses and internal processes (Millero et al., 2001; Stabenau & Kotun, 2012; Swart et al., 1989a,b). Some of the data that fall above the proposed mixing model could potentially be explained by multiple groundwater sources. The Sr/Ca composition of groundwater in Florida Bay is poorly constrained (Böhlke et al., 1999; Corbett et al., 1999; Stalker et al., 2009), but it is thought that saline groundwater measurably impacts the salt balance in Florida Bay (Stabenau & Kotun, 2012; Swart & Price, 2002). Therefore, its potential to influence Sr/Ca variability in this region cannot be dismissed.

Alternatively, non-conservative processes such as seasonal changes in carbonate precipitation and dissolution could explain a significant portion of both the observed summer maxima and winter minima in Florida Bay. While aragonite is the most common mineral to precipitate in Florida Bay, its precipitation and dissolution would only impact seawater Sr/Ca during winter months, when Florida Bay experiences net dissolution (Millero et al., 2001) and when the K of aragonite is sufficiently larger than one (Smith et al., 1979). Biogenic production of high magnesium calcite (HMC), which has a K less than 0.05 within the temperature range of Florida Bay (Malone & Baker, 1999), could help explain both summer maxima and winter minima. However, HMC is not as commonly produced by organisms in Florida Bay as aragonite (Nelson & Ginsburg, 1986), and its impact relative to aragonite is likely very small. With respect to abiotic mineral production, low magnesium calcite (LMC) and dolomite are commonly occurring minerals in Florida Bay and the nearby Great Bahama Bank (Liu et al., 2019; Millero et al., 2001; Shinn, 1968). Marine diagenesis of aragonite into LMC or dolomitization could increase porewater Sr/Ca substantially (Brand & Veizer, 1980; Liu et al., 2019; Schijf & Byrne, 2007; Swart et al., 1989a), but further study is needed to determine the role of carbonate diagenesis on Florida Bay Sr/Ca variability.

4.3 Seawater Sr/Ca Variability in the Virgin Islands

The decreased mean and increased variance in seawater Sr/Ca that occurred around June 2018 is similar in magnitude at both VI sites (Table 5), and may therefore be driven by the same regional process. Both sites receive open ocean water from the Caribbean and the northern tropical Atlantic (Johns et al., 2002). The Amazon and Orinoco rivers are known to impact SSS and biogeochemistry in surface waters of the Caribbean and immediately east of the Lesser Antilles on seasonal timescales (Hellweger & Gordon, 2002; Hu et al., 2004; Müller-Karger et al., 1989). These river plumes spread northward annually in the Ekman layer, beginning around mid-summer (Nikiema et al., 2007). Therefore, the decrease in mean and increase in variance after June 2018 at both STJN and ANEE could be driven by Ekman-induced seasonal advection of Amazon and Orinoco river water.

Table 5. Mean seawater Sr/Ca and standard error at both VI sites prior to and after June 2018. All units are in mmol/mol. *Samples from STJN that were estimated to be collected between Oct. 24th and Nov. 25th 2018 were clearly an unusual local event and were therefore not included in this analysis (see text).

Site	**February – June 2018**	**June 2018 – January 2019**	**Difference**
ANEE	8.684 ± 0.002	8.631 ± 0.006	0.053 ± 0.006
STJN*	8.722 ± 0.003	8.689 ± 0.009	0.033 ± 0.009

Generally speaking, rivers have lower Sr/Ca ratios than seawater (e.g., Mackenzie & Garrels, 1966). Considering the potential impact of the Amazon and Orinoco plumes on both seawater Sr/Ca and SSS (Chérubin & Richardson, 2007), seawater Sr/Ca at ANEE may be compared with regionally integrated satellite-derived SSS (Kerr et al., 2010; Mecklenburg et al., 2012) over the study period (Figure 10).

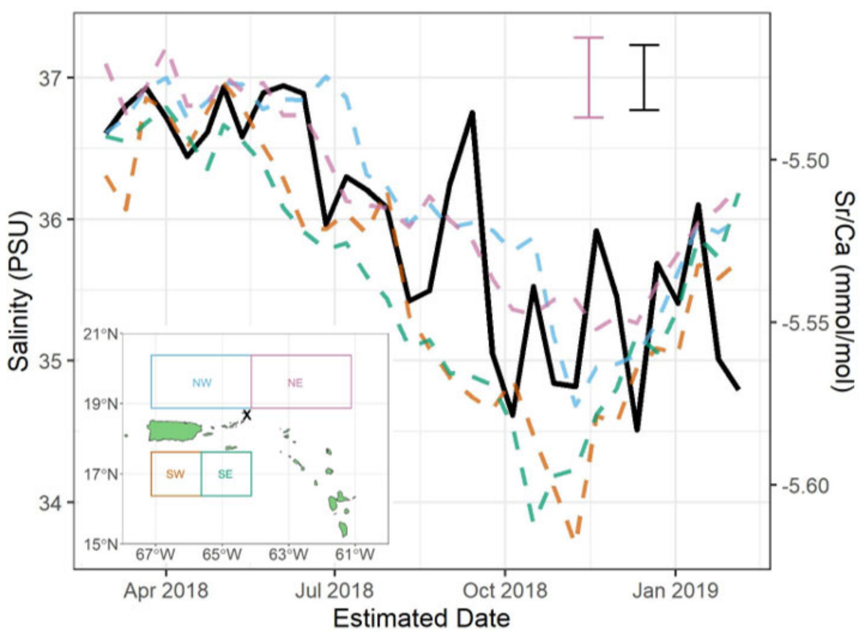

Figure 9. Seawater Sr/Ca at the ANEE site (black line) plotted with satellite-derived SSS measurements acquired during the study period (Kerr et al., 2010) (dashed lines). The color of each dashed line corresponds to SSS integrated over an area indicated by the inset map during the study period. Errors for Sr/Ca (solid) and SSS (dashed) are 0.01 mmol/mol and 0.28, respectively. Salinity in each region is positively correlated with seawater Sr/Ca from ANEE ($r^2 > 0.54$), most strongly in the Northeast quadrant ($r^2 = 0.61$).

Values of SSS from each region of the northeastern Caribbean are correlated with seawater Sr/Ca at ANEE ($r^2 > 0.54$), with the strongest correlation from the northeast quadrant closest to Anegada ($r^2 = 0.61$). This is consistent with the direction of mean flow through the Anegada Passage (Schmuker & Schiebel, 2002).

To explore the possibility that Amazon and Orinoco river plumes could decrease seawater Sr/Ca in the northern Caribbean, published values of Sr and Ca concentrations were compiled for the Amazon and Orinoco river basins (Bouchez et al., 2010; Gaillardet et al., 1997; Hartmann et al., 2014). Results are varied, but yield an average Sr/Ca ratio for the Amazon and Orinoco rivers of 2.41 ± 1.77 and 4.57 ± 0.65 mmol/mol, respectively. If the mean shift in seawater Sr/Ca at ANEE around June is due solely to mixing of seawater and Amazon and Orinoco river water, then river water should constitute approximately 0.62 – 1.45% of our samples. This corresponds to a salinity decrease of 0.23 – 0.53, which is consistent with previous estimates of salinity deviations propagated by Amazon and Orinoco river inputs in the northern Caribbean (~0.5; Froelich et al., 1978; Grodsky et al., 2015). The remaining salinity depression observed in 2018 is likely due to increased rainfall. The results from this preliminary investigation suggest that the decrease in mean seawater Sr/Ca at ANEE after June is consistent with seasonal northward transport of relatively low Sr/Ca Amazon and Orinoco river water (Chérubin & Richardson, 2007; Corredor & Morell, 2001; Hu et al., 2004).

Other potential mechanisms for the increase in variance around June 2018 at the ANEE site are more difficult to evaluate. One possibility is that wind-driven upwelling along the northern coast of Anegada would occur more frequently in fall and winter, when the tradewinds are relatively stronger. If originating at sufficient depth, this could increase seawater Sr/Ca variability at the surface in episodic events. Alternatively, cyclonic eddies shedding from the North Brazil Current (Johns et al., 1990, 1998) increase in both frequency and magnitude around August and reach a maximum between December and February (Aguedjou et al., 2019). These eddies are distinct water masses with unknown Sr/Ca values that intermittently pass through the region (Fratantoni & Richardson, 2006; Goni & Johns, 2001), potentially advecting seawater Sr/Ca signatures from river plumes, equatorial upwelling, and local biogeochemistry.

Unlike ANEE, seawater Sr/Ca variability at STJN exhibits short-duration, high-magnitude deviations that are specific to this site. Large sediment plumes are often seen in the bays surrounding St. John after substantial rainfall (Edmunds & Gray, 2014; Gray et al., 2012). Reich et al. (2013) postulated that one of these events may have altered ambient seawater chemistry and resulted in anomalous coral Sr/Ca measurements. The same type of event could have caused our measured seawater Sr/Ca excursions, including the large negative excursion in late 2018. Therefore, the relationship between seawater Sr/Ca and rainfall was explored at STJN as a potential mechanism for sudden excursions in seawater Sr/Ca (Figure 11). These meteorological data indicate an ambiguous relationship between rainfall on St. Thomas and seawater Sr/Ca at STJN, where rain events and periods of low barometric pressure do not always correspond to changes in seawater Sr/Ca. Anna's Retreat at east end of St. Thomas is the closest source of continuous precipitation data known to us throughout any portion of the study period. Convective rainfall is notoriously patchy on tropical islands, thus precipitation events recorded on St. Thomas did not necessarily occur in St. John at our Coral Bay site. However, it is worth noting that the large negative excursion of late 2018 follows a prolonged period of low barometric pressure that appears to have produced significant local rainfall.

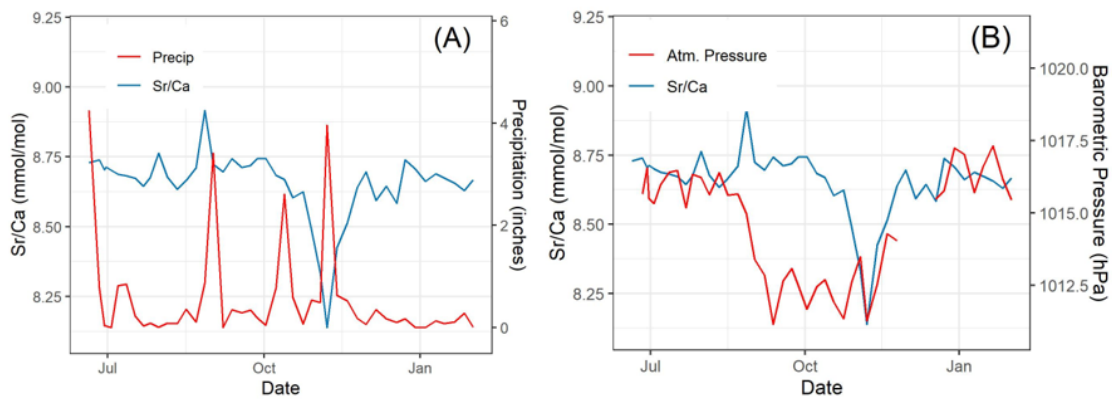

Figure 10. Seawater Sr/Ca at the STJN OsmoSampler plotted with (A) precipitation data from the east end of St. Thomas (~15 km from STJN) collected by the Community Collaborative Rain, Hail, and Snow Network (Reges et al., 2016), and (B) barometric pressure measurements from National Data Buoy Center Station 41052 (Hamilton, 1986), approximately 10 km south of Cruz Bay on the southwest corner of St. John. The negative excursion in seawater Sr/Ca from STJN is coincident with a sustained drop in barometric pressure, but available precipitation data does not appear anomalous at this time.

4.4 Implications for Coral Sr/Ca-based Paleothermometry

4.4.1 Implications for Coral Sr/Ca-based SST Reconstructions

The seawater Sr/Ca variability observed in this study has significant implications for coral Sr/Ca – based paleothermometry at each site. Perhaps most important is its potential impact on site-specific coral Sr/Ca – SST calibrations. In both the Florida Keys and the Virgin Islands, mean seawater Sr/Ca was higher in spring and summer than in winter and fall. Given the direct effect of seawater Sr/Ca on coral Sr/Ca and the inverse relationship between coral Sr/Ca and SST, these summer maxima and winter minima should have the effect of reducing the slope obtained from coral Sr/Ca – SST calibrations that assume constant seawater Sr/Ca, causing the annual temperature cycle to be underestimated. This is consistent with previous coral Sr/Ca – SST calibrations along the FKRT, which on average have significantly lower slopes than their Pacific counterparts (DeLong et al., 2011; Flannery et al., 2017; Maupin et al., 2008; Smith et al., 2006; Swart et al., 2002). Furthermore, interannual variability in seawater Sr/Ca would compromise the fidelity of the SST reconstruction from year to year by further diminishing the correlation between coral Sr/Ca and SST. This may be the case in Swart et al. (2002), who observed two statistically different coral Sr/Ca – SST calibrations over two consecutive years within a single specimen.

To illustrate how seawater Sr/Ca variability may impact a coral Sr/Ca-based SST reconstruction, hypothetical Sr/Ca-based SST reconstructions were generated for four of the six study sites based on the current understanding of how corals record climate and geochemical signals in their environment (i.e., forward modeling; Thompson et al., 2011). These hypothetical Sr/Ca-based SST reconstructions are hereafter simply referred to as 'pseudo SST'. Pseudo SST (red lines) was obtained by calculating coral Sr/Ca at each location using the following equation:

$$K = \frac{c_i}{s_i} = aT + b \tag{6}$$

where K is the distribution coefficient for Sr and Ca between aragonite and seawater, c_i is coral Sr/Ca at time i, s_i is seawater Sr/Ca at time i, and T is temperature (°C). Equation 6 can be rewritten in terms of c_i to explicitly account for seawater Sr/Ca variability.

$$c_i = (aT + b)s_i \quad (7)$$

Standard coral Sr/Ca – SST regressions often assume constant s ($\bar{s}$) to obtain a fixed slope ($m = a\bar{s}$). This slope can also be obtained by taking the partial derivative of c with respect to T in equation (7).

$$c = mT + \beta \quad (8)$$

$$\frac{\partial c}{\partial T} = m = a\bar{s} \quad (9)$$

Therefore, coral Sr/Ca (c_i) is calculated using known instantaneous temperature (T), recorded by Onset HOBO© temperature loggers (See Ch. 2), and measured seawater Sr/Ca (s_i). The value of c_i is then applied to a standard calibration equation (that assumes a constant seawater Sr/Ca, or s) to yield a 'pseudo SST reconstruction'. The calibration of Swart et al. (2002) was used to create pseudo SST reconstructions at OS1, OS4, ANEE, and STJN (Figure 12). As stated previously, this calibration likely carries an implicit bias due to seawater Sr/Ca variability that reduces the sensitivity of the coral Sr/Ca – SST relationship and shifts mean reconstructed SST. If a steeper calibration slope were used, it would increase the temperature offset in the pseudo SST reconstructions accordingly. If mean seawater Sr/Ca at each site were significantly different, then the pseudo SST would be offset directly according to that difference. Among the four sites chosen for this analysis, ANEE is the only site whose mean is significantly different from the others (Wilcoxon Rank Sum Test, $p = 0.02$).

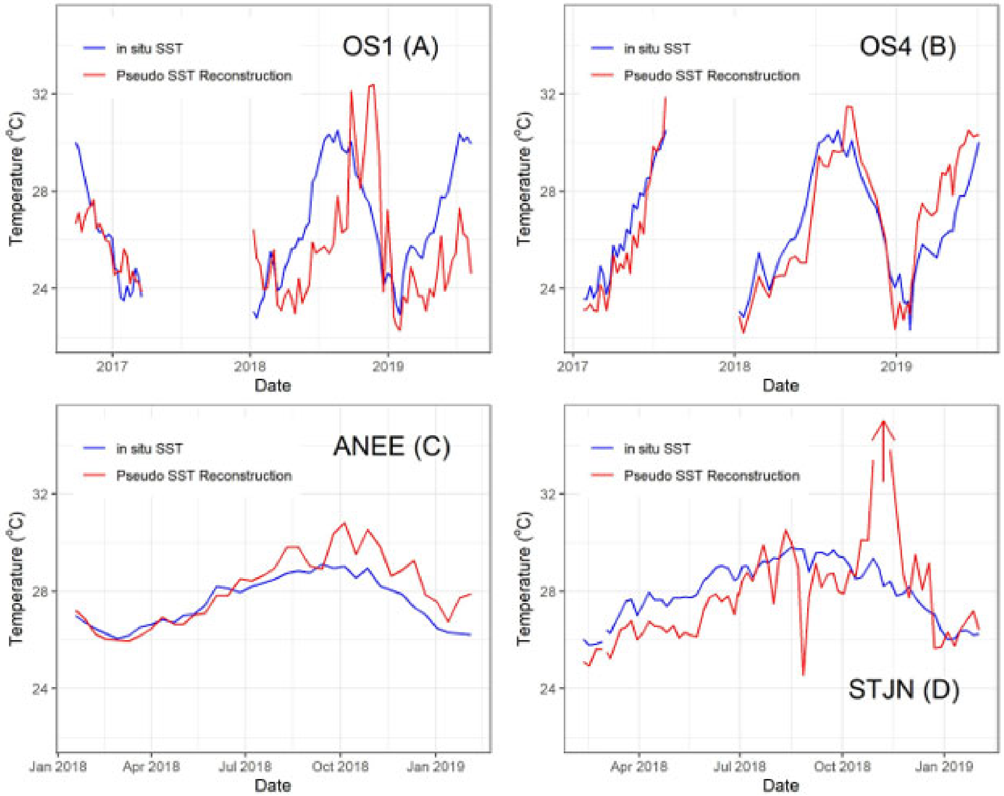

Figure 11. Coral Sr/Ca-based reconstructed pseudo SST (red) *versus in situ* SST (blue) measured using Onset HOBO© loggers at OS1 (A), OS4 (B), ANEE (C), and STJN (D). Pseudo SST was calculated using the coral Sr/Ca – SST regression from Swart et al. (2002). Pseudo SST is more variable at all sites compared to *in situ* SST. In November 2018, pseudo SST at STJN peak at almost 40ºC, which is clearly an unrealistic temperature.

Temperature offsets from each pseudo SST reconstruction are summarized in Table 6. Absolute mean temperature offset, or the absolute difference between *in situ* SST and pseudo SST, is highest at OS1, where seasonal variations in seawater Sr/Ca are out of phase with *in situ* SST. This phase lag is consistent with observations from both Swart et al. (2002) and Smith et al. (2006). At OS4, pseudo SST and *in situ* SST are generally in good agreement, although there are periods of time when discrepancies of ~2ºC persist. ANEE exhibits the lowest absolute mean temperature offset out of all sites. This is because mean seawater Sr/Ca at ANEE prior to June 2018 is not significantly different from mean seawater Sr/Ca at either of the Florida Keys sites (Wilcoxon Rank Sum Test, $p = 0.18$). However, the decreased mean and increased variance after June 2018 significantly enhance the apparent seasonal cycle and hence the mean temperature offset. STJN exhibits the second-highest absolute mean temperature offset, in large part due to the inclusion of the excursion in late 2018. In general, pseudo SST and *in situ* SST are not in good agreement with each other at this site. Positive and negative excursions in seawater Sr/Ca create corresponding variations in pseudo SST that poorly represent actual *in situ* SST variations.

Table 6. A summary of the error for the pseudo SST reconstructions at OS1, OS4, ANEE, and STJN. Values are reported as the difference between measured *in situ* SST and SST theoretically obtained from a coral growing under the measured *in situ* seawater Sr/Ca conditions (pseudo SST). Negative values indicate that pseudo SST is lower than *in situ* SST. Absolute mean temperature offset is low at all sites except for OS1, where the temperature offset is seasonal rather than episodic.

Site	**Minimum error (ºC)**	**Maximum error (ºC)**	**Absolute Mean Offset (ºC)**
OS1	−5.33	5.67	1.92
OS4	−2.36	2.72	0.98
ANEE	−0.37	1.92	0.66
STJN	−5.17	11.61	1.33

4.4.2 Implications for Seawater Sr/Ca Variability Across the FKRT

This thesis study into seawater Sr/Ca variability along the FKRT was partly inspired by incongruous coral Sr/Ca – SST calibrations in different years measured by Swart et al. (2002) and calculated seawater Sr/Ca at Looe Key from Smith et al. (2006). The findings from these two studies were reexamined in light of the continuous seawater Sr/Ca measurements undertaken during this study. Monthly averages of calculated seawater Sr/Ca and $\delta^{18}O$ from Looe Key were recalculated using the Swart et al. (2002) calibration and then compared to seawater Sr/Ca from OS1 and OS2

(Figure 13). Originally, Smith et al. (2006) calculated seawater Sr/Ca from Looe Key using a generic calibration for the *Porites* genus from Smith et al. (1979) (Figure 13C – red).

$$K = \frac{c}{s} = 1.30 - 0.0094T \tag{10}$$

$$s = \frac{c}{(1.30 - 0.0094T)} \tag{11}$$

Because Smith et al. (2006) measured coral Sr/Ca in *Montastraea (Orbicella) faveolata*, it is more appropriate to use the calibration equation from Swart et al. (2002) (Figure 13C – green), which was derived using the related species *Montastraea (Orbicella) annularis* from just outside of Biscayne Bay in the Upper Keys, ~140 km from Looe Key.

$$R = c = 10.165 - 0.0471T \tag{12}$$

where $R = K \times s$, and *s,* the seawater Sr/Ca ratio, is assumed constant (see Smith et al., 1979). To obtain calculated seawater Sr/Ca, the calibration of Swart et al. (2002) can be rewritten in terms of *K* to determine *s*.

$$K = \frac{c}{s} = \frac{10.165 - 0.0471T}{8.69} = 1.17 - 0.0054T \tag{13}$$

$$s = \frac{c}{(1.17 - 0.0054T)} \tag{14}$$

Mean seawater at OS2 (8.69 mmol/mol) is used to make the conversion because it occupies a similar cross-shelf position along the FKRT as Looe Key, assuming that the two sites are similarly influenced by Florida Bay. If, for example, mean seawater Sr/Ca from de Villiers (1999) (8.54 mmol/mol) was used to make the conversion, it would lower all calculated seawater Sr/Ca values by 0.15 mmol/mol accordingly.

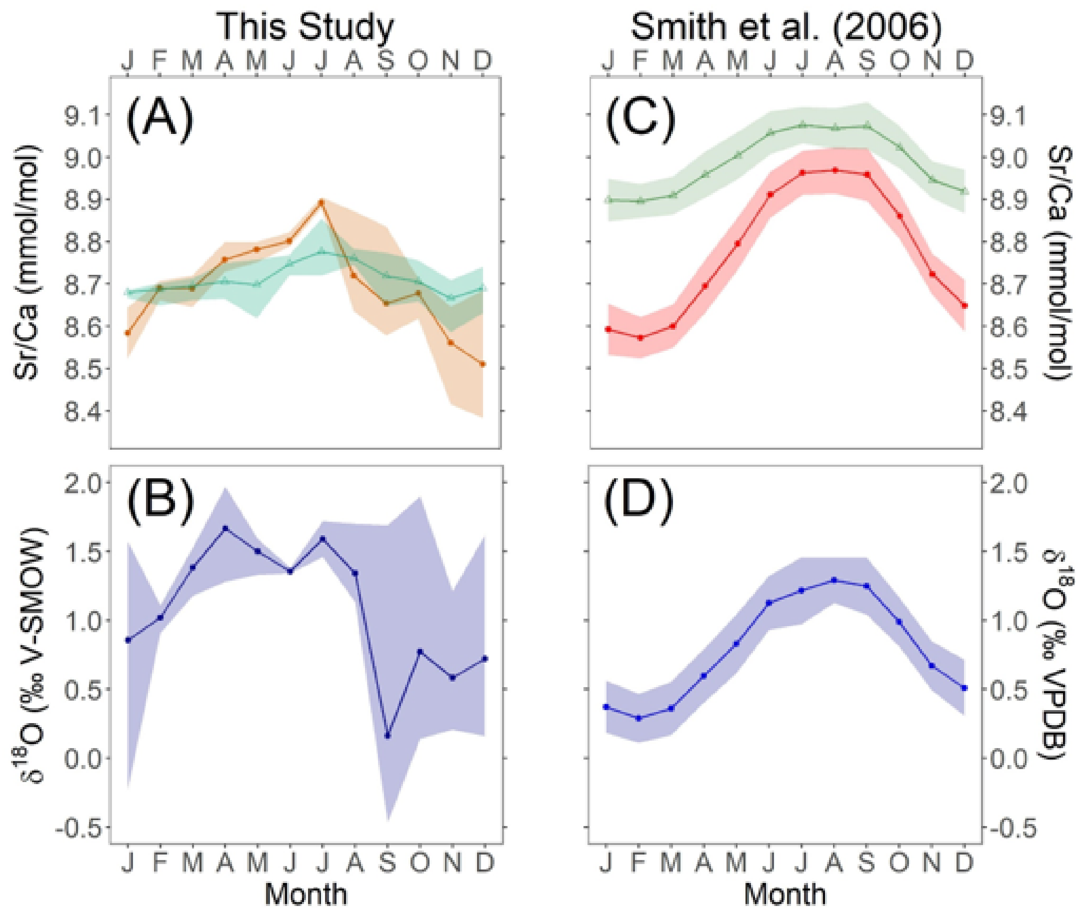

Figure 12. (A) Monthly averages of measured seawater Sr/Ca at OS1 (orange) and OS2 (green). (B) Monthly averages of measured seawater $\delta^{18}O$ at OS1. (C) Monthly averages of calculated seawater Sr/Ca at Looe Key (Smith et al., 2006) using calibration equations from Smith et al. (1979) (red) and Swart et al. (2002) (green). (D) Monthly averages of calculated seawater $\delta^{18}O$ at Looe Key (Smith et al., 2006) using a calibration equation from Leder et al. (1996). The shaded regions in (A) and (B) represent the range of values observed at OS1 during the study period, while the shaded regions in (C) and (D) represent the standard deviation of the reported values associated with sampling. Notes the similarities in the summer maxima and winter minima between the current study and Smith et al. (2006).

The similarities in phase and magnitude between calculated seawater Sr/Ca at Looe Key (C) and *in situ* seawater Sr/Ca at OS1 and OS2 (A) are encouraging, but only qualitative. Using the Swart et al. (2002) calibration leads to better agreement between the magnitude of calculated seawater Sr/Ca at Looe Key and *in situ* seawater Sr/Ca at OS2. The difference in mean calculated seawater Sr/Ca between the Swart et al. (2002) and Smith et al. (1979) calibrations is due to the conversion of the regression components using mean seawater Sr/Ca at OS2. Using the Swart et al. (2002) calibration changes annual mean seawater at Looe Key from 8.77 to 8.99 mmol/mol, either of which is significantly higher than measured seawater Sr/Ca at OS1 (8.69 mmol/mol) and OS2 (8.71 mmol/mol).

The results from this analysis support the conclusion that, given its proximity to Florida Bay and the channels between the islands of the Florida Keys, seawater Sr/Ca variability at Looe Key, like OS2, is also influenced by Sr/Ca variability in Florida Bay. Given that these two sites are ~70 km apart and encompass most of the Middle Keys, these results have important implications for coral Sr/Ca-based paleothermometry along the FKRT.

Chapter 5: Conclusion

The goal of this study is the quantification of seawater Sr/Ca variability across coral reefs in the tropical western Atlantic basin, represented by four study sites in the Florida Keys and two study sites in the U.S. and British Virgin Islands. All six sites exhibit significant seawater Sr/Ca variability. Although differences in mean seawater Sr/Ca among sites is not significant, the magnitude of variance at each site differs greatly. Even the site that shows the smallest variance (ANEE) would still exhibit an apparent seasonal cycle of ~2ºC in reconstructed coral temperature from seawater Sr/Ca variability alone. Perhaps most important is the impact that the observed seawater Sr/Ca variations may have on local coral Sr/Ca – SST calibrations. At four of the six study sites, seawater Sr/Ca was higher in spring-summer and lower in fall-winter. This may lower the slope of local coral Sr/Ca – SST regressions, which could explain why calibrations of coral Sr/Ca to SST at some sites are lower than others.

This study corroborates results from both Smith et al. (2006) and Khare (2018) who surmised that Florida Bay is a major driver for seawater Sr/Ca variability along the middle portion of the FKRT. The OS1 site in Florida Bay exhibits the greatest variance out of all our study sites (0.10 mmol/mol). Seawater Sr/Ca variability at this site displays a clear annual cycle, with pronounced high summer and low winter ratios. The same is true for OS2, but to a lesser extent, indicating that both sites are influenced by seawater Sr/Ca variability in Florida Bay.

Results from both the Florida Keys and Virgin Islands suggest that nearshore processes (e.g., runoff, groundwater, drainage geology) have a greater influence on seawater Sr/Ca variability than offshore processes (upwelling, eddies). Potential sources of variability appear mainly related to local and regional hydrography rather than geology. This is supported by the fact that, excluding a single excursion at the siliciclastic STJN site, the mean and variance of Sr/Ca ratios were not significantly different from the other carbonate platform sites. On the other hand, there are large differences in seawater Sr/Ca between the other five carbonate platform sites, despite the relative proximity of four of them. Mechanisms of seawater variability moreover appear highly complex, with multiple local drivers.

Future studies in coral reef environments should focus on using appropriate tracers to identify and resolve specific mechanisms underlying seawater Sr/Ca variability, in order to target the most stable locations for coral paleoclimate work. Mechanisms to explore include: runoff, groundwater discharge, reef productivity, and diagenesis. More studies need to be conducted before a particular offshore process, such as upwelling and eddy migration, can be dismissed as a major mechanism of variability. Future coral Sr/Ca-based paleoclimate studies should monitor seawater Sr/Ca at prospective study sites for as long as possible prior to collecting coral samples to demonstrate the stability of seawater Sr/Ca at the site. As a note of caution, sites that are known to be significantly influenced by runoff, groundwater discharge, or large shallow lagoons should be avoided.

Appendix

Sample ID	Date	Sr/Ca (mmol/mol)	SE (mmol/mol)	δ^{18}O (‰ VSMOW)	SD (‰ VSMOW)	Temp. (ºC)	V. (mL)	Salinity
17W FLKS OS1-1	1/14/2017	8.68	0.007	NA	NA	24.7	5.85	37.0
17W FLKS OS1-2	1/6/2017	8.69	0.007	NA	NA	24.9	5.45	NA
17W FLKS OS1-3	12/30/2016	8.71	0.007	NA	NA	26.1	5.60	NA
17W FLKS OS1-4	12/22/2016	8.69	0.005	NA	NA	26.2	5.60	NA
17W FLKS OS1-5	12/14/2016	8.68	0.005	NA	NA	26.1	5.60	NA
17W FLKS OS1-6	12/6/2016	8.67	0.006	NA	NA	26.3	5.50	36.0
17W FLKS OS1-7	11/28/2016	8.66	0.007	NA	NA	26.3	5.65	NA
17W FLKS OS1-8	11/20/2016	8.68	0.006	NA	NA	26.6	5.60	NA
17W FLKS OS1-9	11/12/2016	8.67	0.008	NA	NA	27.5	5.55	NA
17W FLKS OS1-10	11/4/2016	8.68	0.004	NA	NA	27.4	5.65	NA
17W FLKS OS1-11	10/28/2016	8.71	0.007	NA	NA	28.0	5.55	35.0
17W FLKS OS1-12	10/20/2016	8.75	0.004	NA	NA	28.5	5.60	NA
17W FLKS OS1-13	10/12/2016	8.80	0.009	NA	NA	29.1	5.55	NA
17W FLKS OS1-14	10/4/2016	8.80	0.006	NA	NA	29.7	5.45	NA
17W FLKS OS1-15	9/26/2016	8.83	0.007	NA	NA	30.0	5.65	NA
17W FLKS OS1-16	9/21/2016	8.80	0.006	NA	NA	NA	1.21	NA
17S FLKS OS1-1	3/19/2017	8.67	0.010	NA	NA	23.6	4.75	38.0
17S FLKS OS1-2	3/11/2017	8.68	0.005	NA	NA	24.5	6.40	38.0
17S FLKS OS1-3	3/3/2017	8.70	0.006	NA	NA	24.8	5.50	38.0
17S FLKS OS1-4	2/23/2017	8.64	0.007	NA	NA	23.9	5.45	38.0
17S FLKS OS1-5	2/16/2017	8.65	0.004	NA	NA	23.7	5.55	37.5
17S FLKS OS1-6	2/8/2017	8.62	0.004	NA	NA	24.1	5.55	36.5
17S FLKS OS1-7	1/31/2017	8.58	0.002	NA	NA	23.5	5.55	35.0
17S FLKS OS1-8	1/23/2017	8.63	0.005	NA	NA	23.6	5.30	33.0
18W FLKS OS1-1	1/4/2018	8.50	0.017	NA	NA	NA	5.05	NA
18W FLKS OS1-2	12/28/2017	8.42	0.007	0.16	0.06	NA	5.25	NA
18W FLKS OS1-3	12/20/2017	8.38	0.011	0.16	0.05	NA	5.40	NA
18W FLKS OS1-4	12/12/2017	8.47	0.007	0.26	0.06	NA	5.40	NA

18W FLKS OS1-5	12/5/2017	8.56	0.011	0.37	0.05	NA	5.30	34.0
18W FLKS OS1-6	11/27/2017	8.59	0.009	0.38	0.08	NA	5.45	NA
18W FLKS OS1-7	11/19/2017	8.61	0.016	0.41	0.08	NA	5.45	NA
18W FLKS OS1-8	11/11/2017	8.65	0.024	0.29	0.06	NA	5.40	NA
18W FLKS OS1-9	11/4/2017	8.64	0.015	0.21	0.09	NA	5.35	NA
18W FLKS OS1-10	10/27/2017	8.68	0.023	0.14	0.06	NA	5.45	37.0
18W FLKS OS1-11	10/19/2017	8.68	0.017	0.29	0.05	NA	5.45	NA
18W FLKS OS1-12	10/11/2017	8.71	0.008	0.26	0.07	NA	5.45	NA
18W FLKS OS1-13	10/4/2017	8.69	0.022	0.14	0.05	NA	5.40	NA
18W FLKS OS1-14	9/26/2017	8.72	0.009	0.04	0.07	NA	4.95	NA
18W FLKS OS1-15	9/22/2017	8.64	0.009	-0.05	0.07	NA	0.68	NA
18W FLKS OS1-16	9/21/2017	8.62	0.020	-0.05	0.05	NA	0.68	NA
18W FLKS OS1-17	9/20/2017	8.66	0.028	-0.06	0.06	NA	0.68	NA
18W FLKS OS1-18	9/19/2017	8.64	0.034	-0.20	0.06	NA	0.68	NA
18W FLKS OS1-19	9/18/2017	8.66	0.015	-0.11	0.06	NA	0.68	NA
18W FLKS OS1-20	9/17/2017	8.62	0.011	-0.12	0.04	NA	0.68	NA
18W FLKS OS1-21	9/16/2017	8.62	0.045	-0.11	0.06	NA	0.68	NA
18W FLKS OS1-22	9/15/2017	8.67	0.007	0.05	0.06	NA	0.68	NA
18W FLKS OS1-23	9/14/2017	8.59	0.027	-0.25	0.08	NA	0.68	NA
18W FLKS OS1-24	9/13/2017	8.60	0.004	-0.17	0.07	NA	0.68	NA
18W FLKS OS1-25	9/13/2017	8.61	0.023	-0.40	0.04	NA	0.68	NA
18W FLKS OS1-26	9/12/2017	8.63	0.032	-0.17	0.05	NA	0.68	NA
18W FLKS OS1-27	9/11/2017	8.62	0.023	-0.47	0.10	NA	0.68	NA
18W FLKS OS1-28	9/10/2017	8.60	0.006	-0.23	0.07	NA	0.68	NA
18W FLKS OS1-29	9/9/2017	8.66	0.033	-0.14	0.04	NA	0.68	NA
18W FLKS OS1-30	9/8/2017	8.65	0.032	-0.19	0.08	NA	0.68	NA
18W FLKS OS1-31	9/7/2017	8.66	0.027	-0.16	0.06	NA	0.68	NA
18W FLKS OS1-32	9/6/2017	8.66	0.005	-0.17	0.06	NA	0.68	NA
18W FLKS OS1-33	9/5/2017	8.64	0.002	0.01	0.05	NA	0.68	NA
18W FLKS OS1-34	9/4/2017	8.64	0.038	0.24	0.07	NA	0.68	NA
18W FLKS OS1-35	9/3/2017	8.60	0.032	0.30	0.04	NA	0.68	NA
18W FLKS OS1-36	9/2/2017	8.67	0.003	0.85	0.06	NA	0.68	NA

18W FLKS OS1-37	9/1/2017	8.75	0.011	1.60	0.06	NA	0.68	NA	
18W FLKS OS1-38	8/31/2017	8.72	0.012	1.70	0.09	NA	0.68	NA	
18W FLKS OS1-39	8/30/2017	8.78	0.026	1.44	0.06	NA	0.68	NA	
18W FLKS OS1-40	8/29/2017	8.75	0.011	1.27	0.04	NA	0.68	NA	
18W FLKS OS1-41	8/28/2017	8.66	0.003	1.23	0.07	NA	0.68	NA	
18W FLKS OS1-42	8/27/2017	8.70	0.002	1.15	0.05	NA	0.68	NA	
18W FLKS OS1-43	8/26/2017	8.72	0.037	1.13	0.06	NA	0.68	NA	
18W FLKS OS1-44	8/25/2017	8.70	0.011	1.22	0.04	NA	0.68	NA	
18W FLKS OS1-45	8/24/2017	8.64	0.001	1.15	0.06	NA	0.68	NA	
18W FLKS OS1-46	8/23/2017	8.70	0.024	1.20	0.05	NA	0.68	NA	
18W FLKS OS1-47	8/22/2017	8.70	0.027	1.35	0.05	NA	0.68	NA	
18W FLKS OS1-48	8/21/2017	8.73	0.008	1.47	0.05	NA	0.68	NA	
18W FLKS OS1-49	8/20/2017	8.74	0.005	1.54	0.06	NA	0.68	NA	
18W FLKS OS1-50	8/19/2017	8.67	0.045	1.33	0.02	NA	0.68	NA	
18W FLKS OS1-51	8/18/2017	8.69	0.031	1.31	0.06	NA	0.68	NA	
18W FLKS OS1-52	8/17/2017	8.67	0.009	1.33	0.03	NA	0.68	NA	
18W FLKS OS1-53	8/16/2017	8.69	0.025	1.25	0.04	NA	0.68	NA	
18W FLKS OS1-54	8/15/2017	8.65	0.001	1.32	0.02	NA	0.68	NA	
18W FLKS OS1-55	8/11/2017	8.81	0.013	1.62	0.03	NA	5.10		40.5
18W FLKS OS1-56	8/5/2017	8.83	0.016	-1.26	0.04	NA	3.52		37.5
18S FLKS OS1-1	6/23/2018	8.82	0.010	1.38	0.04	28.6	5.15		33.5
18S FLKS OS1-2	6/14/2018	8.79	0.019	1.34	0.07	28.4	5.25	NA	
18S FLKS OS1-3	6/5/2018	8.79	0.007	1.34	0.03	26.7	5.40	NA	
18S FLKS OS1-4	5/27/2018	8.80	0.006	1.33	0.03	26.5	5.35	NA	
18S FLKS OS1-5	5/18/2018	8.79	0.009	1.58	0.03	26.0	5.40	NA	
18S FLKS OS1-6	5/9/2018	8.75	0.007	1.59	0.02	26.1	5.40		35.0
18S FLKS OS1-7	4/29/2018	8.80	0.009	1.28	0.03	25.7	5.40	NA	
18S FLKS OS1-8	4/20/2018	8.77	0.010	1.88	0.02	25.6	5.35	NA	
18S FLKS OS1-9	4/11/2018	8.73	0.002	1.97	0.03	25.2	5.35	NA	
18S FLKS OS1-10	4/2/2018	8.73	0.011	1.54	0.03	24.8	5.40	NA	
18S FLKS OS1-11	3/24/2018	8.72	0.008	1.18	0.02	24.1	5.45		34.0
18S FLKS OS1-12	3/14/2018	8.70	0.009	1.53	0.03	23.9	5.45	NA	

18S FLKS OS1-13	3/5/2018	8.65	0.006	1.44	0.04	24.9	5.40	NA
18S FLKS OS1-14	2/24/2018	8.71	0.004	1.04	0.04	25.5	5.45	NA
18S FLKS OS1-15	2/15/2018	8.70	0.005	1.11	0.03	24.6	5.45	NA
18S FLKS OS1-16	2/5/2018	8.66	0.008	0.91	0.03	23.6	5.35	33.5
18S FLKS OS1-17	1/27/2018	8.60	0.016	1.11	0.04	23.3	5.40	NA
18S FLKS OS1-18	1/18/2018	8.57	0.005	0.96	0.04	22.8	5.45	NA
18S FLKS OS1-19	1/10/2018	8.52	0.008	-0.22	0.02	23.1	3.47	NA
19W FLKS OS1-1	1/8/2019	8.64	0.008	1.57	0.03	24.5	3.60	NA
19W FLKS OS1-2	12/30/2018	8.56	0.009	1.62	0.04	24.6	4.40	38.0
19W FLKS OS1-3	12/19/2018	8.68	0.009	1.35	0.04	24.1	5.05	NA
19W FLKS OS1-4	12/7/2018	8.51	0.005	1.12	0.03	25.8	5.05	NA
19W FLKS OS1-5	11/24/2018	8.42	0.004	0.80	0.02	26.7	5.10	NA
19W FLKS OS1-6	11/12/2018	8.46	0.007	0.79	0.03	27.5	5.00	36.0
19W FLKS OS1-7	11/1/2018	8.58	0.005	1.21	0.02	27.8	5.10	NA
19W FLKS OS1-8	10/19/2018	8.69	0.005	1.90	0.04	28.4	5.05	NA
19W FLKS OS1-9	10/7/2018	8.62	0.005	1.89	0.02	28.7	5.05	NA
19W FLKS OS1-10	9/25/2018	8.58	0.007	1.00	0.02	30.0	5.05	NA
19W FLKS OS1-11	9/14/2018	8.82	0.005	1.62	0.03	29.6	5.05	35.0
19W FLKS OS1-12	9/1/2018	8.84	0.006	1.69	0.02	29.7	5.10	NA
19W FLKS OS1-13	8/20/2018	8.80	0.006	1.35	0.03	30.5	5.00	NA
19W FLKS OS1-14	8/9/2018	8.87	0.011	1.47	0.03	30.0	5.00	NA
19W FLKS OS1-15	7/28/2018	8.91	0.007	1.46	0.02	30.4	5.00	NA
19W FLKS OS1-16	7/16/2018	8.88	0.005	1.72	0.03	30.1	5.00	35.5
19S FLKS OS1-1	8/8/2019	8.92	0.006	NA	NA	29.9	5.20	39.0
19S FLKS OS1-2	7/29/2019	8.87	0.005	NA	NA	30.2	5.50	NA
19S FLKS OS1-3	7/19/2019	8.85	0.005	NA	NA	30.0	5.50	NA
19S FLKS OS1-4	7/9/2019	8.82	0.004	NA	NA	30.4	5.50	NA
19S FLKS OS1-5	6/29/2019	8.87	0.006	NA	NA	29.5	5.50	NA
19S FLKS OS1-6	6/19/2019	8.84	0.009	NA	NA	28.8	5.50	37.5
19S FLKS OS1-7	6/9/2019	8.85	0.005	NA	NA	28.0	5.50	NA
19S FLKS OS1-8	5/31/2019	8.85	0.008	NA	NA	27.7	5.50	NA
19S FLKS OS1-9	5/21/2019	8.75	0.015	NA	NA	27.8	5.50	NA

19S FLKS OS1-10	5/11/2019	8.78	0.007	NA	NA	27.0	5.50	NA
19S FLKS OS1-11	5/1/2019	8.80	0.009	NA	NA	26.3	5.50	37.5
19S FLKS OS1-12	4/21/2019	8.78	0.007	NA	NA	26.3	5.50	NA
19S FLKS OS1-13	4/11/2019	8.81	0.008	NA	NA	26.0	5.50	NA
19S FLKS OS1-14	4/1/2019	8.75	0.009	NA	NA	25.2	5.50	NA
19S FLKS OS1-15	3/22/2019	8.75	0.007	NA	NA	25.4	5.50	NA
19S FLKS OS1-16	3/12/2019	8.74	0.004	NA	NA	25.7	5.50	37.5
19S FLKS OS1-17	3/2/2019	8.72	0.005	NA	NA	25.8	5.50	NA
19S FLKS OS1-18	2/20/2019	8.77	0.011	NA	NA	25.4	5.50	NA
19S FLKS OS1-19	2/10/2019	8.72	0.007	NA	NA	24.6	5.50	NA
19S FLKS OS1-20	1/31/2019	8.71	0.007	NA	NA	22.9	5.50	NA
19S FLKS OS1-21	1/21/2019	8.71	0.007	NA	NA	23.4	5.50	35.5
19S FLKS OS1-22	1/15/2019	8.73	0.013	NA	NA	24.0	1.61	NA
17W FLKS OS2-1	1/15/2017	8.68	0.005	NA	NA	22.7	4.35	36.0
17W FLKS OS2-2	1/9/2017	8.68	0.005	NA	NA	23.4	4.70	NA
17W FLKS OS2-3	1/2/2017	8.68	0.006	NA	NA	24.4	4.70	NA
17W FLKS OS2-4	12/26/2016	8.68	0.012	NA	NA	25.5	4.70	NA
17W FLKS OS2-5	12/19/2016	8.68	0.009	NA	NA	25.6	4.75	NA
17W FLKS OS2-6	12/12/2016	8.70	0.006	NA	NA	25.5	4.75	36.0
17W FLKS OS2-7	12/5/2016	8.69	0.005	NA	NA	26.0	4.60	NA
17W FLKS OS2-8	11/28/2016	8.70	0.006	NA	NA	24.8	4.75	NA
17W FLKS OS2-9	11/22/2016	8.71	0.006	NA	NA	24.4	4.65	NA
17W FLKS OS2-10	11/15/2016	8.71	0.004	NA	NA	25.7	4.65	NA
17W FLKS OS2-11	11/8/2016	8.69	0.006	NA	NA	25.9	4.60	34.0
17W FLKS OS2-12	11/1/2016	8.69	0.007	NA	NA	25.8	4.70	NA
17W FLKS OS2-13	10/25/2016	8.70	0.010	NA	NA	26.3	4.75	NA
17W FLKS OS2-14	10/19/2016	8.70	0.008	NA	NA	27.7	4.65	NA
17W FLKS OS2-15	10/12/2016	8.75	0.006	NA	NA	28.6	4.75	NA
17W FLKS OS2-16	10/5/2016	8.76	0.009	NA	NA	29.8	4.65	36.0
17W FLKS OS2-17	9/28/2016	8.77	0.007	NA	NA	30.5	4.60	37.0
17W FLKS OS2-18	9/23/2016	8.77	0.005	NA	NA	31.7	2.85	NA
17S FLKS OS2-1	7/29/2017	8.73	0.007	NA	NA	31.4	4.00	37.5

17S FLKS OS2-2	7/20/2017	8.72	0.007	NA	NA	31.4	5.30	NA
17S FLKS OS2-3	7/9/2017	8.73	0.010	NA	NA	30.9	5.30	NA
17S FLKS OS2-4	6/29/2017	8.76	0.008	NA	NA	30.6	5.35	NA
17S FLKS OS2-5	6/18/2017	8.77	0.015	NA	NA	29.5	5.40	37.0
17S FLKS OS2-6	6/8/2017	8.76	0.005	NA	NA	29.5	5.40	NA
17S FLKS OS2-7	5/28/2017	8.70	0.008	NA	NA	29.7	5.30	NA
17S FLKS OS2-8	5/20/2017	8.71	0.005	NA	NA	27.9	2.95	NA
17S FLKS OS2-9	5/13/2017	8.63	0.006	NA	NA	27.7	4.90	NA
17S FLKS OS2-10	5/3/2017	8.62	0.007	NA	NA	27.2	5.35	37.5
17S FLKS OS2-11	4/22/2017	8.67	0.006	NA	NA	25.5	5.15	NA
17S FLKS OS2-12	4/12/2017	8.66	0.007	NA	NA	24.9	5.00	NA
17S FLKS OS2-13	4/6/2017	8.68	0.006	NA	NA	26.9	1.30	NA
17S FLKS OS2-14	4/2/2017	8.69	0.006	NA	NA	26.4	2.70	37.5
17S FLKS OS2-15	3/29/2017	8.71	0.005	NA	NA	24.5	2.25	NA
17S FLKS OS2-16	3/24/2017	8.71	0.009	NA	NA	23.5	1.95	NA
17S FLKS OS2-17	3/20/2017	8.69	0.009	NA	NA	22.5	2.75	NA
17S FLKS OS2-18	3/13/2017	8.66	0.006	NA	NA	24.1	3.95	NA
17S FLKS OS2-19	3/4/2017	8.67	0.008	NA	NA	24.0	5.30	37.0
17S FLKS OS2-20	2/22/2017	8.69	0.012	NA	NA	24.0	5.35	NA
17S FLKS OS2-21	2/11/2017	8.69	0.006	NA	NA	24.1	5.30	NA
17S FLKS OS2-22	2/1/2017	8.65	0.008	NA	NA	22.1	5.30	NA
17S FLKS OS2-23	1/23/2017	8.68	0.009	NA	NA	23.8	3.82	NA
18S FLKS OS2-1	6/25/2018	8.75	0.005	NA	NA	30.8	4.85	35.5
18S FLKS OS2-2	6/17/2018	8.72	0.006	NA	NA	29.7	5.15	NA
18S FLKS OS2-3	6/9/2018	8.73	0.007	NA	NA	29.3	5.10	NA
18S FLKS OS2-4	6/1/2018	8.74	0.005	NA	NA	27.0	5.15	NA
18S FLKS OS2-5	5/24/2018	8.74	0.009	NA	NA	26.4	5.15	NA
18S FLKS OS2-6	5/15/2018	8.72	0.005	NA	NA	27.1	5.10	35.0
18S FLKS OS2-7	5/7/2018	8.76	0.006	NA	NA	26.8	5.20	NA
18S FLKS OS2-8	4/29/2018	8.74	0.003	NA	NA	27.5	5.10	NA
18S FLKS OS2-9	4/21/2018	8.75	0.007	NA	NA	26.3	5.10	NA
18S FLKS OS2-10	4/13/2018	8.73	0.007	NA	NA	27.2	5.10	NA

18S FLKS OS2-11	4/5/2018	8.73	0.005	NA	NA	25.8	5.10	35.5
18S FLKS OS2-12	3/28/2018	8.70	0.007	NA	NA	23.6	5.10	NA
18S FLKS OS2-13	3/20/2018	8.71	0.006	NA	NA	23.6	5.15	NA
18S FLKS OS2-14	3/12/2018	8.70	0.007	NA	NA	22.5	5.15	NA
18S FLKS OS2-15	3/4/2018	8.70	0.006	NA	NA	25.1	5.20	NA
18S FLKS OS2-16	2/24/2018	8.70	0.018	NA	NA	25.1	5.15	34.0
18S FLKS OS2-17	2/16/2018	8.70	0.015	NA	NA	24.9	5.10	NA
18S FLKS OS2-18	2/8/2018	8.70	0.012	NA	NA	23.8	5.10	34.0
18S FLKS OS2-19	1/31/2018	8.68	0.005	NA	NA	22.0	5.05	NA
18S FLKS OS2-20	1/23/2018	8.67	0.004	NA	NA	21.4	5.10	34.0
18S FLKS OS2-21	1/15/2018	8.68	0.009	NA	NA	21.5	5.15	NA
18S FLKS OS2-22	1/9/2018	8.68	0.006	NA	NA	21.6	1.26	NA
19W FLKS OS2-1	1/8/2019	8.68	0.010	NA	NA	23.8	4.55	36.0
19W FLKS OS2-2	12/30/2018	8.74	0.007	NA	NA	24.1	5.15	NA
19W FLKS OS2-3	12/21/2018	8.72	0.007	NA	NA	22.6	5.25	NA
19W FLKS OS2-4	12/11/2018	8.67	0.005	NA	NA	23.9	5.25	NA
19W FLKS OS2-5	12/2/2018	8.63	0.005	NA	NA	24.8	5.00	37.0
19W FLKS OS2-6	11/23/2018	8.59	0.008	NA	NA	26.3	5.25	NA
19W FLKS OS2-7	11/13/2018	8.61	0.003	NA	NA	27.5	5.20	NA
19W FLKS OS2-8	11/4/2018	8.63	0.010	NA	NA	26.8	5.25	NA
19W FLKS OS2-9	10/25/2018	8.66	0.008	NA	NA	28.1	5.25	NA
19W FLKS OS2-10	10/15/2018	8.66	0.009	NA	NA	28.9	5.30	37.0
19W FLKS OS2-11	10/6/2018	8.72	0.006	NA	NA	28.7	5.25	NA
19W FLKS OS2-12	9/26/2018	8.72	0.008	NA	NA	31.0	5.25	NA
19W FLKS OS2-13	9/17/2018	8.68	0.005	NA	NA	31.0	5.25	NA
19W FLKS OS2-14	9/7/2018	8.65	0.006	NA	NA	29.6	5.25	NA
19W FLKS OS2-15	8/28/2018	8.75	0.007	NA	NA	30.6	5.30	36.5
19W FLKS OS2-16	8/19/2018	8.78	0.006	NA	NA	31.1	5.25	NA
19W FLKS OS2-17	8/9/2018	8.75	0.007	NA	NA	30.6	5.25	NA
19W FLKS OS2-18	7/31/2018	8.85	0.004	NA	NA	31.3	4.40	36.0
19W FLKS OS2-19	7/23/2018	8.83	0.005	NA	NA	32.6	5.05	36.0
19W FLKS OS2-20	7/13/2018	8.78	0.003	NA	NA	32.0	4.95	36.0

19S FLKS OS2-1	4/30/2019	8.35	0.008	NA	NA	27.2	5.75	37.0
19S FLKS OS2-2	4/19/2019	8.50	0.007	NA	NA	26.9	5.50	NA
19S FLKS OS2-3	4/9/2019	8.51	0.007	NA	NA	26.6	5.50	NA
19S FLKS OS2-4	3/30/2019	8.57	0.009	NA	NA	24.9	5.50	NA
19S FLKS OS2-5	3/20/2019	8.65	0.006	NA	NA	25.0	5.50	NA
19S FLKS OS2-6	3/10/2019	8.65	0.003	NA	NA	25.9	5.50	36.0
19S FLKS OS2-7	2/28/2019	8.70	0.005	NA	NA	26.6	5.50	NA
19S FLKS OS2-8	2/18/2019	8.72	0.006	NA	NA	24.8	5.50	NA
19S FLKS OS2-9	2/8/2019	8.74	0.008	NA	NA	23.7	5.50	NA
19S FLKS OS2-10	1/29/2019	8.68	0.007	NA	NA	21.6	5.50	NA
19S FLKS OS2-11	1/19/2019	8.67	0.003	NA	NA	21.6	5.50	34.0
19S FLKS OS2-12	1/14/2019	8.66	0.007	NA	NA	NA	0.15	NA
17W FLKS OS3-1	1/17/2017	8.75	0.009	NA	NA	24.5	3.35	NA
17W FLKS OS3-2	1/12/2017	8.72	0.007	NA	NA	24.1	5.10	NA
17W FLKS OS3-3	1/5/2017	8.73	0.008	NA	NA	25.2	5.20	36.0
17W FLKS OS3-4	12/29/2016	8.72	0.012	NA	NA	25.9	5.35	NA
17W FLKS OS3-5	12/22/2016	8.71	0.005	NA	NA	26.0	5.35	NA
17W FLKS OS3-6	12/15/2016	8.72	0.004	NA	NA	26.0	5.35	NA
17W FLKS OS3-7	12/8/2016	8.74	0.010	NA	NA	26.2	5.35	NA
17W FLKS OS3-8	11/30/2016	8.67	0.006	NA	NA	26.1	5.40	33.0
17W FLKS OS3-9	11/23/2016	8.85	0.005	NA	NA	26.0	5.45	NA
17W FLKS OS3-10	11/16/2016	8.70	0.009	NA	NA	26.8	5.45	NA
17W FLKS OS3-11	11/9/2016	8.69	0.004	NA	NA	27.2	5.40	NA
17W FLKS OS3-12	11/2/2016	8.70	0.004	NA	NA	27.2	5.40	NA
17W FLKS OS3-13	10/26/2016	8.70	0.005	NA	NA	27.6	5.45	34.0
17W FLKS OS3-14	10/19/2016	8.69	0.004	NA	NA	28.5	5.40	NA
17W FLKS OS3-16	10/5/2016	8.73	0.006	NA	NA	29.5	5.40	NA
17W FLKS OS3-17	9/28/2016	8.71	0.002	NA	NA	30.1	5.45	NA
17W FLKS OS3-18	9/23/2016	8.72	0.005	NA	NA	30.5	2.15	NA
17S FLKS OS3-1	7/29/2017	8.73	0.006	NA	NA	30.8	5.80	36.5
17S FLKS OS3-2	7/21/2017	8.75	0.004	NA	NA	30.8	5.55	NA
17S FLKS OS3-3	7/14/2017	8.74	0.005	NA	NA	29.9	5.55	NA

17S FLKS OS3-4	7/6/2017	8.74	0.006	NA	NA	30.0	5.50	NA
17S FLKS OS3-5	6/29/2017	8.73	0.003	NA	NA	29.4	5.35	37.5
17S FLKS OS3-6	6/22/2017	8.71	0.007	NA	NA	28.8	5.50	NA
17S FLKS OS3-7	6/14/2017	8.73	0.010	NA	NA	28.8	5.55	NA
17S FLKS OS3-8	6/7/2017	8.72	0.009	NA	NA	28.7	5.55	NA
17S FLKS OS3-9	5/30/2017	8.71	0.009	NA	NA	28.4	5.55	NA
17S FLKS OS3-10	5/23/2017	8.70	0.009	NA	NA	27.9	5.55	37.5
17S FLKS OS3-11	5/15/2017	8.70	0.007	NA	NA	27.6	5.55	NA
17S FLKS OS3-12	5/8/2017	8.71	0.007	NA	NA	26.9	5.55	NA
17S FLKS OS3-13	4/30/2017	8.72	0.007	NA	NA	26.6	5.55	NA
17S FLKS OS3-14	4/23/2017	8.72	0.008	NA	NA	25.7	5.45	NA
17S FLKS OS3-15	4/16/2017	8.71	0.006	NA	NA	25.6	5.50	36.5
17S FLKS OS3-16	4/8/2017	8.70	0.009	NA	NA	25.5	5.45	NA
17S FLKS OS3-17	4/1/2017	8.71	0.007	NA	NA	25.8	5.45	NA
17S FLKS OS3-18	3/25/2017	8.70	0.008	NA	NA	24.0	5.50	NA
17S FLKS OS3-19	3/17/2017	8.70	0.010	NA	NA	23.7	5.45	NA
17S FLKS OS3-20	3/10/2017	8.71	0.012	NA	NA	24.5	5.60	37.5
17S FLKS OS3-21	3/2/2017	8.70	0.005	NA	NA	24.8	5.50	NA
17S FLKS OS3-22	2/23/2017	8.68	0.014	NA	NA	24.0	5.55	NA
17S FLKS OS3-23	2/16/2017	8.71	0.009	NA	NA	23.8	5.60	NA
17S FLKS OS3-24	2/8/2017	8.71	0.005	NA	NA	24.1	5.55	NA
17S FLKS OS3-25	2/1/2017	8.70	0.004	NA	NA	23.0	5.55	37.0
17S FLKS OS3-26	1/24/2017	8.70	0.008	NA	NA	24.1	5.55	37.0
17S FLKS OS3-27	1/20/2017	8.70	0.014	NA	NA	NA	0.69	NA
18S FLKS OS3-1	6/25/2018	8.75	0.004	NA	NA	29.8	4.05	35.5
18S FLKS OS3-2	6/18/2018	8.74	0.008	NA	NA	29.2	5.25	NA
18S FLKS OS3-3	6/9/2018	8.74	0.007	NA	NA	28.4	5.00	NA
18S FLKS OS3-4	6/1/2018	8.73	0.007	NA	NA	26.9	5.05	NA
18S FLKS OS3-5	5/24/2018	8.72	0.008	NA	NA	26.5	5.05	NA
18S FLKS OS3-6	5/16/2018	8.72	0.011	NA	NA	26.6	5.05	35.0
18S FLKS OS3-7	5/8/2018	8.69	0.006	NA	NA	26.3	5.00	NA
18S FLKS OS3-8	4/30/2018	8.71	0.006	NA	NA	26.5	5.05	NA

18S FLKS OS3-9	4/22/2018	8.71	0.008	NA	NA	26.1	5.05	NA
18S FLKS OS3-10	4/14/2018	8.71	0.006	NA	NA	25.9	5.05	NA
18S FLKS OS3-11	4/6/2018	8.70	0.007	NA	NA	25.6	5.05	34.0
18S FLKS OS3-12	3/28/2018	8.70	0.013	NA	NA	24.2	5.05	NA
18S FLKS OS3-13	3/20/2018	8.71	0.005	NA	NA	24.2	5.05	NA
18S FLKS OS3-14	3/12/2018	8.71	0.005	NA	NA	23.8	5.00	NA
18S FLKS OS3-15	3/4/2018	8.70	0.007	NA	NA	25.3	5.00	NA
18S FLKS OS3-16	2/24/2018	8.70	0.010	NA	NA	25.6	5.05	34.0
18S FLKS OS3-17	2/16/2018	8.71	0.006	NA	NA	24.9	5.05	34.0
18S FLKS OS3-18	2/8/2018	8.71	0.004	NA	NA	24.1	5.00	NA
18S FLKS OS3-19	1/31/2018	8.71	0.004	NA	NA	23.5	5.10	34.0
18S FLKS OS3-20	1/23/2018	8.71	0.008	NA	NA	22.8	4.95	NA
18S FLKS OS3-21	1/15/2018	8.69	0.004	NA	NA	22.7	5.05	34.0
18S FLKS OS3-22	1/9/2018	8.68	0.005	NA	NA	23.0	1.22	NA
19W FLKS OS3-1	1/11/2019	8.75	0.006	NA	NA	23.6	1.10	NA
19W FLKS OS3-2	1/4/2019	8.77	0.010	NA	NA	24.8	5.85	33.5
19W FLKS OS3-3	12/23/2018	8.75	0.009	NA	NA	23.3	5.40	NA
19W FLKS OS3-4	12/12/2018	8.69	0.010	NA	NA	25.2	5.35	NA
19W FLKS OS3-5	12/1/2018	8.64	0.004	NA	NA	26.0	5.85	35.0
19W FLKS OS3-6	11/19/2018	8.65	0.003	NA	NA	27.0	5.70	35.0
19W FLKS OS3-7	11/7/2018	8.68	0.012	NA	NA	27.6	5.75	NA
19W FLKS OS3-8	10/26/2018	8.68	0.005	NA	NA	27.9	5.70	NA
19W FLKS OS3-9	10/14/2018	8.72	0.003	NA	NA	28.7	5.45	NA
19W FLKS OS3-10	10/3/2018	8.71	0.007	NA	NA	29.2	5.45	36.0
19W FLKS OS3-11	9/22/2018	8.68	0.005	NA	NA	30.6	5.45	NA
19W FLKS OS3-12	9/10/2018	8.69	0.005	NA	NA	29.6	5.45	NA
19W FLKS OS3-13	8/30/2018	8.78	0.002	NA	NA	29.9	5.40	NA
19W FLKS OS3-14	8/19/2018	8.84	0.004	NA	NA	30.8	5.40	NA
19W FLKS OS3-15	8/8/2018	8.71	0.007	NA	NA	30.1	5.45	36.5
19W FLKS OS3-16	7/28/2018	8.80	0.011	NA	NA	31.4	5.40	NA
19W FLKS OS3-17	7/16/2018	8.71	0.008	NA	NA	31.3	5.50	NA
19S FLKS OS3-1	8/9/2019	8.73	0.008	NA	NA	30.5	5.25	35.5

19S FLKS OS3-2	8/1/2019	8.71	0.005	NA	NA	30.5	4.90	NA
19S FLKS OS3-3	7/24/2019	8.72	0.006	NA	NA	30.6	4.90	NA
19S FLKS OS3-4	7/17/2019	8.66	0.007	NA	NA	30.3	4.90	NA
19S FLKS OS3-5	7/10/2019	8.70	0.004	NA	NA	30.7	5.00	NA
19S FLKS OS3-6	7/2/2019	8.75	0.008	NA	NA	30.0	5.10	36.0
19S FLKS OS3-7	6/24/2019	8.72	0.008	NA	NA	29.8	5.10	NA
19S FLKS OS3-8	6/17/2019	8.71	0.005	NA	NA	29.6	5.10	NA
19S FLKS OS3-9	6/9/2019	8.76	0.006	NA	NA	30.0	5.10	NA
19S FLKS OS3-10	6/1/2019	8.77	0.005	NA	NA	28.2	5.00	NA
19S FLKS OS3-11	5/25/2019	8.64	0.007	NA	NA	27.8	5.00	36.0
19S FLKS OS3-12	5/17/2019	8.66	0.007	NA	NA	28.1	5.10	NA
19S FLKS OS3-13	5/9/2019	8.66	0.005	NA	NA	27.9	5.10	NA
19S FLKS OS3-14	5/2/2019	8.64	0.005	NA	NA	26.6	5.10	NA
19S FLKS OS3-15	4/24/2019	8.63	0.008	NA	NA	26.3	5.10	NA
19S FLKS OS3-16	4/16/2019	8.62	0.007	NA	NA	26.7	5.10	36.0
19S FLKS OS3-17	4/9/2019	8.60	0.003	NA	NA	26.1	5.10	NA
19S FLKS OS3-18	4/1/2019	8.67	0.009	NA	NA	25.2	5.10	NA
19S FLKS OS3-19	3/24/2019	8.63	0.010	NA	NA	25.0	5.10	NA
19S FLKS OS3-20	3/16/2019	8.63	0.004	NA	NA	25.8	5.50	NA
19S FLKS OS3-21	3/8/2019	8.64	0.005	NA	NA	25.7	5.50	36.0
19S FLKS OS3-22	2/28/2019	8.69	0.005	NA	NA	26.0	5.50	NA
19S FLKS OS3-23	2/19/2019	8.75	0.007	NA	NA	25.2	5.50	35.5
19S FLKS OS3-24	2/11/2019	8.73	0.008	NA	NA	24.7	5.50	NA
19S FLKS OS3-25	2/3/2019	8.71	0.007	NA	NA	23.1	5.50	35.5
19S FLKS OS3-26	1/26/2019	8.71	0.006	NA	NA	23.2	5.10	NA
19S FLKS OS3-27	1/18/2019	8.71	0.004	NA	NA	23.0	5.10	NA
19S FLKS OS3-28	1/14/2019	8.71	0.012	NA	NA	NA	0.41	NA
17S FLKS OS4-1	7/30/2017	8.59	0.013	NA	NA	30.5	4.85	36.0
17S FLKS OS4-2	7/23/2017	8.67	0.006	NA	NA	30.2	5.05	NA
17S FLKS OS4-3	7/16/2017	8.66	0.006	NA	NA	29.7	5.30	NA
17S FLKS OS4-4	7/9/2017	8.68	0.008	NA	NA	29.7	4.90	NA
17S FLKS OS4-5	7/1/2017	8.64	0.012	NA	NA	29.1	5.35	37.0

17S FLKS OS4-6	6/24/2017	8.68	0.010	NA	NA	28.6	5.30	NA
17S FLKS OS4-7	6/16/2017	8.70	0.011	NA	NA	28.5	5.40	NA
17S FLKS OS4-8	6/9/2017	8.75	0.010	NA	NA	27.8	5.40	NA
17S FLKS OS4-9	6/1/2017	8.73	0.012	NA	NA	27.9	5.40	NA
17S FLKS OS4-10	5/25/2017	8.75	0.011	NA	NA	27.3	5.15	37.5
17S FLKS OS4-11	5/17/2017	8.74	0.011	NA	NA	27.5	5.35	NA
17S FLKS OS4-12	5/10/2017	8.75	0.007	NA	NA	26.2	5.35	NA
17S FLKS OS4-13	5/2/2017	8.72	0.007	NA	NA	26.4	5.35	NA
17S FLKS OS4-14	4/25/2017	8.71	0.005	NA	NA	25.5	5.35	NA
17S FLKS OS4-15	4/17/2017	8.71	0.008	NA	NA	25.8	5.45	37.0
17S FLKS OS4-16	4/10/2017	8.70	0.005	NA	NA	25.3	5.25	NA
17S FLKS OS4-17	4/2/2017	8.69	0.007	NA	NA	25.8	5.30	NA
17S FLKS OS4-18	3/26/2017	8.69	0.010	NA	NA	24.4	5.40	NA
17S FLKS OS4-19	3/18/2017	8.71	0.005	NA	NA	23.8	5.35	NA
17S FLKS OS4-20	3/11/2017	8.71	0.011	NA	NA	24.6	5.05	37.5
17S FLKS OS4-21	3/3/2017	8.71	0.005	NA	NA	24.9	5.35	NA
17S FLKS OS4-22	2/24/2017	8.72	0.011	NA	NA	23.9	5.35	NA
17S FLKS OS4-23	2/16/2017	8.70	0.005	NA	NA	23.6	5.30	NA
17S FLKS OS4-24	2/9/2017	8.71	0.010	NA	NA	24.1	5.35	NA
17S FLKS OS4-25	2/1/2017	8.69	0.010	NA	NA	23.6	5.35	37.5
17S FLKS OS4-26	1/25/2017	8.70	0.007	NA	NA	23.6	5.25	NA
17S FLKS OS4-27	1/21/2017	8.70	0.013	NA	NA	NA	0.40	NA
18S FLKS OS4-1	6/22/2018	8.76	0.011	0.76	0.03	28.6	5.95	36.0
18S FLKS OS4-2	6/10/2018	8.78	0.008	0.78	0.03	27.4	5.60	NA
18S FLKS OS4-3	5/29/2018	8.75	0.011	0.75	0.03	26.6	5.60	NA
18S FLKS OS4-4	5/17/2018	8.71	0.011	0.83	0.03	26.1	5.50	NA
18S FLKS OS4-5	5/5/2018	8.71	0.009	0.89	0.03	26.0	5.45	NA
18S FLKS OS4-6	4/24/2018	8.72	0.006	0.86	0.02	25.6	5.55	36.0
18S FLKS OS4-7	4/12/2018	8.71	0.004	0.83	0.02	25.2	5.50	NA
18S FLKS OS4-8	3/31/2018	8.68	0.006	0.81	0.03	24.6	5.50	NA
18S FLKS OS4-9	3/19/2018	8.69	0.010	0.71	0.02	23.9	5.55	NA
18S FLKS OS4-10	3/8/2018	8.71	0.007	0.77	0.02	24.7	5.55	NA

18S FLKS OS4-11	2/24/2018	8.72	0.012	0.80	0.02	25.5	5.40	35.5
18S FLKS OS4-12	2/12/2018	8.71	0.008	0.75	0.01	24.4	5.45	NA
18S FLKS OS4-13	2/1/2018	8.70	0.006	0.79	0.02	23.5	5.55	NA
18S FLKS OS4-14	1/20/2018	8.70	0.009	0.73	0.04	22.8	5.55	NA
18S FLKS OS4-15	1/11/2018	8.69	0.010	-2.83	0.04	23.1	2.52	NA
19W FLKS OS4-1	1/7/2019	8.73	0.006	1.14	0.02	24.6	5.35	33.0
19W FLKS OS4-2	12/28/2018	8.75	0.011	0.86	0.05	24.0	5.25	NA
19W FLKS OS4-3	12/17/2018	8.69	0.004	0.77	0.03	24.5	5.45	NA
19W FLKS OS4-4	12/6/2018	8.67	0.007	0.63	0.06	25.8	5.45	NA
19W FLKS OS4-5	11/26/2018	8.67	0.010	0.72	0.03	26.7	5.50	35.5
19W FLKS OS4-6	11/15/2018	8.66	0.008	0.69	0.06	27.4	5.45	NA
19W FLKS OS4-7	11/4/2018	8.65	0.009	0.78	0.03	27.7	5.50	NA
19W FLKS OS4-8	10/24/2018	8.64	0.007	0.74	0.04	28.1	5.50	NA
19W FLKS OS4-9	10/13/2018	8.65	0.013	0.78	0.03	28.6	5.45	NA
19W FLKS OS4-10	10/3/2018	8.63	0.009	0.70	0.07	29.2	5.50	35.5
19W FLKS OS4-11	9/22/2018	8.61	0.007	0.57	0.04	30.1	5.40	NA
19W FLKS OS4-12	9/11/2018	8.58	0.007	0.64	0.04	29.4	5.50	NA
19W FLKS OS4-13	8/31/2018	8.68	0.006	0.87	0.04	29.8	5.45	NA
19W FLKS OS4-14	8/21/2018	8.72	0.003	0.78	0.04	30.5	5.35	NA
19W FLKS OS4-15	8/10/2018	8.69	0.006	0.82	0.03	30.0	5.40	35.5
19W FLKS OS4-16	7/30/2018	8.74	0.009	0.85	0.03	30.3	5.35	NA
19W FLKS OS4-17	7/20/2018	8.73	0.003	0.79	0.05	30.1	5.45	NA
19W FLKS OS4-18	7/9/2018	8.70	0.005	0.65	0.03	30.0	5.35	35.5
19S FLKS OS4-1	7/5/2019	8.66	0.009	NA	NA	30.0	5.75	37.0
19S FLKS OS4-2	6/23/2019	8.62	0.008	NA	NA	29.1	5.75	NA
19S FLKS OS4-3	6/12/2019	8.57	0.007	NA	NA	28.3	5.25	NA
19S FLKS OS4-4	6/2/2019	8.58	0.011	NA	NA	27.8	5.25	NA
19S FLKS OS4-5	5/23/2019	8.58	0.007	NA	NA	27.8	5.25	NA
19S FLKS OS4-6	5/13/2019	8.59	0.010	NA	NA	27.1	4.25	36.0
19S FLKS OS4-7	5/7/2019	8.61	0.003	NA	NA	26.4	2.50	NA
19S FLKS OS4-8	4/30/2019	8.55	0.003	NA	NA	26.4	3.75	NA
19S FLKS OS4-9	4/22/2019	8.56	0.005	NA	NA	26.2	4.50	NA

19S FLKS OS4-10	4/12/2019	8.55	0.005	NA	NA	26.1	5.75	NA
19S FLKS OS4-11	4/1/2019	8.59	0.009	NA	NA	25.3	5.60	36.0
19S FLKS OS4-12	3/21/2019	8.61	0.010	NA	NA	25.4	5.60	NA
19S FLKS OS4-13	3/10/2019	8.61	0.005	NA	NA	25.6	5.60	NA
19S FLKS OS4-14	2/27/2019	8.60	0.012	NA	NA	25.8	5.60	NA
19S FLKS OS4-15	2/17/2019	8.60	0.006	NA	NA	25.1	4.50	NA
19S FLKS OS4-16	2/8/2019	8.66	0.012	NA	NA	24.3	4.00	36.0
19S FLKS OS4-17	2/3/2019	8.63	0.008	NA	NA	23.0	1.50	NA
19S FLKS OS4-18	1/31/2019	8.65	0.004	NA	NA	22.3	1.50	NA
19S FLKS OS4-19	1/27/2019	8.68	0.016	NA	NA	23.5	3.00	35.5
19S FLKS OS4-20	1/21/2019	8.68	0.012	NA	NA	23.4	3.00	36.0
19S FLKS OS4-21	1/16/2019	8.71	0.007	NA	NA	23.5	2.10	NA
19W ANEE OS-1	2/4/2019	8.60	0.008	0.89	0.02	26.2	4.70	35.0
19W ANEE OS-2	1/24/2019	8.61	0.006	0.57	0.06	26.3	5.10	NA
19W ANEE OS-3	1/13/2019	8.66	0.007	0.47	0.05	26.3	5.00	NA
19W ANEE OS-4	1/2/2019	8.63	0.010	0.61	0.04	26.5	5.05	NA
19W ANEE OS-5	12/22/2018	8.64	0.005	0.67	0.04	27.0	4.90	NA
19W ANEE OS-6	12/11/2018	8.59	0.005	0.58	0.04	27.3	5.00	34.0
19W ANEE OS-7	11/30/2018	8.63	0.007	0.61	0.03	27.9	5.00	NA
19W ANEE OS-8	11/19/2018	8.65	0.006	0.25	0.03	28.0	5.00	NA
19W ANEE OS-9	11/8/2018	8.60	0.008	0.37	0.04	28.2	5.10	NA
19W ANEE OS-10	10/27/2018	8.60	0.003	0.55	0.01	28.9	5.05	NA
19W ANEE OS-11	10/16/2018	8.63	0.005	0.70	0.04	28.6	5.05	35.0
19W ANEE OS-12	10/5/2018	8.59	0.009	0.58	0.04	29.0	4.95	NA
19W ANEE OS-13	9/24/2018	8.61	0.003	0.67	0.04	28.9	4.90	NA

19W ANEE OS-14	9/13/2018	8.68	0.007	0.73	0.04	29.1	5.20	NA
19W ANEE OS-15	9/1/2018	8.66	0.005	0.72	0.04	28.7	5.10	NA
19W ANEE OS-16	8/21/2018	8.63	0.007	0.76	0.03	28.8	5.10	35.5
19W ANEE OS-17	8/10/2018	8.63	0.004	0.85	0.05	28.7	5.15	NA
19W ANEE OS-18	7/29/2018	8.66	0.007	0.71	0.04	28.5	5.05	NA
19W ANEE OS-19	7/18/2018	8.66	0.006	0.68	0.02	28.3	5.15	NA
19W ANEE OS-20	7/7/2018	8.66	0.007	0.82	0.02	28.2	5.05	NA
19W ANEE OS-21	6/26/2018	8.65	0.006	0.76	0.03	28.0	4.90	35.5
19W ANEE OS-22	6/14/2018	8.69	0.005	0.84	0.05	28.1	5.20	NA
19W ANEE OS-23	6/3/2018	8.69	0.009	0.80	0.03	28.2	4.90	NA
19W ANEE OS-24	5/23/2018	8.69	0.008	0.86	0.04	27.4	5.00	NA
19W ANEE OS-25	5/12/2018	8.68	0.007	0.94	0.02	27.1	5.00	NA
19W ANEE OS-26	5/2/2018	8.69	0.005	0.89	0.02	27.0	4.05	NA
19W ANEE OS-27	4/23/2018	8.68	0.004	1.02	0.01	26.7	4.50	36.5
19W ANEE OS-28	4/12/2018	8.67	0.007	0.87	0.01	26.8	5.00	NA
19W ANEE OS-29	4/1/2018	8.68	0.008	0.85	0.03	26.6	4.70	NA
19W ANEE OS-30	3/21/2018	8.69	0.005	0.78	0.06	26.5	5.00	NA
19W ANEE OS-31	3/10/2018	8.69	0.008	0.87	0.02	26.2	4.95	36.5
19W ANEE OS-32	2/27/2018	8.68	0.005	0.64	0.04	26.1	5.00	NA
19W ANEE OS-33	2/16/2018	8.69	0.006	0.56	0.02	26.3	4.85	NA
19W ANEE OS-34	2/6/2018	8.69	0.010	0.54	0.03	26.5	4.90	36.0

19W ANEE OS-35	1/26/2018	8.67	0.009	0.59	0.01	26.7	4.85	NA
19W ANEE OS-36	1/18/2018	8.67	0.003	NA	NA	27.0	2.19	NA
19W STJN OS-1	2/1/2019	8.67	0.012	NA	NA	26.2	5.55	33.0
19W STJN OS-2	1/27/2019	8.63	0.013	NA	NA	26.2	5.25	NA
19W STJN OS-3	1/21/2019	8.66	0.006	NA	NA	26.4	5.25	NA
19W STJN OS-4	1/15/2019	8.67	0.012	NA	NA	26.4	5.30	NA
19W STJN OS-5	1/10/2019	8.69	0.019	NA	NA	26.0	5.25	NA
19W STJN OS-6	1/4/2019	8.66	0.014	NA	NA	26.0	5.35	34.0
19W STJN OS-7	12/29/2018	8.71	0.014	NA	NA	26.4	5.30	NA
19W STJN OS-8	12/23/2018	8.74	0.009	NA	NA	27.1	5.30	NA
19W STJN OS-9	12/18/2018	8.58	0.018	NA	NA	27.2	5.30	NA
19W STJN OS-10	12/12/2018	8.65	0.009	NA	NA	27.4	5.30	NA
19W STJN OS-11	12/6/2018	8.59	0.016	NA	NA	27.7	5.35	35.0
19W STJN OS-12	11/30/2018	8.70	0.007	NA	NA	28.2	5.30	NA
19W STJN OS-13	11/25/2018	8.64	0.010	NA	NA	27.9	5.25	NA
19W STJN OS-14	11/19/2018	8.51	0.008	NA	NA	27.8	5.20	NA
19W STJN OS-15	11/13/2018	8.43	0.014	NA	NA	28.4	5.25	NA
19W STJN OS-16	11/7/2018	8.14	0.016	NA	NA	28.2	5.40	35.0
19W STJN OS-17	11/3/2018	8.33	0.018	NA	NA	28.9	3.25	35.0
19W STJN OS-18	10/29/2018	8.49	0.016	NA	NA	29.4	4.90	NA
19W STJN OS-19	10/24/2018	8.62	0.008	NA	NA	29.0	5.15	NA
19W STJN OS-20	10/18/2018	8.60	0.011	NA	NA	28.6	4.85	NA
19W STJN OS-21	10/13/2018	8.67	0.008	NA	NA	28.5	5.05	36.5
19W STJN OS-22	10/8/2018	8.68	0.012	NA	NA	29.0	5.00	NA
19W STJN OS-23	10/2/2018	8.74	0.010	NA	NA	29.4	5.00	NA
19W STJN OS-24	9/27/2018	8.74	0.014	NA	NA	29.5	3.95	NA
19W STJN OS-25	9/23/2018	8.72	0.012	NA	NA	29.7	4.45	NA
19W STJN OS-26	9/18/2018	8.71	0.006	NA	NA	29.5	5.05	37.0
19W STJN OS-27	9/12/2018	8.74	0.005	NA	NA	29.6	5.05	NA
19W STJN OS-28	9/7/2018	8.70	0.006	NA	NA	29.6	4.95	NA
19W STJN OS-29	9/1/2018	8.72	0.008	NA	NA	28.8	5.00	NA

19W STJN OS-30	8/27/2018	8.92	0.005	NA	NA	29.7	5.00	NA
19W STJN OS-31	8/22/2018	8.71	0.010	NA	NA	29.7	5.05	36.5
19W STJN OS-32	8/16/2018	8.67	0.007	NA	NA	29.8	5.05	NA
19W STJN OS-33	8/11/2018	8.63	0.005	NA	NA	29.6	5.05	NA
19W STJN OS-34	8/5/2018	8.68	0.010	NA	NA	29.3	5.05	NA
19W STJN OS-35	7/31/2018	8.76	0.006	NA	NA	29.4	5.05	NA
19W STJN OS-36	7/26/2018	8.68	0.007	NA	NA	29.2	4.50	36.0
19W STJN OS-37	7/22/2018	8.65	0.007	NA	NA	29.2	2.80	NA
19W STJN OS-38	7/17/2018	8.67	0.011	NA	NA	29.0	5.05	NA
19W STJN OS-39	7/12/2018	8.68	0.009	NA	NA	28.6	5.00	NA
19W STJN OS-40	7/7/2018	8.69	0.007	NA	NA	29.0	4.15	NA
19W STJN OS-41	7/3/2018	8.70	0.008	NA	NA	29.0	3.40	NA
19W STJN OS-42	6/30/2018	8.71	0.004	NA	NA	28.6	1.65	NA
19W STJN OS-43	6/29/2018	8.70	0.006	NA	NA	28.5	0.80	NA
19W STJN OS-44	6/26/2018	8.74	0.004	NA	NA	28.4	5.15	35.5
19W STJN OS-45	6/20/2018	8.73	0.009	NA	NA	28.9	5.15	NA
19W STJN OS-46	6/14/2018	8.74	0.009	NA	NA	29.0	5.15	NA
19W STJN OS-47	6/9/2018	8.72	0.011	NA	NA	29.0	5.10	NA
19W STJN OS-48	6/3/2018	8.72	0.005	NA	NA	28.6	5.15	NA
19W STJN OS-49	5/29/2018	8.73	0.005	NA	NA	28.4	5.15	NA
19W STJN OS-50	5/23/2018	8.76	0.004	NA	NA	27.9	5.15	NA
19W STJN OS-51	5/18/2018	8.75	0.005	NA	NA	27.7	5.10	34.0
19W STJN OS-52	5/12/2018	8.74	0.008	NA	NA	27.8	5.05	NA
19W STJN OS-53	5/7/2018	8.75	0.009	NA	NA	27.7	4.70	NA
19W STJN OS-54	5/2/2018	8.73	0.005	NA	NA	27.7	4.65	NA
19W STJN OS-55	4/26/2018	8.72	0.011	NA	NA	27.4	5.15	NA
19W STJN OS-56	4/21/2018	8.73	0.009	NA	NA	27.7	5.15	33.5
19W STJN OS-57	4/15/2018	8.73	0.004	NA	NA	27.6	5.15	NA
19W STJN OS-58	4/10/2018	8.73	0.006	NA	NA	28.0	5.10	NA
19W STJN OS-59	4/4/2018	8.73	0.007	NA	NA	27.4	4.85	NA
19W STJN OS-60	3/30/2018	8.72	0.007	NA	NA	27.0	4.80	NA
19W STJN OS-61	3/25/2018	8.72	0.005	NA	NA	27.7	4.70	33.5

19W STJN OS-62	3/20/2018	8.72	0.010	NA	NA	27.6	4.50	NA
19W STJN OS-63	3/15/2018	8.71	0.006	NA	NA	27.1	3.95	NA
19W STJN OS-64	3/10/2018	8.72	0.003	NA	NA	26.7	5.15	NA
19W STJN OS-65	3/6/2018	8.72	0.010	NA	NA	26.3	3.85	NA
19W STJN OS-66	3/3/2018	8.72	0.004	NA	NA	26.4	1.05	NA
19W STJN OS-67	3/2/2018	8.71	0.004	NA	NA	NA	0.20	NA
19W STJN OS-68	3/2/2018	8.70	0.006	NA	NA	NA	0.20	NA
19W STJN OS-69	3/2/2018	8.69	0.009	NA	NA	NA	0.15	NA
19W STJN OS-70	2/27/2018	8.69	0.009	NA	NA	25.9	5.45	34.0
19W STJN OS-71	2/21/2018	8.68	0.009	NA	NA	25.8	5.35	NA
19W STJN OS-72	2/15/2018	8.71	0.005	NA	NA	25.8	5.35	NA
19W STJN OS-73	2/10/2018	8.72	0.004	NA	NA	26.0	4.57	NA
19W STJN OS-72	2/15/18	8.71	0.005	NA	NA	25.8	5.35	NA
19W STJN OS-73	2/10/18	8.72	0.004	NA	NA	26.0	4.57	NA

Bibliography

Aguedjou, H. M. A., Dadou, I., Chaigneau, A., Morel, Y., & Alory, G. (2019). Eddies in the Tropical Atlantic Ocean and their seasonal variability. *Geophys. Res. Lett.*, *46*, 12156–12164. doi: 10.1029/2019GL083925

Alibert, C., Kinsley, L., Fallon, S. J., McCulloch, M. T., Berkelmans, R., & McAllister, F. (2003). Source of trace element variability in Great Barrier Reef corals affected by the Burdekin flood plumes. *Geochim. Cosmochim. Acta*, *67*, 231–246. doi: 10.1016/S0016-7037(02)01055-4

Andersson, P. S., Wasserburg, G. J., & Ingri, J. (1992). The sources and transport of Sr and Nd isotopes in the Baltic Sea. *Earth Planet. Sci. Lett.*, *113*, 459–472. doi: 10.1016/0012-821X(92)90124-E

Barry, R. G., & Chorley, R. J. (2009). *Atmosphere, weather and climate*, 1st ed. Routledge, London. doi: 10.4324/9780203871027

Basu, A. R., Jacobsen, S. B., Poreda, R. J., Dowling, C. B., & Aggarwal, P. K. (2001). Large groundwater strontium flux to the oceans from the Bengal Basin and the marine strontium isotope record. *Science*, *293*, 1470–1473. doi: 10.1126/science.1060524

Beck, J. W., Edwards, R. L., Ito, E., Taylor, F. W., Recy, J., Rougerie, F., Joannot, P., Henin, C. (1992). Sea-surface temperature from coral skeletal strontium/calcium ratios. *Science*, *257*, 644–647. doi: 10.1126/science.257.5070.644

Bernstein, R. E., Betzer, P. R., Feely, R. A., Byrne, R. H., Lamb, M. F., & Michaels, A. F. (1987). Acantharian fluxes and strontium to chlorinity ratios in the North Pacific Ocean. *Science*, *237*, 1490–1494. doi: 10.1126/science.237.4821.1490

Bernstein, R. E., Byrne, R. H., Betzer, P. R., & Greco, A. M. (1992). Morphologies and transformations of celestite in seawater: The role of acantharians in strontium and barium geochemistry. *Geochim. Cosmochim. Acta*, *56*, 3273–3279. doi: 10.1016/0016-7037(92)90304-2

Böhlke, J. K., Plummer, L. N., Busenberg, E., Coplen, T. B., Shinn, E. A., & Schlosser, P. (1999). *Origins, residence times, and nutrient sources of marine ground water beneath the Florida Keys and nearby offshore areas* (pp. 2-3, OF 99-0181). US Geological Survey, Boca Raton, FL.

Bouchez, J., Lajeunesse, E., Gaillardet, J., France-Lanord, C., Dutra-Maia, P., & Maurice, L. (2010). Turbulent mixing in the Amazon River: The isotopic memory of confluences. *Earth Planet. Sci. Lett.*, *290*, 37–43. doi: 10.1016/j.epsl.2009.11.054

Bowden, M. J., Fischmann, N., Cook, P., Woods, J., & Omasta, E. (1970). *Climate, water balance, and climatic change in the north-west Virgin Islands*. Caribbean Research Institute, St. Thomas, USVI.

Brand, U., & Veizer, J. (1980). Chemical diagenesis of a multicomponent carbonate system; 1, Trace elements. *J. Sediment. Res.*, *50*, 1219–1236. doi: 10.1306/212F7BB7-2B24-11D7-8648000102C1865D

Brennan, S. R., Fernandez, D. P., Mackey, G., Cerling, T. E., Bataille, C. P., Bowen, G. J., & Wooller, M. J. (2014). Strontium isotope variation and carbonate versus silicate weathering in rivers from across Alaska: Implications for provenance studies. *Chem. Geol.*, *389*, 167–181. doi: 10.1016/j.chemgeo.2014.08.018

Brown, B. E., & Dunne, R. P. (1980). Environmental controls of patch-reef growth and development. *Mar. Biol.*, *56*, 85–96. doi: 10.1007/BF00390598

Budd, D. A., & Vacher, H. L. (1991). Predicting the thickness of fresh-water lenses in carbonate paleo-islands. *J. Sed. Res.*, *61*, 43–53. doi: 10.1306/D4267681-2B26-11D7-8648000102C1865D

Burgman, R., Seager, R., Clement, A., & Herweijer, C. (2010). Role of tropical Pacific SSTs in global medieval hydroclimate: A modeling study. *Geophys. Res. Lett.*, *37*, L06705. doi: 10.1029/2009GL042239

Calvesbert, R. J. (1970). Climate of Puerto Rico and the US Virgin Islands. *Climatography of the United States.* (No. 60-52). Silver Spring, MD: US Department of Commerce, Environmental Science Services Administrations, Environmental Data Service.

Chérubin, L. M., & Richardson, P. L. (2007). Caribbean current variability and the influence of the Amazon and Orinoco freshwater plumes. *Deep Sea Res. I*, *54*, 1451–1473. doi: 10.1016/j.dsr.2007.04.021

Cohen, A. L., Layne, G. D., Hart, S. R., & Lobel, P. S. (2001). Kinetic control of skeletal Sr/Ca in a symbiotic coral: Implications for the paleotemperature proxy. *Paleoceanography*, *16*, 20–26. doi: 10.1029/1999PA000478

Cooper, L. W., Frey, K. E., Logvinova, C., Biasatti, D. M., & Grebmeier, J. M. (2016). Variations in the proportions of melted sea ice and runoff in surface waters of the Chukchi Sea: A retrospective analysis, 1990–2012, and analysis of the implications of melted sea ice in an under-ice bloom. *Deep-Sea Res. II*, *130*, 6–13. doi: 10.1016/j.dsr2.2016.04.014

Coplen, T. B. (1996). New guidelines for reporting stable hydrogen, carbon, and oxygen isotope-ratio data. *Geochim. Cosmochim. Acta*, *60*, 3359–3360. doi:

10.1016/0016-7037(96)00263-3

Corbett, D. R., Chanton, J., Burnett, W., Dillon, K., & Rutkowski, C. (1999). Patterns of groundwater discharge into Florida Bay. *Limnol. Oceanogr.*, *44*, 1045–1055. doi: 10.4319/lo.1999.44.4.1045

Corredor, J. E., & Morell, J. M. (2001). Seasonal variation of physical and biogeochemical features in eastern Caribbean Surface Water. *J. Geophys. Res. Oceans*, *106*, 4517–4525. doi: 10.1029/2000JC000291

Corrège, T. (2006). Sea surface temperature and salinity reconstruction from coral geochemical tracers. *Palaeogeogr. Palaeoclimatol. Palaeoecol.*, 232, 408–428. doi: 10.1016/j.palaeo.2005.10.014

Cosner, O. J. (1972). *Water in St. John, US Virgin Islands.* (pp. 1-49, OF 72-78). US Geological Survey, San Juan, PR. doi: 10.3133/ofr7278

D'Olivo, J. P., Sinclair, D. J., Rankenburg, K., & McCulloch, M. T. (2018). A universal multi-trace element calibration for reconstructing sea surface temperatures from long-lived Porites corals: Removing 'vital-effects.' *Geochim. Cosmochim. Acta*, *239*, 109–135. doi: 10.1016/j.gca.2018.07.035

Davis, K. A., Leichter, J. J., Hench, J. L., & Monismith, S. G. (2008). Effects of western boundary current dynamics on the internal wave field of the Southeast Florida shelf. *J. Geophys. Res. Oceans*, *113*, C09010. doi: 10.1029/2007JC004699

de Villiers, S., Shen, G. T., & Nelson, B. K. (1994). The SrCa-temperature relationship in coralline aragonite: Influence of variability in $(Sr/Ca)_{seawater}$ and skeletal growth parameters. *Geochim. Cosmochim. Acta*, *58*, 197–208. doi: 10.1016/0016-7037(94)90457-X

de Villiers, S., Nelson, B. K., & Chivas, A. R. (1995). Biological controls on coral Sr/Ca and $\delta^{18}O$ reconstructions of sea surface temperatures. *Science*, *269*, 1247–1249. doi: 10.1126/science.269.5228.1247

de Villiers, S. (1999). Seawater strontium and Sr/Ca variability in the Atlantic and Pacific oceans. *Earth Planet. Sci. Lett.*, *171*, 623–634. doi: 10.1016/S0012-821X(99)00174-0

de Villiers, S., Greaves, M., & Elderfield, H. (2002). An intensity ratio calibration method for the accurate determination of Mg/Ca and Sr/Ca of marine carbonates by ICP-AES. *Geochem. Geophys. Geosyst.*, *3*, 1001. doi: 10.1029/2001GC000169

DeLong, K. L., Flannery, J. A., Maupin, C. R., Poore, R. Z., & Quinn, T. M. (2011).

A coral Sr/Ca calibration and replication study of two massive corals from the Gulf of Mexico. *Palaeogeogr. Palaeoclimatol. Palaeoecol.*, *307*, 117–128. doi: 10.1016/j.palaeo.2011.05.005

DeLong, K. L., Quinn, T. M., Taylor, F. W., Shen, C. C., & Lin, K. (2013). Improving coral-base paleoclimate reconstructions by replicating 350 years of coral Sr/Ca variations. *Palaeogeogr. Palaeoclimatol. Palaeoecol.*, *373*, 6–24. doi: 10.1016/j.palaeo.2012.08.019

Dittmar W. (1884). Report on researches into the composition of ocean water collected by HMS Challenger during the years 1873–1876. In: J. Murray (Ed.) *Report on the Scientific Results of the Voyage of HMS Challenger: Physics and Chemistry* (Vol. 1, pp. 1–251). HM Stationery Office, London.

Dodd, J. R., & Crisp, E. L. (1982). Non-linear variation with salinity of Sr/Ca and Mg/Ca ratios in water and aragonitic bivalve shells and implications for paleosalinity studies. *Palaeogeogr. Palaeoclimatol. Palaeoecol.*, *38*, 45–56. doi: 10.1016/0031-0182(82)90063-3

Donnelly, T. W. (1966). Geology of St. Thomas and St. John, US Virgin Islands. In: H. H. Hess, Carol O. Bowin, Thomas W. Donnelly, John T. Whetten, E. R. Oxburgh (Eds.), *Caribbean Geological Investigations* (Vol. 98, pp. 85-176). Geological Society of America, Boulder, CO. doi: 10.1130/MEM98-p85

Duever, M. J., Meeder, J. F., Meeder, L. C., & McCollom, J. M. (1994). The climate of south Florida and its role in shaping the Everglades ecosystem. In: S. M. Davis, J. C. Ogden, & W. A. Park (Eds.), *Everglades: The ecosystem and its restoration* (pp. 225–248). Delray Beach, FL, USA: St. Lucie Press.

Dwyer, G., & Cronin, T. (2001). Ostracode shell chemistry as a paleosalinity proxy in Florida Bay. *Bulletin of American Paleontology*, *361*, 249–276.

Edmunds, P. J., & Gray, S. C. (2014). The effects of storms, heavy rain, and sedimentation on the shallow coral reefs of St. John, US Virgin Islands. *Hydrobiologia*, *734*, 143–158. doi: 10.1007/s10750-014-1876-7

Emile-Geay, J., Cobb, K. M., Carré, M., Braconnot, P., Leloup, J., Zhou, Y., Henderson, S.P., Corrége, T., McGregor, H.V., Collins, M. (2016). Links between tropical Pacific seasonal, interannual and orbital variability during the Holocene. *Nat. Geosci.*, *9*, 168–173. doi: 10.1038/ngeo2608

English, N. B., Quade, J., DeCelles, P. G., & Garzione, C. N. (2000). Geologic control of Sr and major element chemistry in Himalayan Rivers, Nepal. *Geochim. Cosmochim. Acta*, *64*, 2549–2566. doi: 10.1016/S0016-7037(00)00379-3

Epstein, S., & Mayeda, T. (1953). Variation of O^{18} content of waters from natural sources. *Geochim. Cosmochim. Acta*, *4*, 213–224. doi: 10.1016/0016-7037(53)90051-9

Felis, T., Pätzold, J., Loya, Y., Fine, M., Nawar, A. H., & Wefer, G. (2000). A coral oxygen isotope record from the northern Red Sea documenting NAO, ENSO, and North Pacific teleconnections on Middle East climate variability since the year 1750. *Paleoceanography*, *15*, 679–694. doi: 10.1029/1999PA000477

Felis, T., Ionita, M., Rimbu, N., Lohmann, G., & Kölling, M. (2018). Mild and arid climate in the eastern Sahara–Arabian Desert during the late Little Ice Age. *Geophys. Res. Lett.*, *45*, 7112–7119. doi: 10.1029/2018GL078617

Flannery, J. A., Richey, J. N., Thirumalai, K., Poore, R. Z., & DeLong, K. L. (2017). Multi-species coral Sr/Ca-based sea-surface temperature reconstruction using *Orbicella faveolata* and *Siderastrea siderea* from the Florida Straits. *Palaeogeogr. Palaeoclimatol. Palaeoecol.*, *466*, 100–109. doi: 10.1016/j.palaeo.2016.10.022

Forchhammer, G. (1865) On the composition of sea-water in the different parts of the ocean. *Phil. Trans. Royal Soc. London 155,* 203–262. doi: 10.1098/rstl.1865.0004

Fowell, S. E., Sandford, K., Stewart, J. A., Castillo, K. D., Ries, J. B., & Foster, G. L. (2016). Intrareef variations in Li/Mg and Sr/Ca sea surface temperature proxies in the Caribbean reef-building coral *Siderastrea siderea*. *Paleoceanography*, *31*, 1315–1329. doi: 10.1002/2016PA002968

Fratantoni, D. M., & Richardson, P. L. (2006). The evolution and demise of North Brazil Current rings. *J. Phys. Oceanogr.*, *36*, 1241–1264. doi: 10.1175/JPO2907.1

Froelich Jr, P. N., Atwood, D. K., & Giese, G. S. (1978). Influence of Amazon River discharge on surface salinity and dissolved silicate concentration in the Caribbean Sea. *Deep Sea Res.*, *25*, 735–744. doi: 10.1016/0146-6291(78)90627-6

Gagan, M. K., Ayliffe, L. K., Hopley, D., Cali, J. A., Mortimer, G. E., Chappell, J., McCulloch, M.T., Head, M. J. (1998). Temperature and surface-ocean water balance of the Mid-Holocene Tropical Western Pacific. *Science*, *279*, 1014 – 1018. doi: 10.1126/science.279.5353.1014

Gaillardet, J., Dupre, B., Allegre, C. J., & Négrel, P. (1997). Chemical and physical denudation in the Amazon River Basin. *Chem. Geol.*, *142*, 141–173. doi: 10.1016/S0009-2541(97)00074-0

Gelesh, L., Marshall, K., Boicourt, W., & Lapham, L. (2016). Methane concentrations increase in bottom waters during summertime anoxia in the highly eutrophic estuary, Chesapeake Bay, USA. *Limnol. Oceanogr.*, *61*, S253–S266. doi: 10.1002/lno.10272

Gillanders, B. M. (2005). Otolith chemistry to determine movements of diadromous and freshwater fish. *Aquat. Living Resour.*, *18*, 291–300. doi: 10.1051/alr:2005033

Goni, G. J., & Johns, W. E. (2001). A census of North Brazil Current rings observed from TOPEX/POSEIDON altimetry: 1992–1998. *Geophys. Res. Lett.*, *28*, 1–4. doi: 10.1029/2000GL011717

Gray, S. C., Sears, W., Kolupski, M. L., Hastings, Z. C., Przyuski, N. W., Fox, M. D., & DeGrood, A. (2012). Factors affecting land-based sedimentation in coastal bays, US Virgin Islands. *Proceedings of the 12th International Coral Reef Symposium*, 9-13 July. Cairns, AU.

Gray, W. M., Sheaffer, J. D., & Landsea, C. W. (1997). Climate trends associated with multidecadal variability of Atlantic hurricane activity. In: H. F. Diaz, R. S. Pulwarty (Eds.), *Hurricanes* (pp. 15–53). Springer, Berlin, Heidelberg, GER. doi: 10.1007/978-3-642-60672-4_2

Grodsky, S. A., Johnson, B. K., Carton, J. A., & Bryan, F. O. (2015). Interannual Caribbean salinity in satellite data and model simulations. *J. Geophys. Res. Oceans*, *120*, 1375–1387. doi: 10.1002/2014JC010625

Grottoli, A. G. (2001). Past climate from corals. In: J. H. Steele, S. A. Thorpe, & K. K. Turekian (Eds.), *Encyclopedia of Ocean Sciences* (1st ed., pp. 2098–2107). Netherlands: Academic Press. doi: 10.1006/rwos.2001.0270.

Grove, C. A., Kasper, S., Zinke, J., Pfeiffer, M., Garbe-Schönberg, D., & Brummer, G. A. (2013). Confounding effects of coral growth and high SST variability on skeletal Sr/Ca: Implications for coral paleothermometry. *Geochem. Geophys. Geosyst.*, *14*, 1277–1293. doi: 10.1002/ggge.20095

Guilderson, T. P., Fairbanks, R. G., & Rubenstone, J. L. (1994). Tropical temperature variations since 20,000 years ago: modulating interhemispheric climate change. *Science*, *263*, 663–665. doi: 10.1126/science.263.5147.663

Hackert, E., Kovach, R. M., Molod, A., Vernieres, G., Borovikov, A., Marshak, J., & Chang, Y. (2020). Satellite sea surface salinity observations impact on El Niño Southern Oscillation predictions: Case studies from the NASA GEOS Seasonal Forecast System. *J. Geophys. Res. Oceans*, *125*, e2019JC015788. doi: 10.1029/2019JC015788

Halley, R. B., Vacher, H. L., & Shinn, E. A. (1997). Geology and hydrogeology of the Florida Keys. In: L. H. L. Vacher & T. M. Quinn (Eds.), *Geology and hydrogeology of carbonate islands* (Vol. 54, pp. 217–248). Elsevier, Amsterdam. doi: 10.1016/S0070-4571(04)80027-X

Hamilton, G. D. (1986). National data buoy center programs. *Bull. Amer. Meteor. Soc.*, *67*, 411–415. doi: 10.1175/1520-0477(1986)067<0411:NDBCP>2.0.CO;2

Hartmann, J., Lauerwald, R., & Moosdorf, N. (2014). A brief overview of the GLObal RIver CHemistry Database, GLORICH. *Procedia Earth Planet. Sci.*, *10*, 23–27. doi: 10.1016/j.proeps.2014.08.005

Hastenrath, S. (1991) *Climate Dynamics of the Tropics,* updated edition. Kluwer Academic Publishers, Norwell, MA. doi: 10.1007/978-94-011-3156-8

He, H., Li, Y., Wang, S., Ma, Q. and Pan, Y. (2020) A high precision method for calcium determination in seawater using ion chromatography. *Front. Mar. Sci.* 7:231. doi: 10.3389/fmars.2020.00231

Hellweger, F. L., & Gordon, A. L. (2002). Tracing Amazon river water into the Caribbean Sea. *J. Mar. Res.*, *60*, 537–549. doi: 10.1357/002224002762324202

Hetzinger, S., Pfeiffer, M., Dullo, W.-C., Zinke, J., & Garbe-Schönberg, D. (2016). A change in coral extension rates and stable isotopes after El Niño-induced coral bleaching and regional stress events. *Sci. Rep.*, *6*, 32879. doi: 10.1038/srep32879

Hirabayashi, S., Yokoyama, Y., Suzuki, A., Kawakubo, Y., Miyairi, Y., Okai, T., & Nojima, S. (2013). Coral growth-rate insensitive Sr/Ca as a robust temperature recorder at the extreme latitudinal limits of *Porites*. *Geochem. J.*, *47*, e1–e5. doi: 10.2343/geochemj.2.0259

Horibe, Y., Endo, K., & Tsubota, H. (1974). Calcium in the South Pacific, and its correlation with carbonate alkalinity. *Earth Planet. Sci. Lett.*, *23*, 136–140. doi: 10.1016/0012-821X(74)90040-5

Hu, C., Montgomery, E. T., Schmitt, R. W., & Muller-Karger, F. E. (2004). The dispersal of the Amazon and Orinoco River water in the tropical Atlantic and Caribbean Sea: Observation from space and S-PALACE floats. *Deep-Sea Res. II*, *51*, 1151–1171. doi: 10.1016/S0967-0645(04)00105-5

Hughen, K. A., Schrag, D. P., Jacobsen, S. B., & Hantoro, W. (1999). El Niño during the last interglacial period recorded by a fossil coral from Indonesia. *Geophys. Res. Lett.*, *26*, 3129–3132. doi: 10.1029/1999GL006062

IPCC, 2014: *Climate Change 2014: Synthesis Report. Contribution of Working Groups I, II and III to the Fifth Assessment Report of the Intergovernmental Panel on Climate Change* [Core Writing Team, R.K. Pachauri and L.A. Meyer (eds.)]. IPCC, Geneva, Switzerland, 151 pp.

Jannasch, H. W., Wheat, C. G., Plant, J. N., Kastner, M., & Stakes, D. S. (2004). Continuous chemical monitoring with osmotically pumped water samplers: OsmoSampler design and applications. *Limnol. Oceanogr. Meth.*, *2*, 102–113. doi: 10.4319/lom.2004.2.102

Johns, W. E., Lee, T. N., Beardsley, R. C., Candela, J., Limeburner, R., & Castro, B. (1998). Annual cycle and variability of the North Brazil Current. *J. Phys. Oceanogr.*, *28*, 103–128. doi: 10.1175/1520-0485(1998)028<0103:ACAVOT>2.0.CO;2

Johns, W. E., Lee, T. N., Schott, F. A., Zantopp, R. J., & Evans, R. H. (1990). The North Brazil Current retroflection: Seasonal structure and eddy variability. *J. Geophys. Res. Oceans*, *95*, 22,103–22,120. doi: 10.1029/JC095iC12p22103

Johns, W. E., Townsend, T. L., Fratantoni, D. M., & Wilson, W. D. (2002). On the Atlantic inflow to the Caribbean Sea. *Deep-Sea Res. I*, *49*, 211–243. doi: 10.1016/S0967-0637(01)00041-3

Jones, P. D., Briffa, K. R., Osborn, T. J., Lough, J. M., van Ommen, T. D., Vinther, B. M., Luterbacher, J., Wahl, E. R., Zwiers, F. W., Mann, M. E., Schmidt, G. A., Ammann, C. M., Buckley, B. M., Cobb, K. M., Esper, J. et al. (2009). High-resolution palaeoclimatology of the last millennium: a review of current status and future prospects. *The Holocene*, *19*, 3–49. doi: 10.1177/0959683608098952

Katz, A., Sass, E., Starinsky, A., & Holland, H. D. (1972). Strontium behavior in the aragonite-calcite transformation: An experimental study at 40–98ºC. *Geochim. Cosmochim. Acta*, *36*, 481–496. doi: 10.1016/0016-7037(72)90037-3

Kennedy, J. J., Rayner, N. A., Smith, R. O., Parker, D. E., & Saunby, M. (2011). Reassessing biases and other uncertainties in sea surface temperature observations measured in situ since 1850: 2. Biases and homogenization. *J. Geophys. Res.*, *116*, D14104. doi: 10.1029/2010JD015220

Kerr, Y. H., Waldteufel, P., Wigneron, J.-P., Delwart, S., Cabot, F., Boutin, J., Escorihuela, M. -J., Font, J., Reul, N., Gruhier, C. (2010). The SMOS mission: New tool for monitoring key elements of the global water cycle. *Proceedings of the IEEE*, *98*, 666–687. doi: 10.1109/JPROC.2010.2043032

Khare, A. (2018). *Potential Impact of Variation in the Seawater Strontium to Calcium Ratio on Coral Paleothermometry in the Florida Keys, USA,* (master's thesis). Retrieved from DRUM. (https://drum.lib.umd.edu/bitstream/handle/1903/21397/Khare_umd_0117N_19217.pdf?sequence=2). Solomons, MD: University of Maryland Center for Environmental Science.

Khaska, M., La Salle, C. L. G., Lancelot, J., Mohamad, A., Verdoux, P., Noret, A., & Simler, R. (2013). Origin of groundwater salinity (current seawater vs. saline deep water) in a coastal karst aquifer based on Sr and Cl isotopes. Case study of the La Clape massif (southern France). *Appl. Geochem.*, *37*, 212–227. doi: 10.1016/j.apgeochem.2013.07.006

Kilbourne, K. H., Quinn, T. M., Taylor, F. W., Delcroix, T., & Gouriou, Y. (2004). El Niño-Southern Oscillation-related salinity variations recorded in the skeletal geochemistry of a *Porites* coral from Espiritu Santo, Vanuatu. *Paleoceanography*, *19*, 1–8. doi: 10.1029/2004PA001033

Kinsman, D. J., & Holland, H. (1969). The co-precipitation of cations with $CaCO_3$ – IV. The co-precipitation of Sr^{2+} with aragonite between 16 and 96ºC. *Geochim. Cosmochim. Acta*, *33*, 1–17. doi: 10.1016/0016-7037(69)90089-1

Kottek, M., Grieser, J., Beck, C., Rudolf, B., & Rubel, F. (2006). World map of the Köppen-Geiger climate classification updated. *Meteorol. Z.*, *15*, 259–263. doi: 10.1127/0941-2948/2006/0130

Kourafalou, V. H., & Kang, H. (2012). Florida Current meandering and evolution of cyclonic eddies along the Florida Keys Reef Tract: Are they interconnected? *J. Geophys. Res. Oceans*, *117*, C05028. doi: 10.1029/2011JC007383

Kuffner, I. B., Hickey, T. D., & Morrison, J. M. (2013). Calcification rates of the massive coral *Siderastrea siderea* and crustose coralline algae along the Florida Keys (USA) outer-reef tract. *Coral Reefs*, *32*, 987–997. doi: 10.1007/s00338-013-1047-8

Kuffner, I. B., Jokiel, P. L., Rodgers, K. S., Andersson, A. J., & Mackenzie, F. T. (2012). An apparent "vital effect" of calcification rate on the Sr/Ca temperature proxy in the reef coral *Montipora capitata*. *Geochem. Geophys. Geosyst.*, *13*, Q08004. doi: 10.1029/2012GC004128

Leder, J. J., Swart, P. K., Szmant, A. M., & Dodge, R. E. (1996). The origin of variations in the isotopic record of scleractinian corals: I. Oxygen. *Geochim. Cosmochim. Acta*, *60*, 2857–2870. doi: 10.1016/0016-7037(96)00118-4

Lee, T. N. (1986). Coastal circulation in the Key Largo coral reef marine sanctuary. In J. van de Kreeke (Ed.), *Physics of shallow estuaries and bays* (pp. 178–198). doi: 10.1029/LN016p0178

Lee, T. N., Rooth, C., Williams, E., McGowan, M., Szmant, A. F., & Clarke, M. E. (1992). Influence of Florida Current, gyres and wind-driven circulation on transport of larvae and recruitment in the Florida Keys coral reefs. *Cont. Shelf Res.*, *12*, 971–1002. doi: 10.1016/0278-4343(92)90055-O

Lee, T. N., Clarke, M. E., Williams, E., Szmant, A. F., & Berger, T. (1994). Evolution of the Tortugas Gyre and its influence on recruitment in the Florida Keys. *Bull. Mar. Sci.*, *54*, 621–646.

Lee, T. N., & Williams, E. (1999). Mean distribution and seasonal variability of coastal currents and temperature in the Florida Keys with implications for larval recruitment. *Bull. Mar. Sci.*, *64*, 35–56.

Leichter, J. J., Stewart, H. L., & Miller, S. L. (2003). Episodic nutrient transport to Florida coral reefs. *Limnol. Oceanogr.*, *48*, 1394–1407. doi: 10.4319/lo.2003.48.4.1394

Lerouge, C., Gaucher, E. C., Tournassat, C., Négrel, P., Crouzet, C., Guerrot, C., Gautier, A., Michel, P., Vinsot, A., Buschaert, S. (2010). Strontium distribution and origins in a natural clayey formation (Callovian-Oxfordian, Paris Basin, France): A new sequential extraction procedure. *Geochim. Cosmochim. Acta*, *74*, 2926–2942. doi: 10.1016/j.gca.2010.02.013

Levene, H. (1960). Robust tests for equality of variances. In: I. Olkin (Ed.), *Contributions to Probability and Statistics* (pp. 278–292). Standford, CA: Stanford University Press.

Liu, X.-M., Hardisty, D. S., Lyons, T. W., & Swart, P. K. (2019). Evaluating the fidelity of the cerium paleoredox tracer during variable carbonate diagenesis on the Great Bahamas Bank. *Geochim. Cosmochim. Acta*, *248*, 25–42. doi: 10.1016/j.gca.2018.12.028

Lloyd, R. M. (1964). Variations in the oxygen and carbon isotope ratios of Florida Bay mollusks and their environmental significance. *J. Geol.*, *72*, 84–111. doi: 10.1086/626966

Lough, J. M. (2012). Small change, big difference: Sea surface temperature distributions for tropical coral reef ecosystems, 1950–2011. *J. Geophys. Res. Oceans*, *117*, C09018. doi: 10.1029/2012JC008199

Lubarsky, K. A., Silbiger, N. J., & Donahue, M. J. (2018). Effects of submarine groundwater discharge on coral accretion and bioerosion on two shallow reef flats. *Limnol. Oceanogr.*, *63*, 1660–1676. doi: 10.1002/lno.10799

Macdonald, J. I., & Crook, D. A. (2010). Variability in Sr: Ca and Ba: Ca ratios in water and fish otoliths across an estuarine salinity gradient. *Mar. Ecol. Prog. Ser.*, *413*, 147–161. doi: 10.3354/meps08703

Mackenzie, F. T., & Garrels, R. M. (1966). Chemical mass balance between rivers and oceans. *Amer. J. Sci*, *264*, 507–525. doi: 10.2475/ajs.264.7.507

Malone, M. J., & Baker, P. A. (1999). Temperature dependence of the strontium distribution coefficient in calcite; an experimental study from 40º to 200ºC and application to natural diagenetic calcites. *J. Sediment. Res.*, *69*, 216–223. doi: 10.2110/jsr.69.216

Mann, M. E., Zhang, Z., Rutherford, S., Bradley, R. S., Hughes, M. K., Shindell, D., Ammann, C., Faluvegi, G., Ni, F. (2009). Global signatures and dynamical origins of the Little Ice Age and Medieval Climate Anomaly. *Science*, *326*, 1256–1260. doi: 10.1126/science.1177303

Mann, M. E., Steinman, B. A., & Miller, S. K. (2020). Absence of internal multidecadal and interdecadal oscillations in climate model simulations. *Nat. Commun.*, *11*, 1–9. doi: 10.1038/s41467-019-13823-w

Martin-Kaye, P. H. A. (1959). *Reports on the Geology of the Leeward and the British Virgin Islands*. Voice Publishing Company, St. Lucia.

Mather, J. D. (1988). *The influence of geology and karst development on the formation of freshwater lenses on small limestone islands.* Paper presented at the IAH 21st Congress, British Geological Survey, London, UK.

Maupin, C. R., Quinn, T. M., & Halley, R. B. (2008). Extracting a climate signal from the skeletal geochemistry of the Caribbean coral *Siderastrea siderea*. *Geochem. Geophys. Geosyst.*, *9*, Q12012. doi: 10.1029/2008GC002106

McPhaden, M. J., Busalacchi, A. J., Cheney, R., Donguy, J.-R., Gage, K. S., Halpern, D., Ming, J., Julian, P., Meyers, G., Mitchum, G. T., Niiler, P. P., Picaut, J., Reynolds., R. W., Smith, N., Takeuchi, K. (1998). The Tropical Ocean-Global Atmosphere observing system: A decade of progress. *J. Geophys. Res. Oceans*, *103*, 14169–14240. doi: 10.1029/97JC02906

Mecklenburg, S., Drusch, M., Kerr, Y. H., Font, J., Martin-Neira, M., Delwart, S., Buenadicha, G., Reul, N., Daganzo-Eusebio, E., Oliva, R. (2012). ESA's soil moisture and ocean salinity mission: Mission performance and operations. *IEEE Transactions on Geoscience and Remote Sensing*, *50*, 1354–1366. doi: 10.1109/TGRS.2012.2187666

Meibom, A., Yurimoto, H., Cuif, J., Domart-Coulon, I., Houlbreque, F., Constantz, B., Dauphin, Y., Tambutté, E., Tambutté, S., Allemand, D. (2006). Vital effects in coral skeletal composition display strict three-dimensional control. *Geophys. Res. Lett.*, *33*, L11608. doi: 10.1029/2006GL025968

Millero, F. J., Hiscock, W. T., Huang, F., Roche, M., & Zhang, J. Z. (2001). Seasonal variation of the carbonate system in Florida Bay. *Bull. Mar. Sci.*, *68*, 101–123.

Morice, C. P., Kennedy, J. J., Rayner, N. A., & Jones, P. D. (2012). Quantifying uncertainties in global and regional temperature change using an ensemble of observational estimates: The HadCRUT4 data set. *J. Geophys. Res.*, *117*, D08101. doi: 10.1029/2011JD017187

Muehllehner, N., Langdon, C., Venti, A., & Kadko, D. (2016). Dynamics of carbonate chemistry, production, and calcification of the Florida Reef Tract (2009–2010): Evidence for seasonal dissolution. *Global Biogeochem. Cycles*, *30*, 661–688. doi: 10.1002/2015GB005327

Müller-Karger, F. E., McClain, C. R., Fisher, T. R., Esaias, W. E., & Varela, R. (1989). Pigment distribution in the Caribbean Sea: Observations from space. *Prog. Oceanogr.*, *23*, 23–64. doi: 10.1016/0079-6611(89)90024-4

Nelson, J. E., & Ginsburg, R. N. (1986). Calcium carbonate production by epibionts on *Thalassia* in Florida Bay. *J. Sediment. Petrol.*, *56*, 622–628. doi: 10.1306/212F89EF-2B24-11D7-8648000102C1865D

Nikiema, O., Devenon, J.-L., & Baklouti, M. (2007). Numerical modeling of the Amazon River plume. *Cont. Shelf Res.*, *27*, 873–899. doi: 10.1016/j.csr.2006.12.004

Olesik, J. W. (1991). Elemental analysis using ICP-OES and ICP/MS. *Anal. Chem.*, *63*, 12A-21A. doi: 10.1021/ac00001a711

Paul, J. H., Rose, J. B., Jiang, S. C., Zhou, X., Cochran, P., Kellogg, C., Kang, J. B., Griffin, D., Farrah, S., Lukasik, J. (1997). Evidence for groundwater and surface marine water contamination by waste disposal wells in the Florida Keys. *Water Res.*, *31*, 1448–1454. doi: 10.1016/S0043-1354(96)00374-0

Paytan, A., Shellenbarger, G. G., Street, J. H., Gonneea, M. E., Davis, K., Young, M. B., & Moore, W. S. (2006). Submarine groundwater discharge: An important source of new inorganic nitrogen to coral reef ecosystems. *Limnol. Oceanogr.*, *51*, 343–348. doi: 10.4319/lo.2006.51.1.0343

Peixoto, J. P., & Oort, A. H. (1992). *Physics of climate*, 520 pp. New York, NY, USA: American Institute of Physics. doi: 10.1063/1.2809772

Philander, S. G. (1990). *El Niño, La Niña, and the Southern Oscillation*, 293 pp. San Diego, CA: Academic Press.

Pilson, M. E. Q. (2012). *An Introduction to the Chemistry of the Sea* (2nd ed.) New York, NY, USA: Cambridge University Press.

Pitts, P. A. (1994). An investigation of near-bottom flow patterns along and across Hawk Channel, Florida Keys. *Bull. Mar. Sci.*, *54*, 610–620.

Prat, O. P., & Nelson, B. R. (2013). Precipitation contribution of tropical cyclones in the southeastern United States from 1998 to 2009 using TRMM satellite data. *J. Clim.*, *26*, 1047–1062. doi: 10.1175/JCLI-D-11-00736.1

Quinn, T. M., Taylor, F. W., & Crowley, T. J. (2006). Coral-based climate variability in the Western Pacific Warm Pool since 1867. *J. Geophys. Res. Oceans*, *111*, C11006. doi: 10.1029/2005JC003243

Rankin, D. W. (2002). *Geology of St. John, US Virgin Islands* (Rep. USGS 1631). US Geological Survey, Reston, VA. doi: 10.3133/pp1631

Rayner, N., Parker, D. E., Folland, C. K., Horton, E. B., Alexander, L. V, & Rowell, D. P. (2003). The global sea-ice and sea surface temperature (HadISST) data sets. *J. Geophys. Res.*, *108*, 4407. doi: 10.1029/2002JD002670

Reges, H. W., Doesken, N., Turner, J., Newman, N., Bergantino, A., & Schwalbe, Z. (2016). CoCoRaHS: The evolution and accomplishments of a volunteer rain gauge network. *Bull. Amer. Meteor. Soc.*, *97*, 1831–1846. doi: 10.1175/BAMS-D-14-00213.1

Reich, C. D., Shinn, E. A., Hickey, T. D., & Tihansky, A. B. (2002). Tidal and meteorological influences on shallow marine groundwater flow in the upper Florida Keys. In: J. W. Porter & K. G. Porter (Eds.), *The Everglades, Florida Bay, and coral reefs of the Florida Keys* (pp. 659–676). doi: 10.1201/9781420039412-30

Reich, C. D., Kuffner, I. B., Hickey, T. D., Morrison, J. M., & Flannery, J. A. (2013). *Complexity of nearshore strontium-to-calcium ratio variability in a core sample of the massive coral Siderastrea siderea obtained in Coral Bay, St. John, U.S. Virgin Islands* (OF 2013-1092). US Geological Survey, Reston, VA. doi: 10.3133/ofr20131092

Robins, N. S. (2012). Island hydrogeology: Highlights from early experience in the West Indies and Bermuda. In: N. Howden & J. Mather (Eds.), *History of Hydrogeology* (1st ed., pp. 29–40). CRC Press, Boca Raton, FL.

Ross, C. L., DeCarlo, T. M., & McCulloch, M. T. (2019). Calibration of Sr/Ca, Li/Mg and Sr-U paleothermometry in branching and foliose corals. *Paleoceanogr. Paleoclimatol.*, *34*, 1271–1291. doi: 10.1029/2018PA003426

Saenger, C., Cohen, A. L., Oppo, D. W., & Hubbard, D. (2008). Interpreting sea surface temperature from strontium/calcium ratios in *Montastraea* corals: Link with growth rate and implications for proxy reconstructions. *Paleoceanography*, *23*, PA3102. doi: 10.1029/2007PA001572

Schijf, J., & Byrne, R. H. (2007). Progressive dolomitization of Florida limestone recorded by alkaline earth element concentrations in saline, geothermal, submarine springs. *J. Geophys. Res. Oceans*, *112*, C01003. doi: 10.1029/2006JC003659

Schmuker, B., & Schiebel, R. (2002). Planktic foraminifers and hydrography of the eastern and northern Caribbean Sea. *Mar. Micropaleontol.*, *46*, 387–403. doi: 10.1016/S0377-8398(02)00082-8

Schneider, K., Levy, O., Dubinsky, Z., & Erez, J. (2009). In situ diel cycles of photosynthesis and calcification in hermatypic corals. *Limnol. Oceanogr.*, *54*, 1995–2002. doi: 10.4319/lo.2009.54.6.1995

Schrag, D. P. (1999). Rapid analysis of high-precision Sr/Ca ratios in corals and other marine carbonates. *Paleoceanography*, *14*, 97–102. doi: 10.1029/1998PA900025

Seeberg-Elverfeldt, J., Schlüter, M., Feseker, T., & Kölling, M. (2005). Rhizon sampling of porewaters near the sediment-water interface of aquatic systems. *Limnol. Oceanogr. Methods*, *3*, 361–371. doi: 10.4319/lom.2005.3.361

Shackleton, N. J., & Matthews, R. K. (1977). Oxygen isotope stratigraphy of Late Pleistocene coral terraces in Barbados. *Nature*, *268*, 618–620. doi: 10.1038/268618a0

Shen, C.-C., Lee, T., Chen, C.-Y., Wang, C.-H., Dai, C.-F., & Li, L.-A. (1996). The calibration of D [Sr/Ca] versus sea surface temperature relationship for *Porites* corals. *Geochim. Cosmochim. Acta*, *60*, 3849–3858. doi: 10.1016/0016-7037(96)00205-0

Shinn, E. A. (1968). Selective dolomitization of recent sedimentary structures. *J. Sediment. Res.*, *38*, 612–616. doi: 10.1306/74D719F1-2B21-11D7-8648000102C1865D

Shinn, E. A., Lidz, B. H., Halley, R. B., Hudson, J. H., & Kindinger, J. L. (1989). Reefs of Florida and the Dry Tortugas: Miami to Key West, Florida July 2 - 7, 1989. *Field Trip Guidebook* (Vol. 176, pp. 53). American Geophysical Union, Washington, D.C. doi: 10.1029/FT176

Sinclair, D. J., Williams, B., & Risk, M. (2006). A biological origin for climate signals in corals—Trace element "vital effects" are ubiquitous in Scleractinian coral skeletons. *Geophys. Res. Lett.*, *33*, L17707. doi: 10.1029/2006GL027183

Smerdon, J. E., & Pollack, H. N. (2016). Reconstructing Earth's surface temperature over the past 2000 years: the science behind the headlines. *WIREs Clim Change*, *7*, 746–771. doi: 10.1002/wcc.418

Smith, D. M., Scaife, A. A., Eade, R., Athanasiadis, P., Bellucci, A., Bethke, I., Bilbao, R., Borchert, L. F. et al. (2020). North Atlantic climate far more predictable than models imply. *Nature*, *583*, 796–800. doi: 10.1038/s41586-020-2525-0

Smith, J. M., Quinn, T. M., Helmle, K. P., & Halley, R. B. (2006). Reproducibility of geochemical and climatic signals in the Atlantic coral *Montastraea faveolata*. *Paleoceanography*, *21*, PA1010. doi: 10.1029/2005PA001187

Smith, S. V., Buddemeier, R. W., Redalje, R. C., & Houck, J. E. (1979). Strontium-calcium thermometry in coral skeletons. *Science*, *204*(4391), 404–407. doi: 10.1126/science.204.4391.404

Stabenau, E., & Kotun, K. (2012). *Salinity and Hydrology of Florida Bay: Status and Trends 1990 – 2009. National Park Service, Everglades National Park, South Florida Natural Resources Center, Homestead, FL.* Status and Trends Report. SFNRC Technical Series 2012:1. 39pp.

Stalker, J. C., Price, R. M., & Swart, P. K. (2009). Determining spatial and temporal inputs of freshwater, including submarine groundwater discharge, to a subtropical estuary using geochemical tracers, Biscayne Bay, South Florida. *Estuaries Coasts*, *32*, 694–708. doi: 10.1007/s12237-009-9155-y

Steuber, T., & Veizer, J. (2002). Phanerozoic record of plate tectonic control of seawater chemistry and carbonate sedimentation. *Geology*, *30*, 1123–1126.

Stoll, H. M., & Schrag, D. P. (1998). Effects of Quaternary sea level cycles on strontium in seawater. *Geochim. Cosmochim. Acta*, *62*, 1107–1118. doi: 10.1016/S0016-7037(98)00042-8

Surge, D. M., & Lohmann, K. C. (2002). Temporal and spatial differences in salinity and water chemistry in SW Florida estuaries: Effects of human-impacted watersheds. *Estuaries*, *25*, 393–408. doi: 10.1007/BF02695982

Swart, P. K., Berier, D., McNeill, D., Guzikowski, M., Harrison, S. A., & Dedick, E. (1989a). Interstitial water geochemistry and carbonate diagenesis in the sub-surface of a Holocene mud island in Florida Bay. *Bull. Mar. Sci.*, *44*, 490–514.

Swart, P. K., Sternberg, L. D. S. L., Steinen, R., & Harrison, S. A. (1989b). Controls on the oxygen and hydrogen isotopic composition of the waters of Florida Bay, U.S.A. *Chem. Geol.*, *79*. doi: 10.1016/0168-9622(89)90014-6

Swart, P. K., Healy, G. F., Dodge, R. E., Kramer, P., Hudson, J. H., Halley, R. B., & Robblee, M. B. (1996). The stable oxygen and carbon isotopic record from a coral growing in Florida Bay: A 160 year record of climatic and anthropogenic influence. *Palaeogeogr. Palaeoclimatol. Palaeoecol.*, *123*, 219–237. doi: 10.1016/0031-0182(95)00078-X

Swart, P. K., Elderfield, H., & Greaves, M. J. (2002). A high-resolution calibration of Sr/Ca thermometry using the Caribbean coral *Montastraea annularis*. *Geochem. Geophys. Geosyst.*, *3*, 1–11. doi: 10.1029/2002GC000306

Swart, P. K., & Price, R. (2002). Origin of salinity variations in Florida Bay. *Limnol. Oceanogr.*, *47*, 1234–1241. doi: 10.4319/lo.2002.47.4.1234

Thode, H. C. (2002). *Testing for normality,* 1st ed. CRC Press, New York, NY. doi: 10.1201/9780203910894

Thompson, D. M., Ault, T. R., Evans, M. N., Cole, J. E., & Emile-Geay, J. (2011). Comparison of observed and simulated tropical climate trends using a forward model of coral $\delta^{18}O$. *Geophys. Res. Lett.*, *38*, L14706. doi: 10.1029/2011GL048224

Tierney, J. E., Abram, N. J., Anchukaitis, K. J., Evans, M. N., Giry, C., Kilbourne, K. H., Saenger, C. P., Wu, H. C., Zinke, J. (2015). Tropical sea surface temperatures for the past four centuries reconstructed from coral archives. *Paleoceanography*, *30*, 226–252. doi: 10.1002/2014PA002717

Top, Z., Brand, L. E., Corbett, R. D., Burnett, W., & Chariton, J. (2001). Helium and radon as tracers of groundwater input into Florida Bay. *J. Coast. Res.*, *17*, 859–868.

Wang, C., & Zhang, L. (2013). Multidecadal ocean temperature and salinity variability in the tropical North Atlantic: Linking with the AMO, AMOC, and subtropical cell. *J. Clim.*, *26*, 6137–6162. doi: 10.1175/JCLI-D-12-00721.1

Watanabe, T. K., Watanabe, T., Ohmori, K., & Yamazaki, A. (2020). Improving analytical method of Sr/Ca ratios in coral skeletons for paleo-SST reconstructions using ICP-OES. *Limnol. Oceanogr. Methods*, *18*, 297–310. doi: 10.1002/lom3.10357

Wei, G., Sun, M., Li, X., & Nie, B. (2000). Mg/Ca, Sr/Ca and U/Ca ratios of a *Porites* coral from Sanya Bay, Hainan Island, South China Sea and their relationships to sea surface temperature. *Palaeogeogr. Palaeoclimatol. Palaeoecol.*, *162*, 59–74. doi: 10.1016/S0031-0182(00)00105-X

Wheat, C. G., Jannasch, H. W., Kastner, M., Hulme, S., Cowen, J. P., Edwards, K. J., Orcutt, B. N., Glazer, B. T. (2011). Fluid sampling from oceanic borehole observatories: Design and methods for CORK activities (1990-2010). In: A. T. Fisher, T. Tsuji, & K. Petronotis (Eds.), *Proceedings of the Integrated Ocean Drilling Program* (Vol. 327, pp. 36). Integrated Ocean Drilling Program Management International Inc., Tokyo. doi: 10.2204/iodp.proc.327.109.2011

Xu, Y.-Y., Pearson, S., & Kilbourne, K. H. (2015). Assessing coral Sr/Ca–SST calibration techniques using the species Diploria strigosa. *Palaeogeogr. Palaeoclimatol. Palaeoecol.*, *440*, 353–362. doi: 10.1016/j.palaeo.2015.09.016

Yates, K. K., & Halley, R. B. (2006). Diurnal variation in rates of calcification and carbonate sediment dissolution in Florida Bay. *Estuaries Coasts*, *29*, 24–39. doi: 10.1007/BF02784696